CHARLES UNIVERSITY

FACULTY OF SCIENCE

Study programme: Physical Geography and Geoecology

Mgr. Martin Hynčica

NONSTATIONARITY OF THE EFFECTS OF MODES OF ATMOSPHERIC CIRCULATION VARIABILITY ON SURFACE CLIMATE ELEMENTS

NESTACIONARITA VLIVU MÓDŮ PROMĚNLIVOSTI ATMOSFÉRICKÉ CIRKULACE NA PŘÍZEMNÍ KLIMATICKÉ PRVKY

Doctoral thesis

Supervisor: prof. RNDr. Radan Huth, DrSc.

Praha, 2023

I declare that I have written this doctoral thesis independently and cited all information sources and literature. The work, either in full or in part, has not been previously submitted for any other academic degree.

Prohlašuji, že jsem předloženou dizertační práci zpracoval samostatně a že jsem řádně odcitoval všechny informační zdroje a literaturu. Tato práce ani její část nebyla předložena k získání jiného nebo stejného akademického titulu.

.....

Újezdeček, 2 February 2023

ACKNOWLEDGEMENTS

I would like to express my thanks to my supervisor prof. Radan Huth, whose deep knowledge of the field has contributed not only to this work but also to my personal growth. His invaluable ideas and advice substantially elevate the quality of this work and they force me to think about scientific topics from different perspectives.

I acknowledge the Charles University Grant Agency (grant No. 426216) and the Czech Science Foundation (projects 17-07043S and 21-07954S) for supporting my research. Furthermore, I acknowledge the following organisations for providing data: NOAA for the 20CR reanalyses, ECMWF for ERA-40 and ERA-20C, JMA for JRA-55, CRU for CRU TS, and the GHCN for station data.

Abstract

Circulation modes are highly correlated, yet often distant areas detected in a field of a circulation variable, such as sea level pressure, geopotential heights, wind speed, and wind components. They consist typically of two or more action centres, which simultaneously weaken or strengthen, hence affecting the intensity and direction of atmospheric circulation and consequently surface climatic elements, such as temperature and precipitation. Temporal variability of action centres affects spatiotemporal distribution of impact on surface climatic variables. The availability of gridded datasets allows investigation of temporal behaviour of action centres and its impact on surface climatic variables on long time scales over large regions, which is, therefore, the main scientific topic of this work.

Due to a large amount of reanalyses differing in e.g. assimilated type of data and model used for their calculation, the comparison of representation of circulation modes and their temporal evolution of relationships with surface climatic elements is conducted between reanalyses. Circulation modes in reanalyses assimilating both surface and upper troposphere/satellite data (ERA40, JRA-55, NCEP-1) are mostly similar whereas the 20CRv2c reanalysis, which utilizes surface data only, contains biases. Although the ERA-20C reanalysis assimilates surface data only as well, it does not hold any substantial biases. Furthermore, temporal evolution of relationships between circulation modes and temperature in ERA-20C is similar to other reanalyses. Owing to a large agreement of ERA-20C with other reanalyses and its long temporal coverage spanning the whole 20th century, it is consequently utilized for identification of circulation modes in further century-long analyses. To evaluate also the gridded data containing surface climatic variables, relationships with circulation modes between station data and the nearest gridpoints from the CRUTS dataset are compared. It is shown that the temporal evolution of relationships at the majority of station-gridpoint pairs is similar. Thus, both ERA-20C and CRUTS datasets are proved to be reliable for our purposes. Then, the temporal evolution of relationships, determined by running correlations between circulation modes (from ERA-20C) and temperature and precipitation (from CRUTS), is investigated between 1901 and 2010 over the Northern Extratropics. Clustering of running correlations delimits areas where temporal evolution of the effect of circulation modes on temperature and precipitation is similar. Generally, the variation of action centres – mainly in their position, shape, and intensity – is responsible for the nonstationarity of relationships with surface climatic elements.

Key words: circulation modes, principal component analysis, running correlations, reanalyses

Abstrakt

Cirkulační módy jsou silně korelované, avšak často geograficky vzdálené oblasti, které lze detekovat v poli cirkulační proměnné, jako jsou přízemní tlak vzduchu, geopotenciální výšky či rychlosti větru a jeho složky. Zpravidla se skládají ze dvou nebo více akčních center, která současně slábnou nebo sílí, čímž ovlivňují intenzitu a směr atmosférické cirkulace, a následně i přízemní klimatické prvky, jako jsou teplota a srážky. Dlouhodobé změny akčních center ovlivňují časoprostorový dopad cirkulačních módů na přízemní klimatické prvky. S využitím gridovaných datasetů je možné tyto dlouhodobé změny akčních center a jejich dopady na přízemní klimatické prvky analyzovat v dlouhém časovém měřítku a v rozsáhlých oblastech, což je také hlavní vědeckou náplní této práce.

Protože existuje mnoho reanalýz, které se odlišují například v tom, jaká data reanalýza asimiluje, nebo v modelu, který je využíván pro jejich výpočet, je nejprve nutné srovnat podobu cirkulačních módů a vývoj vztahů mezi nimi a přízemními klimatickými prvky v různých reanalýzách. Ukazuje se, že reanalýzy, které asimilují jak přízemní data, tak i data z vyšší troposféry nebo satelitů (ERA40, JRA-55, NCEP-1), jsou si navzájem většinou podobné, zatímco reanalýza 20CRv2c, která využívá jen přízemní data, obsahuje chyby. Třebaže reanalýza ERA-20C využívá taktéž jen přízemní data, významněji se od ostatních reanalýz neodlišuje. Časový vývoj vztahů mezi cirkulačními módy a teplotou v ERA-20C je rovněž velmi podobný ostatním reanalýzám. Protože ERA-20C se tedy většinou shoduje s ostatními reanalýzami, neobsahuje významnější chyby a zároveň pokrývá celé 20. století, je použita pro detekci cirkulačních módů v dalších částech, ve kterých se analyzují dlouhodobé změny atmosférické cirkulace. Spolehlivost gridovaných přízemních dat obsahující přízemní klimatické prvky (z CRUTS datasetu) byla potvrzena srovnáním se staničními daty, neboť byly detekovány pouze malé rozdíly v časovém vývoji vztahů mezi teplotou a cirkulačními módy na stanici a nejbližším gridovém bodě. Vývoj časových vztahů, které jsou určeny klouzavými korelacemi mezi cirkulačními módy (z ERA-20C) a přízemní teplotou nebo srážkami (z CRUTS), jsou analyzovány v období 1901 až 2010 pro mimotropické oblasti severní polokoule. Clusterovou analýzou jsou vymezeny regiony, ve kterých je časový vývoj vztahů mezi cirkulačními módy a teplotou nebo srážkami přibližně stejný. Ukazuje se, že změny vlastností akčních center, zejména jejich pozice, tvaru a intenzity, způsobují nestacionaritu jejich vztahů s přízemními klimatickými prvky.

Klíčová slova: cirkulační módy, analýza hlavních komponent, klouzavé korelace, reanalýzy

Table of contents

1. Introduction

1.1 Modes of circulation variability

Modes of low-frequency circulation variability (in short "circulation modes"), also entitled as teleconnections in literature, are composed of action centres either positively or negatively correlated in a field of a circulation variable (e.g. geopotential heights, stream function, and wind speed) on large geographical scales. Action centres simultaneously weaken or strengthen, which affect the direction and intensity of circulation and consequently climatic elements in the entire troposphere (etc. temperature, winds, precipitation). Circulation modes have also large socioeconomic impact due to their linkage with occurrence of droughts (López-Moreno and Vicente-Serrano 2008) and floods (Zanardo et al. 2019), agricultural yields (Gimeno et al. 2002), fish population (Stige et al. 2006), condition of ecosystems (Ottersen et al. 2001), and many others.

Pioneering research exposes circulation modes with the use of one-point autocorrelation maps in pressure fields (Wallace and Gutzler 1981). Instead of autocorrelation maps, principal component analysis (PCA) was shown to be a more suitable method for identification of circulation modes (Barnston and Livezey 1987; Horel 1981), and this approach is widely used to present, although other approaches, such as neural networks (Monahan 2000) are also possible. While autocorrelation maps are computed for a single point only and a huge pile of such maps would be needed for an accurate and complete description of teleconnections, PCA operates with a whole pressure level and produces a large set of outputs, which represent circulation modes. Some climatological studies determine circulation modes as a difference between stations or gridpoints, which concerns mainly the North Atlantic Oscillation, typically defined by normalized pressure differences between Iceland and the Azores/Gibraltar/Lisbon (Hurrell 1995; Rogers 1984), but this approach is limited by the assumption that centres of the mode are stationary and located nearby the utilized station (Pokorná and Huth 2015).

The most studied circulation mode is the North Atlantic Oscillation (NAO), which consists of two main centres in the North Atlantic: the negative action centre residing approximately near Iceland and its positive counterpart located nearby the Azores. Pressure difference

between these action centres governs the intensity of zonal circulation and advection of relatively warmer and humid Atlantic air masses toward large parts of Eurasia: the positive phase of NAO is associated with stronger westerlies toward Eurasia and thereby positive temperature and precipitation response over its large parts, even to the Far East (e.g. Hurrell et al. 2003). Two other most prominent circulation modes are the Pacific-North American pattern (PNA; Leathers et al. 1991) with its four centres located over the eastern North Pacific and North America, and West Pacific Oscillation (WPO; Linkin and Nigam 2008), the spatial representation of which is similar to NAO but situated in the western North Pacific. Both patterns substantially affect climate in North America and eastern Asia. It is worth noticing that circulation modes are most often studied for winter (December, January, and February) when a sharper temperature contrast between the tropics and the Arctic causes stronger upper troposphere circulation and similarly stronger circulation modes. In summer, on the contrary, circulation modes are weaker, more regionalized, and some of those recognized in winter not detected at all.

Circulation modes are not stable entities; they exhibit temporal variability from days to decades. The interdecadal variability of circulation modes affects long-term relationships with surface climatic elements; the relationships thus undergo changes, which result in their strengthening and weakening. The first study to notice and examine non-stationarity of effects of extratropical circulation modes on surface temperature was that by Chen and Hellström (1999) on NAO effects on temperature in Sweden. Non-stationarities of the climatic effects of tropical modes were pointed out even earlier, e.g. Opoku-Ankomah and Cordery (1993) who examined effects of the Southern Oscillation on temperature in southeast Australia. Generally, studies confirm that fluctuations of relationships with surface climatic variables are controlled by spatial changes of circulation modes, which in turn also influence spatial impact of the mode (Beranová and Huth 2008; Filippi et al. 2014; Gu et al. 2009; Krichak et al. 2002; Jung et al. 2003; Vicente-Serrano and López-Moreno 2008; Xu et al. 2016). For example, larger impact of NAO on temperature and precipitation in Eurasia from the late 1970s to the early 1990s is attributed to the eastward shift of the mode (Beranová and Huth 2008; Slonosky et al. 2001). Several causes were suggested to explain this dislocation, such as intensity of the background flow (Luo and Gong 2006), greenhouse gas forcing (Ulbrich and Christoph 1999), changes in solar activity (Gimeno et al. 2003), stratospheric circulation (Dong et al.

2011), and Atlantic Multidecadal Oscillation (Börgel et al. 2020). Generally, there are not many studies investigating interdecadal changes of relationships with surface climatic elements and the causes of such nonstationarity. Recently, for example, Soulard et al. (2019) analyze temporal variation of impact of some circulation modes on North America, whereas Marshall (2021) describes unstable relationships between circulation modes and temperature and precipitation over northern Russia.

1.2 Reanalyses

Reanalyses are commonly used as a data source for studies of various aspects of atmospheric circulation, including the identification of circulation modes. They assimilate observed data, which are subsequently processed by a numerical weather prediction model into a regularly gridded form. A number of reanalyses exist, differing in the amount and type of assimilated data, resolution, temporal coverage, and the model utilized. Depending on the type of observed data assimilated, reanalyses can be divided into two categories (Fujiwara et al. 2017). First category – full-input reanalyses – utilizes surface station observations (e.g. pressure, humidity, wind) and also upper troposphere and satellite data. Most of them start around 1950 or later due to the lack of availability of relevant upper air data before the 1950's. On the contrary, surface-input reanalyses use surface observations only, upper-air data being completely computed by model, which may bring about various inaccuracies or errors. Surface-input reanalyses cover at least the whole 20th century. In this thesis, both categories of reanalyses are analysed and compared (Table 1).

Reanalyses are influenced mainly by the amount and spatial coverage of assimilated observations (Wang et al. 2013); for example, the introduction of satellite data after 1979 may cause inhomogeneities in reanalyses (Dee and Uppala 2009). Decreased reliability of reanalyses is expected over areas with the lack of observations and also in the 19th century and the first half of the 20th century, due to lower density of assimilated observations. Thus, although changes in atmospheric circulation can be tracked even to the 19th century in some reanalyses (Table 1), one has to take into account decreased reliability in the early periods.

Name	Abbreviation	Temporal coverage	Category	Reference
NOAA-CIRES-DOE Twentieth Century Reanalysis version 2c	20CRv2c	1851 - 2014	Surface-input	Compo et al. (2011)
NOAA-CIRES-DOE Twentieth Century Reanalysis version 3	20CRv3	1836 - 2015	Surface-input	Slivinski et al. (2021)
ECMWF Twentieth Century Reanalysis	ERA-20C	1900 - 2010	Surface-input	Poli et al. (2016)
ECMWF 40-year Second Generation Reanalysis	ERA-40	1957 - 2002	Full-input	Uppala et al. (2005)
Japanese 55-Year Reanalysis (JRA) Project	JRA-55	1957 - 2022	Full-input	Kobayashi et al. (2015)
NCEP/NCAR Reanalysis 1	NCEP-1	1948 - 2022	Full-input	Kalnay et al. (1996)

Table 1: Reanalyses used in the thesis.

1.3 Motivation and goals of the theses

The availability of datasets spanning the 20th century provides an excellent opportunity for studying long-term changes in circulation modes and their impact on relationships with surface climatic variables. However, papers published on this topic are limited to selected geographical areas and typically study one mode or a few of them. Also, there are only a few papers analysing circulation modes in the first half of the 20th century. A complex picture of how the nonstationarity of circulation modes affects their relationships with surface climatic elements during the 20th century on large spatial scales and in various reanalyses is missing. This research gap is addressed here; the main goal is to give a compact view on how the association between circulation modes and surface climatic elements, that is temperature and precipitation, has been changing since the beginning of the 20th century over the Northern Extratropics in winter.

Firstly, one has to select reanalysis that will be utilized for detection of circulation modes. Various characteristics of atmospheric circulation have been compared between reanalyses, e.g. the number of cyclones (Wang et al. 2016), circulation types (Stryhal and Huth 2017), and blocking activity (Rohrer et al. 2018), but no study has investigated differences in circulation modes and temporal evolution of relationships with surface climatic elements

among reanalyses yet. We may ask, for example, whether circulation modes are similar between reanalyses. Does temporal evolution of relationships with surface climatic elements correspond between reanalyses? Are there substantial differences between full-input and surface-input reanalyses? For the purposes of this study, the reanalysis has to be selected from the surface-input category, because we intend to cover the whole 20th century.

Furthermore, there are also several datasets containing surface climatic variables. Gridded surface datasets are created by interpolation of observed data into a regular network. The question on whether interpolation may substantially change temporal evolution of relationships with circulation modes at gridpoints is certainly relevant, but has until now been neither answered nor even posed. Is this evolution at a station similar to the nearest gridpoint? If so, a gridded dataset is preferred in further analyses due to its spatial (gridpoints are organized in a regular form) and temporal consistency (the same full temporal coverage at all gridpoints).

Hence, the aims of the thesis are:

- Comparison of reanalyses (Table 1) and selection of the reanalysis, in which circulation modes are detected;
- Evaluation of relationships between temperature and circulation modes in gridded datasets and observations and their comparison;
- Analysis of temporal variation of relationships between circulation modes and surface climatic variables.

1.4 Structure of results and overview of papers

Results are divided into three parts. Comparison of reanalyses is carried out in the first part (Sec. 2).

Paper I. Comparison of circulation modes between five reanalyses (Sec. 2.1)

> Hynčica, M., Huth, R. (2020). Modes of atmospheric circulation variability in the Northern Extratropics: A comparison of five reanalyses. *Journal of Climate*, 33, 10707-10726.

Paper II. Comparing relationships with circulation modes between reanalyses (Sec 2.2)

> Hynčica, M., Huth, R. (2021). Temporal evolution of relationships between temperature and circulation modes in five reanalyses. *International Journal of Climatology*, 42, 4391-4404.

The second part of results (Sec. 3) provides comparison of temporal evolution of relationships of circulation modes with temperature between stations and their nearest gridpoints from the Climatic Research Unit gridded Time Series Dataset (Harris et al. 2020, the CRU dataset).

Paper III. Temporal evolution of relationships between circulation modes and temperature at station and the nearest gridpoint from the CRU.

> Hynčica, M., Huth, R. (2020). Gridded versus station temperatures: Time evolution of relationships with atmospheric circulation. *Journal of Geophysical Research: Atmospheres*, 125, e2020JD033254.

Temporal evolution of relationships between circulation modes and temperature and precipitation is investigated over the Northern Extratropics since the beginning of the 20th century in Sec. 4.

Paper IV. Evolution of relationships between surface climatic variables and circulation modes.

> Hynčica, M., Huth, R. (2022). Temporal variation of relationships between circulation modes and surface climatic variables in the 20th century in winter. *Journal of Climate*. In Review.

2. Comparison of reanalyses

The main goal of this section is to select a reliable reanalysis, which does not hold biases affecting circulation modes and their temporal evolution with surface climatic variables. In addition, the reanalysis has to be selected from the surface-input category due to the necessity of its long temporal coverage. In the first subsection, the representation of circulation modes is compared between five reanalyses (Sec. 2.1) in the second half of the 20th century. In the second subsection (Sec. 2.2), the temporal evolution of relationships between surface temperature and circulation modes detected in five reanalyses is compared. It is shown that the most suitable reanalysis for purposes of this study is ERA-20C.

2.1 Comparison of circulation modes between reanalyses

Paper I: Hynčica, M., Huth, R. (2020). Modes of atmospheric circulation variability in the Northern Extratropics: A comparison of five reanalyses. *Journal of Climate*, 33 10707-10726.

Modes of Atmospheric Circulation Variability in the Northern Extratropics: A Comparison of Five Reanalyses

MARTIN HYNČICA[a,b] AND RADAN HUTH[a,c]

[a] *Department of Physical Geography and Geoecology, Faculty of Science, Charles University, Prague, Czech Republic*
[b] *Czech Hydrometeorological Institute, Ústí nad Labem, Czech Republic*
[c] *Institute of Atmospheric Physics, Czech Academy of Sciences, Prague, Czech Republic*

(Manuscript received 4 December 2019, in final form 4 September 2020)

ABSTRACT: Modes of low-frequency circulation variability in the Northern Hemisphere extratropics are compared between five reanalyses. Circulation modes are detected by rotated principal component analysis (PCA) of monthly mean 500-hPa geopotential heights between 1957 and 2002, separately for individual seasons. The quantification of differences between reanalyses is based on the percentage of grid points (approximately corresponding to the percentage of area) where the spatial representations of a mode (loadings) significantly differ between reanalyses. The differences between surface-input reanalyses (20CRv2c, ERA-20C) and full-input reanalyses (NCEP-1, ERA-40, JRA-55) are larger than differences within the reanalysis groups in all seasons except for autumn. The causes of the differences are of two kinds. First, the differences may be inherent to PCA: namely, the spatial structure of the modes may be sensitive to the number of components rotated. This concerns only a few modes. Second, the differences may reflect real correlation structures in reanalysis data. We demonstrate that the differences concentrate in three or fewer modes in each season. The reanalysis most different from the rest is 20CRv2c, with the differences concentrating over the southern half of Asia and in the subtropical belt over the Pacific and adjacent southwestern North America. The 20CRv2c reanalysis disagrees from other reanalyses there predominantly before the 1980s, which points to the impact of insufficient amount of assimilated observations. On the contrary, ERA-20C exhibits a higher agreement with full-input reanalyses, which is why we recommend it for studies of atmospheric circulation over the entire twentieth century.

KEYWORDS: Atmosphere; Extratropics; Teleconnections; Principal components analysis; Reanalysis data

1. Introduction

Atmospheric circulation can be described in a number of ways, one of which is as modes of low-frequency circulation variability (hereafter referred to simply as "circulation modes"). They typically consist of two or more remote centers between which circulation variables (usually sea level pressure or geopotential heights) are highly (whether negatively or positively) correlated. Circulation modes influence not only conditions in free atmosphere, such as wind speed and direction, humidity, and temperature, but also climate variables at the ground.

Wallace and Gutzler (1981) were the first to have detected circulation modes (referred to as "teleconnections" by them) in the Northern Hemisphere in winter. They used one-point correlation maps for the detection. Pioneering studies in the 1980s (Horel 1981; Rogers 1981; Barnston and Livezey 1987) proved that rotated principal component analysis (PCA) is a suitable tool for identifying circulation modes. Most studies using PCA to detect circulation modes are based on correlation or covariance matrix of gridded geopotential heights or sea level pressure (e.g., Thompson and Wallace 2000; Huth 2006; Compagnucci and Richman 2008), although other options are also possible. The principle of PCA is to obtain a set of new variables (principal components), which are uncorrelated both in space and time. Circulation modes appear as a few leading components, which explain high amounts of variance. Every component (mode) is characterized by its eigenvalue (which quantifies the variance that the component explains), loading, and score. In the setting of PCA used for detection of circulation modes, loadings are maps of correlations or covariances of the modes with the original data field, while scores are time series quantifying the intensity of the mode at a particular time instant (e.g., a month if monthly means are used as data input). Rotation of relevant principal components (i.e., a linear transformation of components into a new set of coordinates) is usually necessary to secure that the detected modes are realistic—that is, that they correspond to the underlying autocorrelations structures, represented by one-point autocorrelation maps (e.g., Richman 1986; Huth 2006; Compagnucci and Richman 2008; Lian and Chen 2012; Kohyama and Hartmann 2016). The realism of modes in this sense does not imply that they represent known dynamical processes. In fact, the association of individual modes with specific dynamical and physical processes is far from straightforward. The existence and maintenance of very few modes in the northern extratropics only has so far been explained in terms of physical processes, the North Atlantic Oscillation (NAO) being such an example (Spensberger et al. 2020).

The possible limitation of PCA is that it is a linear method, whereas many atmospheric processes contributing to variability

Supplemental information related to this paper is available at the Journals Online website: https://doi.org/10.1175/JCLI-D-19-0904.s1.

Corresponding author: Martin Hynčica, martin.hyncica@natur.cuni.cz; Radan Huth, huth@ufa.cas.cz

DOI: 10.1175/JCLI-D-19-0904.1

TABLE 1. Reanalyses used in this study, their category, and references.

Name	Abbreviation	Category	References
NOAA-CIRES-DOE Twentieth Century Reanalysis version 2c	20CRv2c	Surface input	Compo et al. (2011)
ECMWF twentieth century reanalysis	ERA-20C	Surface input	Poli et al. (2016)
ECMWF 40-year second generation reanalysis	ERA-40	Full input	Uppala et al. (2005)
Japanese 55-Year Reanalysis (JRA) Project	JRA-55	Full input	Kobayashi et al. (2015)
NCEP/NCAR 40-Year Reanalysis Project	NCEP-1	Full input	Kalnay et al. (1996)

of atmospheric circulation are nonlinear. Although some attempts have been made to extend the concept of PCA toward nonlinearity by using artificial neural networks and to implement nonlinear PCA to studies of atmospheric circulation (Monahan 2000; Hsieh 2004; Teng et al. 2007), this research direction appears to have been abandoned later. The possible reasons are that the interpretation of outputs of nonlinear PCA is much less straightforward, the calculations require substantially more computer time, and nonlinearity tends to be detected even where none in fact exists (Christiansen 2005).

The choice of specific parameters in PCA influences both spatial structure and temporal behavior of circulation modes. First, one has to make a decision on whether a correlation or covariance matrix is employed. Huth (2006) demonstrates that spatial structure of circulation modes is influenced only marginally by this choice. Second, there are several approaches to account for a decreasing area of grid boxes toward the pole, which may affect spatial representation of circulation modes. And finally, the number of principal components to be retained and rotated must be determined.

Any method to describe and analyze atmospheric circulation captures only a part of the continuum of its variability. Certain uncertainty is inherent to all approaches: for example, the choice of the detection and tracking method in analyses of blockings and cyclone tracks (Ulbrich et al. 2009; Woollings et al. 2018) and the choice of the classification method and number of types in classifications of circulation patterns (Stryhal and Huth 2017). In analyses of circulation modes, this uncertainty is manifested in the sensitivity to the number of modes (i.e., number of components rotated). We chose the particular methodology, which is described below, with the objective to minimize these uncertainties.

Reanalyses are the most suitable datasets for identification of circulation modes because they contain data on a regular grid. Reanalyses are produced by a numerical weather prediction model, into which the observed data are assimilated. However, both the model characteristics (resolution, model configuration, data assimilation design, etc.) and assimilated observations (their quantity, quality, and coverage) cause differences between individual reanalyses. Wang et al. (2013) note that uncertainty in reanalyses is brought about by temporal changes in the amount of assimilated data. The introduction of satellite observations after 1979 (e.g., Sturaro 2003; Dee and Uppala 2009; Dee et al. 2011) and operational vertical sounder after 1998 (Fujiwara et al. 2017; Long et al. 2017) have also been reported to cause inhomogeneities in reanalyses. All these potential biases and discontinuities, which project into reanalyses, may also affect the circulation modes.

Reanalyses differ in the data they assimilate: surface-input reanalyses make use of surface data only, such as pressure, surface winds, sea ice distribution, and sea surface temperature, whereas full-input (standard) reanalyses use also observations of free atmosphere, including radiosonde and satellite data (Fujiwara et al. 2017). In surface-input reanalyses, data in free atmosphere are completely calculated by the model and are constrained by surface observations only, which is also likely to introduce bias. Surface-input reanalyses cover more than a century-long period, starting at least in the beginning of the twentieth century. Full-input reanalyses span a shorter time period when radiosondes are routinely available (approximately since the middle of the twentieth century).

Intercomparisons of reanalyses generally conclude that differences between them are mostly small over areas with a high density of observational data, while considerably larger where data are sparse (Harnik and Chang 2004; Wang et al. 2006; Bromwich et al. 2007; Hodges et al. 2011; Wang et al. 2016). Furthermore, various processes and phenomena in the upper atmosphere are poorly reproduced or completely absent in surface-input reanalyses simply because data from the free atmosphere are not available to them. For example, a rather unreal response of the upper troposphere and stratosphere to volcanic eruptions (Fujiwara et al. 2015), missing sudden stratospheric warmings and quasi-biennial oscillation (Pišoft et al. 2013; Butler et al. 2017), an overestimation of 500-hPa geopotential heights over Greenland in summer (Belleflamme et al. 2013), fewer cyclones in the Northern Hemisphere (Wang et al. 2016), stronger easterlies and higher blocking activity over Europe (Rohrer et al. 2018), and lower occurrence of westerly and northwesterly circulation types (Stryhal and Huth 2017) have been detected in 20CRv2 relative to full-input reanalyses. The last study points to a considerably different representation of circulation types in reanalyses even over the data-rich region of central Europe. On the other hand, major storm tracks in the Northern Hemisphere in 20CRv2, ERA-20C, and JRA-55 agree well with radiosonde observations, in contrast to NCEP-1 and ERA-40 where large biases were detected (Chang and Yau 2016).

Representation of cyclones in full-input reanalyses shows rather good agreement (Zahn et al. 2018). The number of pressure formations over the Northern Hemisphere appears to depend on the horizontal resolution: the reanalyses with a higher resolution, such as MERRA and ERA-Interim, produce

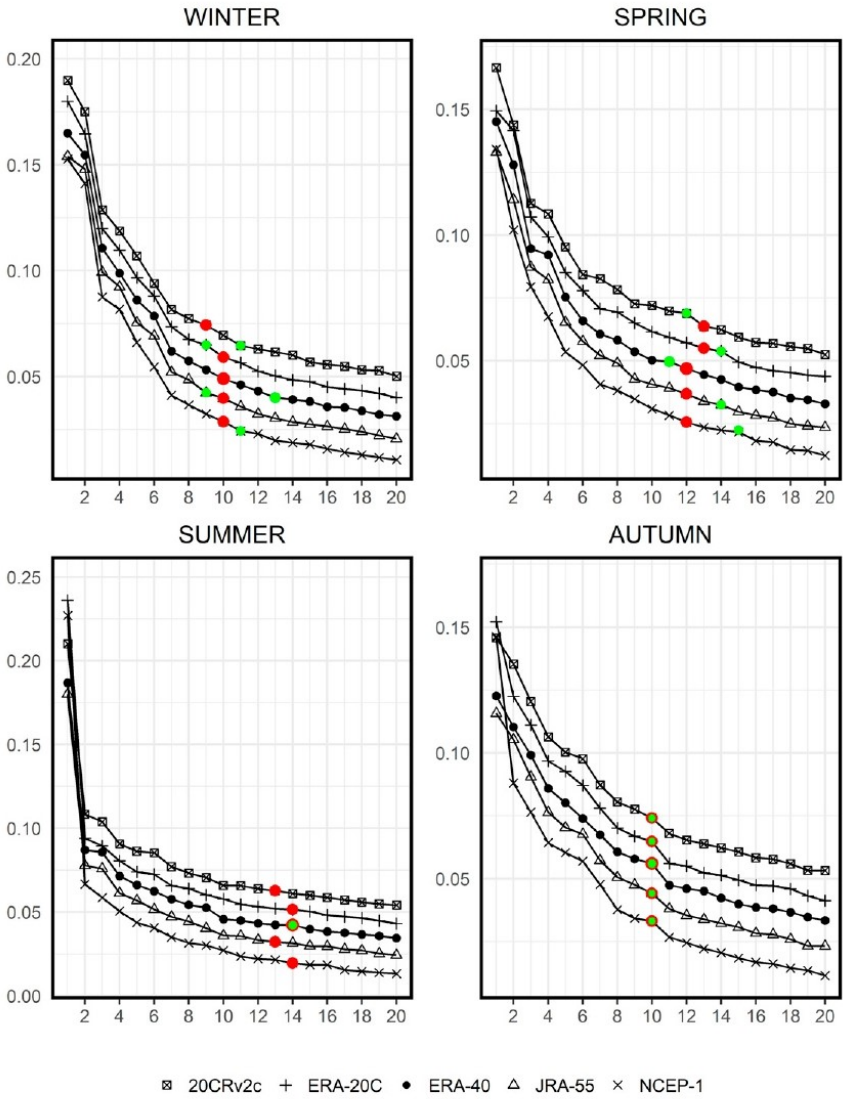

FIG. 1. Scree plots with 20 leading principal components and the percentage of their explained variance (on the *y* axis) in five reanalyses for individual seasons. Red dots show the numbers of rotated components that we apply; green dots show candidate drops, i.e., the numbers of components complying with O'Lenic and Livezey's (1988) criterion. The graphs are indented from each other by 0.01 in order to facilitate display.

more cyclones with stronger intensity (Tilinina et al. 2013; Wang et al. 2016; Pingree-Shippee et al. 2018) and also more anticyclones (Pepler et al. 2018). Differences in the number of cyclones between NCEP-1 and ERA-40 were reported by Trigo (2006) and Wang et al. (2006).

We are not aware of any study that would compare reanalyses from the point of view of circulation modes. This paper is intended to fill this gap, its goal being to compare the spatial representation of circulation modes between five reanalyses that have been most commonly used in climatological studies

TABLE 2. Number of rotated and used principal components and variance explained by the rotated modes.

	Components rotated/used	Variance explained (%)	Components rotated/used	Variance explained (%)
	Winter		Spring	
20CRv2c	9/9	68.7	13/10	69.9
ERA-20C	10/9	72.4	13/12	70.8
ERA-40	10/9	71.5	12/12	68.0
JRA-55	10/9	72.1	12/12	68.0
NCEP-1	10/9	72.2	12/12	68.3
	Summer		Autumn	
20CRv2c	13/12	64.4	10/10	62.3
ERA-20C	14/14	68.6	10/10	64.2
ERA-40	14/13	66.4	10/10	61.4
JRA-55	13/12	64.3	10/9	62.5
NCEP-1	14/12	69.8	10/10	64.5

recently. We intentionally investigate circulation modes in all seasons since only few studies analyze circulation modes in other seasons than winter and if so, they typically focus on the strongest modes, such as the NAO (e.g., Folland et al. 2009; Linderholm et al. 2011; Sun and Wang 2012; Lin 2014; Soulard and Lin 2017). No study that looks at all the modes in the northern extratropics in all seasons has been published for more than 25 years (i.e., since the reanalyses have become available and widely used). We evaluate the realism of the modes in the statistical sense, that is, whether and to what extent they correspond to the underlying correlation structures; it is not our intention to associate the modes with physical and dynamical processes that induce and maintain them. The analysis is performed by rotated PCA of 500-hPa heights in the Northern Hemisphere extratropics.

2. Data and methodology

We evaluate five widely used reanalyses (Table 1) that cover the period from September 1957 to August 2002 (i.e., 45 years altogether). The exception is JRA-55, which starts only in January 1958; its analysis period is therefore shifted one season forward, covering March 1958–February 2003, so that the number of months in each season is equal in all reanalyses (135). Our choice of reanalyses has been governed by two requirements: 1) we examine reanalyses that have been frequently utilized in climatological studies, and those of atmospheric circulation and variability modes in particular, and 2) we intend to cover the longest possible period in which all the reanalyses overlap. Moreover, the period covering a sufficiently long time both before and after 1979 enables us to evaluate the impact of the assimilation of satellite data in full-input reanalyses (see section 4d).

PCA in S-mode (i.e., with grid points arranged in columns and months in rows of the input data matrix) with a correlation matrix is employed for identification of circulation modes in the Northern Hemisphere extratropics delimited by 20°N. Circulation modes are calculated for each season separately—winter (DJF), spring (MAM), summer (JJA), and autumn (SON). Monthly anomalies of 500-hPa geopotential heights from the long-term monthwise average are used. Computation of circulation modes is performed on the grid with 5° × 5° resolution. All reanalyses except 20CRv2c are directly downloaded in 2.5° × 2.5° resolution; then only every other point in both directions is included in the analysis. 20CRv2c is downloaded in its original resolution (2° × 2°) and subsequently interpolated by spline interpolation to 2.5° × 2.5°.

Because meridians converge toward the pole, there is higher density of points in the vicinity of polar regions. There are some options how to deal with this issue (Huth 2006); here we opt for using a quasi-equal-area grid where points are randomly excluded from the regular latitude–longitude grid so that the mean area of a grid box is approximately the same for all parallels (Araneo and Compagnucci 2004). The number of excluded points increases toward the pole while all of them are kept on parallels in low latitudes. The exact position of excluded points does not affect the shape of circulation modes (Huth 2006). The total number of grid points included in the analysis is 699, the North Pole being excluded.

The components are rotated by varimax rotation (Richman 1986), which leads to a better representation of modes. There are several criteria to determine the optimum number of rotated components, which may give outputs differing even more than by an order of magnitude (e.g., Serrano et al. 1999). Here

TABLE 3. Abbreviations and full names of circulation modes.

EA	East Atlantic pattern
EP	East Pacific pattern
EU1	Eurasian pattern type 1
EU2	Eurasian pattern type 2
NA	North Asian pattern
NAO	North Atlantic Oscillation
NP	North Pacific pattern
PNA	Pacific–North American pattern
PT	Pacific transition pattern
SZ	Subtropical zonal pattern
TNH	Tropical/Northern Hemisphere pattern
WPO	West Pacific oscillation

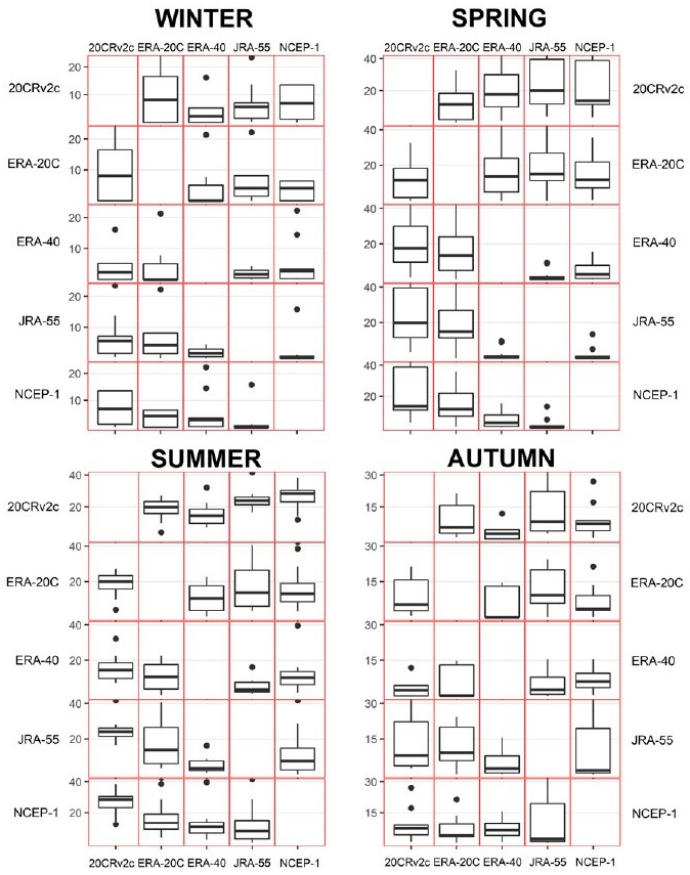

FIG. 2. Tables with boxplots showing the normalized proportion (%) of grid points with significant differences (for a detailed explanation see text) for all pairs of reanalyses in all seasons. The central line of the boxplot is the median; the lower and upper edges denote the lower and upper quartile. The upper and lower whiskers extend to 1.5 times the interquartile range from the respective edges, with the outliers lying beyond the whiskers denoted by dots.

we follow O'Lenic and Livezey (1988), who recommend a criterion based on a scree plot (i.e., graph showing the dependence of variance explained by each component on its rank) where the components are ordered by explained variance. The general guidance is that the components should be cut at a noticeable drop (step) in the graph; typically, the rightmost drop (i.e., the largest possible number) is chosen. In an ideal case, the drop is clearly present and occurs for the same number of components for all reanalyses. In reality, however, one has to make compromise between the presence of a drop, the amount of explained variance, the stability of the modes (the stability meaning here the insensitivity of their spatial patterns to the number of rotated components), and their similarity across reanalyses, which makes the determination of the optimum number of components to rotate a subjective task to some extent. Figure 1 displays the scree plots for all the four seasons, with candidate drops and the rotated numbers of components highlighted. Note that in summer, the eigenvalue spectra are rather flat, without pronounced drops, with the exception of ERA-40, in which the candidate drop is localized to the 14th component; that position is therefore used to approximate the number of components to rotate in other reanalyses, too.

The number of components that we interpret, compare between reanalyses, and discuss may be different from (i.e., smaller than) the number of components rotated (Table 2).

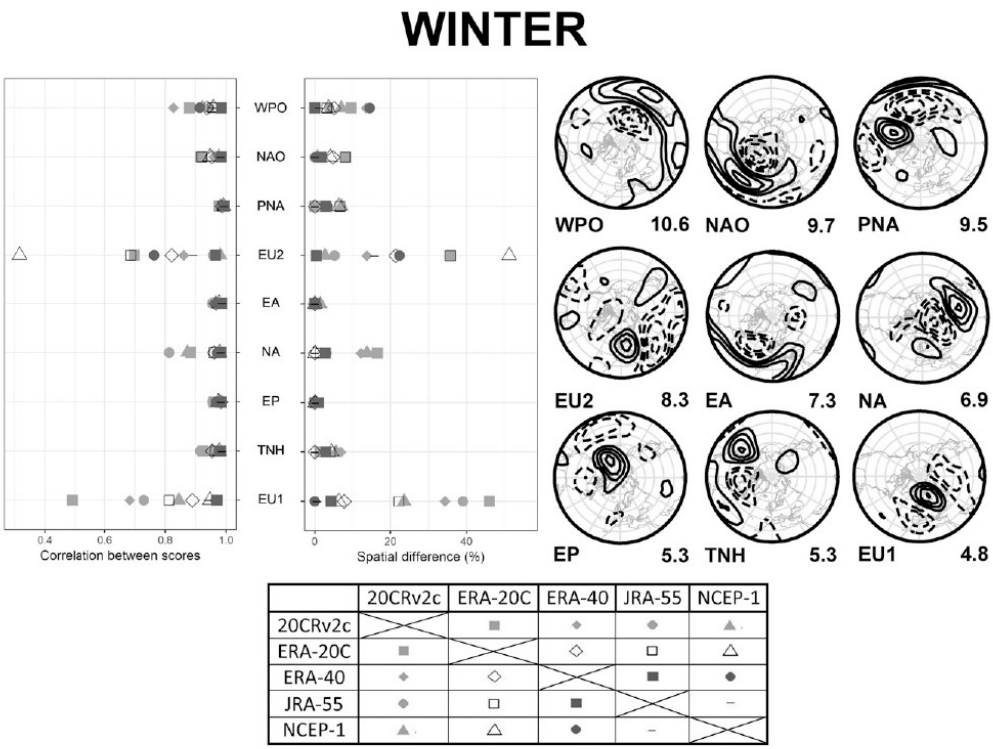

FIG. 3. (top right) Circulation modes in winter in ERA-40: PCA loadings (contour interval is 0.2; positive contours are solid, negative contours are dashed; zero contour is omitted for the sake of clarity), their abbreviated name, and percentage of explained variance are shown below the maps. (top center) Proportion (%) of area with statistically significant differences between loadings normalized by the area with nonzero loadings. (top left) Correlation of scores for all pairs of reanalyses. (bottom) Pairs of reanalyses are denoted by symbols defined in the bottom table.

This is because we have to seek a compromise between the interpretability and realism (in terms of the correspondence with correlation structures) of all the rotated modes and their stability and similarity between reanalyses. That is, in some cases (combinations of reanalysis and season) it is necessary to rotate more components than how many modes seem to actually occur. There are two reasons for it. First, if the lower number of components, equal to the number of really occurring modes, is rotated, one of the really occurring modes is, somewhat paradoxically, not detected; it only appears in the analysis if an additional component is included into rotation. Second, the rotation of the lower number of components results in a substantially lowered similarity of the modes with other reanalyses; this happens because of a somewhat random redistribution of variance among the rotated modes. As we intend to maximize the similarity of modes between reanalyses, we sacrifice the use of the "correct" number of modes to this maximization in some cases. The additional modes typically do not correspond to autocorrelation structures and/or are different in individual reanalyses; therefore, we tend to look at them as representations of noise and do not keep them in the further analyses and discussions.

Loadings represent correlations between the principal component and monthly mean 500-hPa heights. Therefore, statistical significance of differences between loadings is evaluated as statistical significance of a difference between correlations, that is, with the use of Fisher transformation: correlation coefficients r_1, r_2 are transformed to (Huth et al. 2006; Pokorná and Huth 2015)

$$z_i = 0.5\ln[(1+r_i)/(1-r_i)],$$

and the test statistic is then

$$u = (z_1 - z_2)\left[\frac{1}{(n_1-3)} + \frac{1}{(n_2-3)}\right]^{-1/2},$$

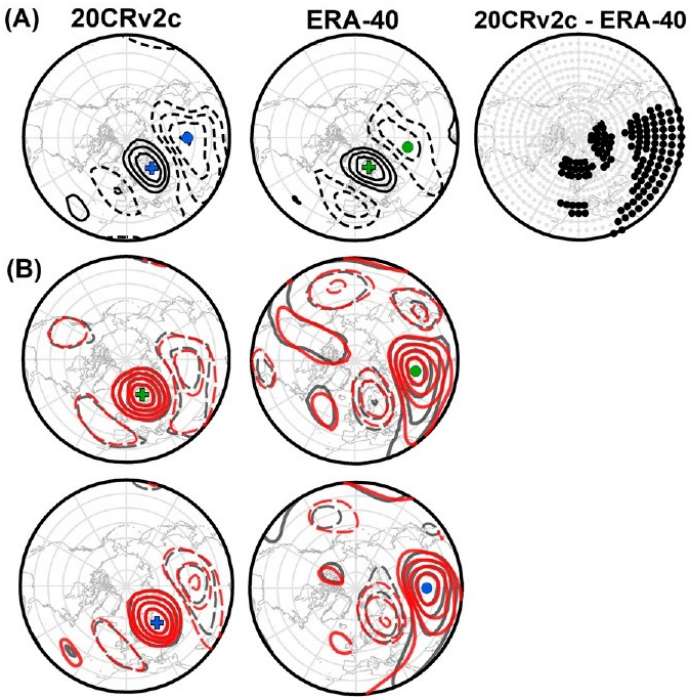

FIG. 4. (a) EU1 in winter in 20CRv2c and ERA-40 and the position of grid points with significant differences in loadings between 20CRv2c and ERA-40. (b) Autocorrelation maps for the grid points with the most positive (crosses) and negative (dots) loadings in (top) ERA-40 and (bottom) 20CRv2c; 20CRv2c in red, ERA-40 in gray.

where n_i is the sample size. We are entitled to employ Fisher transformation because the principal component loadings are approximately normally distributed. The number of grid points with a significant difference between reanalyses closely approximates the area of the northern extratropics where loadings are significantly different from each other. That area is then weighted by the area where the loading is significantly different from zero in at least one of the two compared reanalyses. Thus, a proportion (in %) of the area with nonzero loadings where the differences of loadings between reanalyses are significant is calculated.

The terminology of circulation modes (Table 3) is adopted from Barnston and Livezey (1987, hereinafter BL). The modes not recognized in BL are identified by their rank according to the variance explained in ERA-40 (e.g., "mode 3" if it explains the third largest amount of variance), unless explicitly stated otherwise. The polarity of loadings as provided by PCA is random to some extent; we set the polarity to be equal to modes in BL. The polarity of the modes not appearing in BL follows that in ERA-40.

3. Results

a. General characteristics of circulation modes

In this section, general remarks on differences between reanalyses and a brief explanation of some methodological options are provided.

The variance explained by the retained and rotated principal components is roughly similar in all reanalyses; the spread is of the order of a few percent, with the largest (5.5%) occurring in summer (Table 2). In winter and autumn, 9–10 circulation modes are identified in all reanalyses. Circulation modes in winter explain more variance due to a stronger and more pronounced circulation, the spatial structures of which are larger than in other seasons and concentrate in fewer modes as a result. Autumn, on the contrary, is the season with the lowest explained variance (Table 2), which is caused by a relatively small number of detected modes (the drop in Fig. 1 occurs after the 10th mode). However, the rotation of more than 10 components, that is, a larger share of variance explained, in autumn does not bring additional interpretable modes; that is why we deem that a relatively low explained

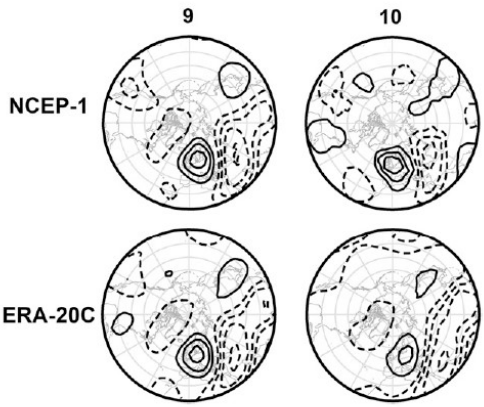

FIG. 5. EU2 in winter in NCEP-1 and ERA-20C for 9 and 10 rotated components.

variance in autumn is a real feature. In spring and summer, circulation is generally more scattered and regionalized, with a shorter autocorrelation distance. More circulation modes (12–14) with somewhat lower explained variance are needed to reasonably describe it.

The normalized percentage of grid points with significant differences between loadings was calculated for all pairs of reanalyses, all circulation modes, and all seasons. It is presented in Fig. 2 where boxplots display the percentage of grid points with significant differences of all circulation modes between all pairs of reanalyses in all seasons. The higher the values of boxplot, the lower the similarity of the two compared reanalyses. Generally, reanalyses have the highest agreement in winter and autumn, while the lowest agreement is found in summer. In winter, spring, and also in summer, the different behavior of surface-input reanalyses, which exhibit larger differences from the other reanalyses, is evident. In autumn, the distinction of the two groups of reanalyses is not visible: the differences are rather similar among reanalyses and tending to concentrate in the circulation modes sensitive to the number of rotated components (see section 3e).

Figure 2 also helps determine the most representative reanalysis, which we use as a reference for the display of circulation modes thereinafter. We select from full-input reanalyses, which should be, considering the amount of assimilated data, more reliable and opt for ERA-40 because it exhibits the lowest differences from 20CRv2c and ERA-20C in all seasons but spring (Fig. 2). Circulation modes in ERA-40 are displayed and discussed later; modes in other reanalyses are displayed for all seasons in the online supplemental material in Figs. S1–S4 in the online supplemental material. The modes are displayed in the order of the explained variance in the particular reanalysis.

b. Winter

All circulation modes in ERA-40, the normalized percentage of the area where all pairs of reanalyses significantly differ from each other, and correlations of scores between all circulation modes in all pairs of reanalyses are displayed in Fig. 3. Most of the circulation modes identified in winter in ERA-40 are highly similar to those in BL. Three most prominent modes in ERA-40 are WPO, NAO, and PNA. The variance that all the modes together explain in individual reanalyses is in the range of 69%–72%.

The spatial differences and correlations of scores are closely related, which is evident in Fig. 3 (top center and left): larger differences between loadings correspond to lower correlations of scores and vice versa. Perfectly spatially matching modes would have identical temporal course of scores; the scores of modes with entirely dissimilar spatial patterns would have uncorrelated scores. The information provided by comparisons of loadings and comparisons of scores thus largely overlaps; therefore, we limit the display and discussion of differences in the further text to the spatial representation of loadings.

The differences between reanalyses are largest for two Eurasian modes, EU1 and EU2 (Fig. 3, top left). EU1 consists of a positive center over northern Europe and two negative centers—one over northern Asia and another, less pronounced, over southwestern Europe. In 20CRv2c, all of its centers have a different shape or position (Fig. 4a): the negative center over southwestern Europe is shifted northeastward, the main positive center is shifted eastward to northeastern Europe and the negative Asian center is located more southeastward, approximately over northwestern China. Additionally, the latter is stronger and more extensive in 20CRv2c. The different position and shape of centers is the main cause of spatial dissimilarity between 20CRv2c and other reanalyses, which is confirmed by the position of points with significant differences in the top-right map in Fig. 4a. Autocorrelation maps for the two grid points with the highest and lowest loadings in ERA-40 and 20CRv2c (Fig. 4b) localize the differences to southern and southeastern parts of Asia where one can see different magnitudes of autocorrelations. It is particularly evident in the autocorrelation maps for the eastern center (Fig. 4b, right column). Since autocorrelation maps in the other reanalyses for the same grid points as in Fig. 4b are very similar to those in ERA-40 (not shown), one may conclude that the differences manifest different behavior of 20CRv2c over southern half of Asia, which is likely why EU1 is displayed in 20CRv2c differently from other reanalyses.

Differences in the appearance of EU2 are illustrated for ERA-20C and NCEP-1 in Fig. 5. They have their roots in the sensitivity to the number of rotated principal components: Fig. 5 shows that 9 and 10 rotated components result in different shapes of EU2 in both reanalyses. The difference concentrates particularly in the negative Eurasian center, which is smaller and has no extension toward eastern Eurasia in NCEP-1 for 10 rotated components. Also the main positive center over Europe/North Atlantic is shifted and has a slightly different shape. EU2 looks very similar in both reanalyses if 9 components are rotated, but the similarity is much lower for 10 rotated components. This is a manifestation of the compromise in the number of components to rotate; a better overall correspondence of modes between reanalyses is achieved at the expense of a reduced correspondence for one particular mode. If we decided to rotate 9 instead of 10 components, the better

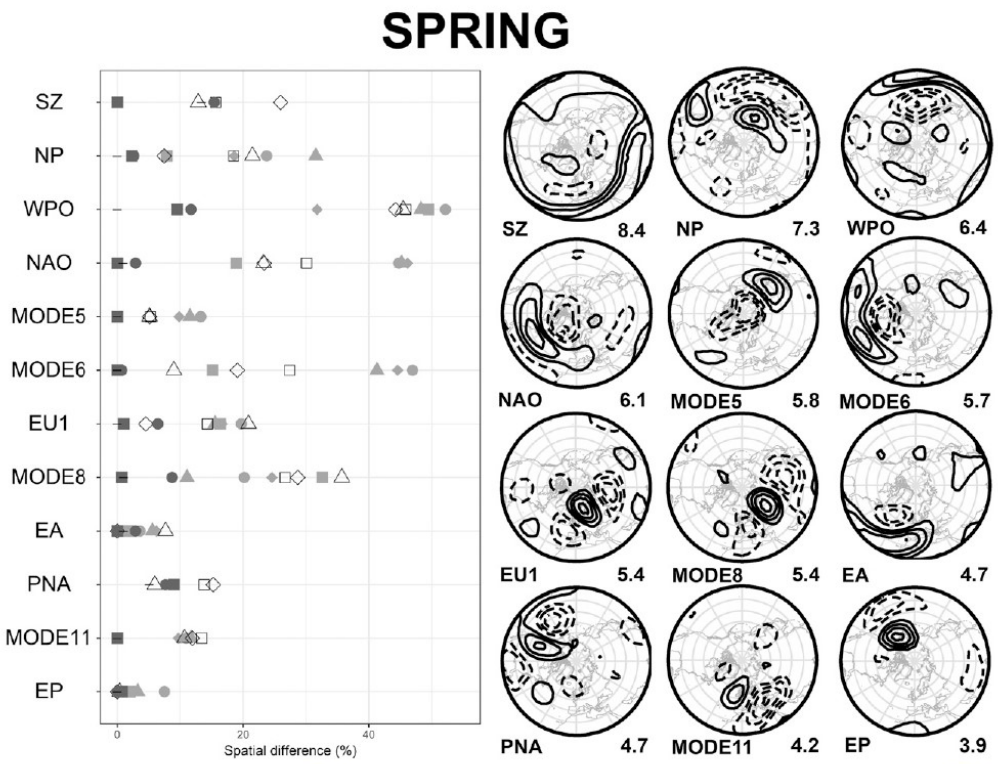

FIG. 6. As in the center and right top part of Fig. 3, but for spring. For the explanation of symbols in the left graph, see the bottom part of Fig. 3.

correspondence of reanalyses in the display of EU2 would be outweighed by a generally worse correspondence for most other modes.

c. Spring

In spring, 12 circulation modes are identified (Fig. 6). Circulation modes explain roughly about 69% of variance in all reanalyses. The most prominent modes in ERA-40 are SZ, NP, and WPO (see Table 3 for expansions of mode names). SZ is, however, absent in 20CRv2c; it does not appear even if different (smaller or larger) numbers of components are rotated. It seems to be at least partly attached to WPO, being reflected in its stronger zonal center over subtropical Eurasia, and to the third mode (explaining 6.8% of variance, not appearing in any other reanalysis, and denoted as ''xxx'' in Fig. S1), which forms a strong center over Asia. The highest differences are, similarly to winter, revealed between surface-input and full-input reanalyses. The differences are particularly large for WPO and NAO (Fig. 6), which we discuss below.

WPO consists of two main zonally elongated centers over the North Pacific along the 50° and 25°N parallels, both attaining maximum loadings near the date line. The representation of the southern center is fairly different in the three reanalyses shown in Fig. 7a. In 20CRv2c, it forms a long belt over the subtropics almost around the globe. This belt is particularly strong over Eurasia and northern Africa and also over large parts of Pacific Ocean as is documented by the position of points with significant differences from ERA-40 in Fig. 7a. On the other hand, the belt over the subtropics is weaker, shifted northward, and confined to the Pacific in ERA-20C. The northern center has also a different shape and position in the three reanalyses, but the difference is less pronounced. The autocorrelation maps for the grid point with the highest loading in the subtropical center provide no clue for a different appearance of WPO in different reanalyses (left column in Fig. 7b) since they look fairly similar in all three reanalyses. This suggests that reanalyses do not differ from each other in correlations within the subtropical belt. There are, however, some differences in correlations of the subtropical belt with the WPO northern center. Although the differences are rather weak, they are notable: the autocorrelations tend to be strongest and their values over 0.2 to be most spatially extensive for 20CRv2c, while weakest and least extensive for

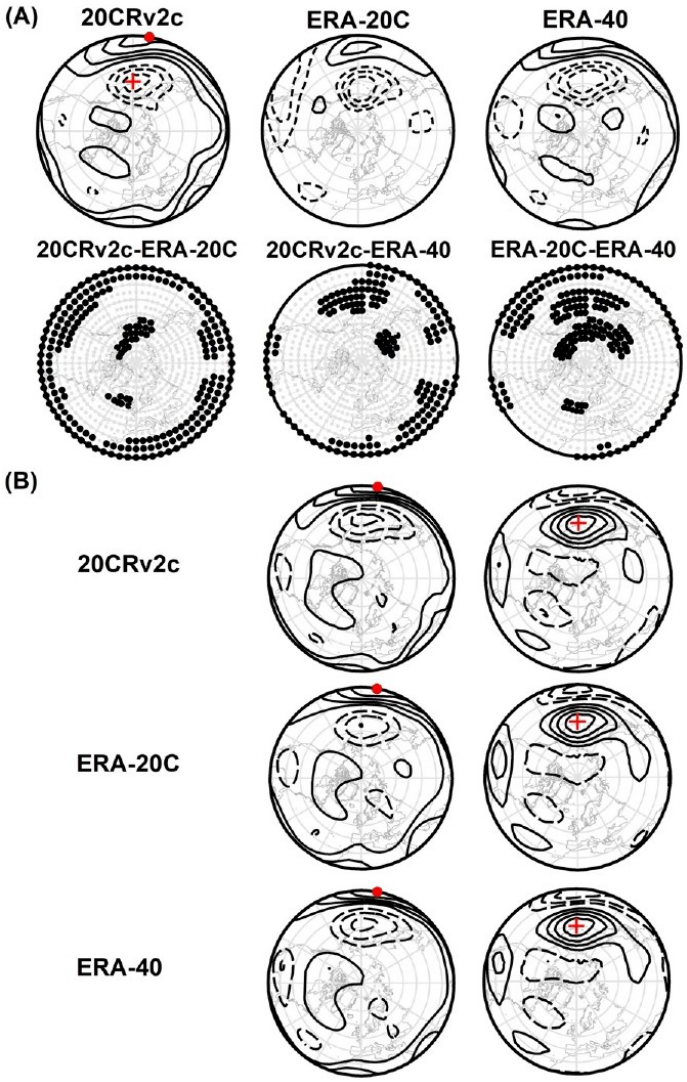

FIG. 7. (a) WPO in spring in three reanalyses in the top row and the position of grid points with significant differences in loadings between the reanalyses in the bottom row. (b) Autocorrelation maps for the points with the most positive (red dots) and negative (red crosses) loadings in 20CRv2c for 20CRv2c, ERA-20C, and ERA-40.

ERA-20C. The extent and strength of subtropical autocorrelations with the WPO northern center are thus in agreement with the strength and spatial extent of the southern center of WPO: they are largest and strongest in 20CRv2c, moderate in ERA-40, and smallest and weakest in ERA-20C.

The appearance of NAO is very different in 20CRv2c (Fig. 8a): in comparison with full-input reanalyses (note that NAO in NCEP-1 and JRA-55 is almost identical to ERA-40 as shown here), the negative North Atlantic center is weaker and less extensive, the positive southern center splits into two separated

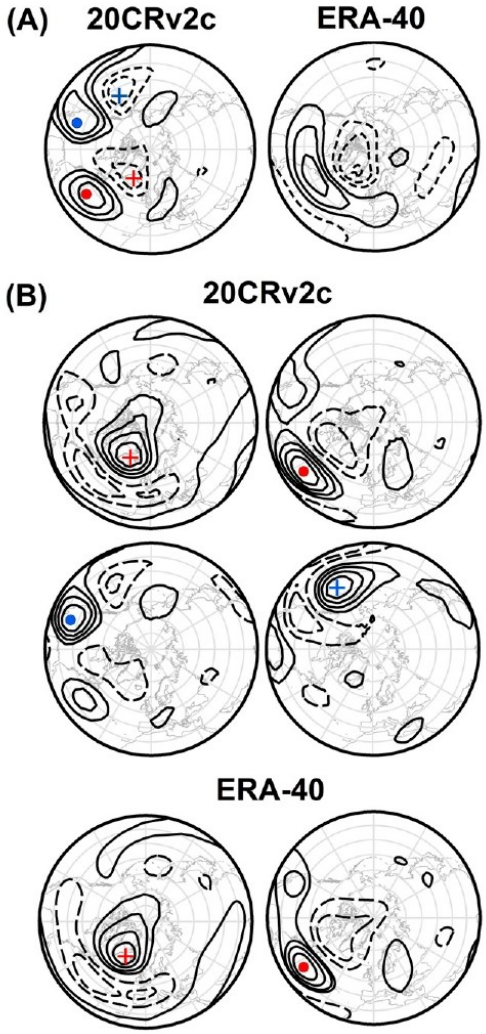

FIG. 8. (a) NAO in spring in 20CRv2c and ERA-40. (b) Autocorrelation maps for the four points with the most positive (dots) and negative (crosses) loadings in 20CRv2c and ERA-40 (only for the pair of eastern points).

parts, and the southernmost negative center is completely missing. The entire pattern over the North Atlantic appears to be shifted southward in 20CRv2c. NAO in ERA-20C (Fig. S2) is more similar to full-input reanalyses than to 20CRv2c. Nevertheless, the surface-input reanalyses share the feature that additional centers over North America and North Pacific are attached to the NAO pattern. Autocorrelation maps for the two Atlantic centers of NAO in 20CRv2c (Fig. 8b, top) are fairly similar to ERA-40 (Fig. 8b, bottom). There is no hint in the autocorrelation maps for 20CRv2 of the link with the upstream center over the northeastern Pacific along 150°E. On the other hand, the southern Atlantic center tends to separate into two cores, one over the western Atlantic and the other over the western United States, in the autocorrelation maps for 20CRv2c, unlike those for ERA-40 where the southern Atlantic center is more compact. Autocorrelation maps for the western centers of NAO in 20CRv2c (middle row in Fig. 8b) exhibit only a very weak link with the Atlantic centers; they clearly resemble PNA, however, which itself is not detected in 20CRv2c as a separate mode. This suggests a (probably unrealistic) connection of NAO with PNA in 20CRv2c through exaggerated correlations between the two southern positive centers. The NAO in 20CRv2c is thus likely an amalgamation of two actually independent modes, PNA and NAO.

d. Summer

In summer, 14 circulation modes are identified (Fig. 9), although not all of them appear in all reanalyses (e.g., mode 11 occurs in the surface-input reanalyses only). Only six of the modes have been described earlier in BL. Total explained variance ranges from 64.3% to 69.8%. The four strongest modes in ERA-40 (SZ, NAO, mode 3, and NP) explain more than 4% of variance and are among the six most important circulation modes in all other reanalyses. Although most of summer circulation modes may seem to be rather weak (explaining only 3%–4% of variance), their realism is supported by autocorrelation maps (Figs. S5 and S6).

The most prominent mode in summer, SZ, is characterized by a circumglobal belt in the subtropics and is noted for the highest spatial differences: for example, in 20CRv2c it is located farther south, especially in the Eastern Hemisphere, and lacks a ridge visible in all other reanalyses over central to eastern Asia (Fig. 10a and Figs. S1–S4). Yet, its representation is particularly different in NCEP-1; significant differences from other reanalyses are located over large regions of Eurasia and northern Africa, reflecting that SZ is stronger there than in other reanalyses, while being weaker over the western North Pacific and North America (Fig. 10a). This is confirmed in autocorrelation maps in Fig. 10b. Moreover, time series of SZ in NCEP-1 do not fit other reanalyses either, particularly before 1965 when SZ attains suspiciously negative values (Fig. 10c).

e. Autumn

Ten circulation modes are identified in autumn, all of them being identified also in BL. The strongest modes are SZ, PNA, and EU1. The modes exhibit a relatively high resemblance between reanalyses (Fig. 11) except the two modes featuring a circumglobal belt in the subtropics, SZ and EA. Autumn is the only season when differences between surface-input and full-input reanalyses do not stand out.

SZ differs between reanalyses over vast parts of Eurasia and central and southern Atlantic (Fig. S7), which may imply different autocorrelation structures in reanalyses predominantly over the low latitudes. Weaker circulation

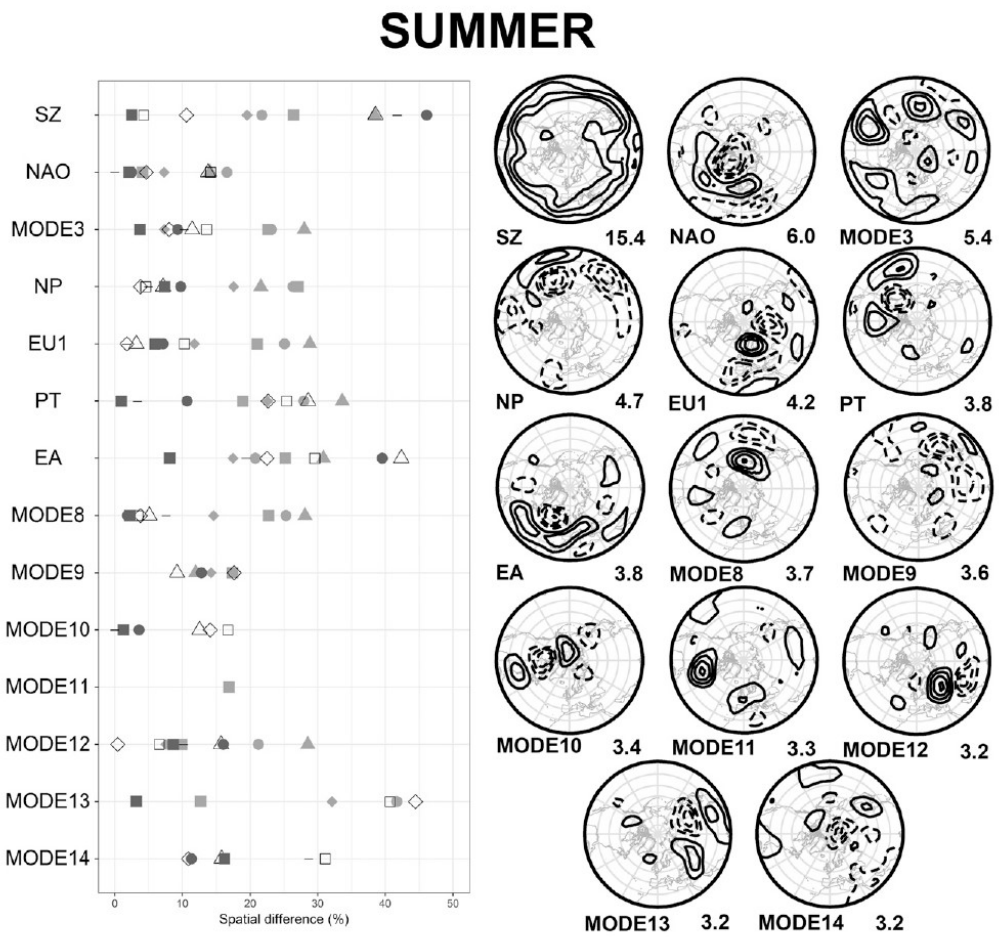

FIG. 9. As in the center and right top part of Fig. 3, but for summer, with the exception of mode 11, which is taken from ERA-20C because it is not identified in ERA-40. For the explanation of symbols in the left graph, see the bottom part of Fig. 3.

variability there may also contribute to this difference. Moreover, SZ does not appear in ERA-40, even when fewer or more components are rotated. The circulation mode in ERA-40 closest to SZ is displayed in Fig. S7; however, its similarity with SZ is fairly low.

The representation of EA in JRA-55 and ERA-40 is different from the other reanalyses, which strongly contributes to the overall higher dissimilarity of the two reanalyses from the rest. It is, however, largely an artifact of PCA. EA in ERA-40 is sensitive to the number of rotated components as it exhibits a larger correspondence with other reanalyses if 11 instead of 10 principal components are rotated (Fig. 12), mainly because the circumglobal subtropical belt is detached from it. Nonetheless, a better agreement of most other circulation modes is achieved when 10 principal components are rotated, which is demonstrated by mode 6 and EU2 in Fig. 12: centers of both modes are shifted for 11 components, changing their appearance in comparison to the 10-component solution and worsening their correspondence with other reanalyses. This is the reason why rotation of 10 components is preferred, even though the spatial representation of EA has lower resemblance with other reanalyses then. In JRA-55, PCA cannot reveal the structure of EA similar to other reanalyses, even after various numbers of components are rotated. Nevertheless, the autocorrelation maps for centers of EA in JRA-55 resemble other reanalyses (Fig. S8), which suggests

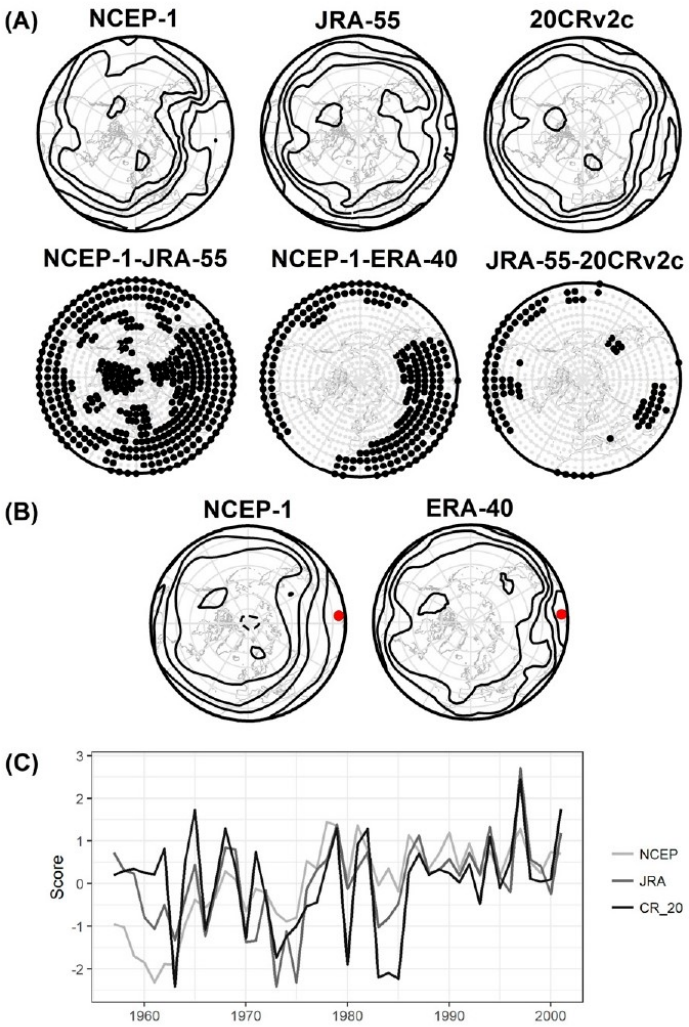

FIG. 10. (a) SZ in summer in NCEP-1, JRA-55, and 20CRv2c and positions of the grid points with statistically significant differences between loadings. (b) Autocorrelation maps for the most positive loading from ERA-40 in NCEP-1 and ERA-40 (red dots). (c) Time series of scores of SZ in summer in NCEP-1, JRA-55, and 20CRv2c.

that a different appearance of EA in JRA-55 is again an artifact of the analysis method.

4. Discussion

The previous section suggests that there are two major reasons for differences in how individual modes are identified in reanalyses: (i) real differences (biases) in correlation structures and (ii) reasons inherent to PCA, in particular the sensitivity of modes to the number of principal components rotated. Higher sensitivity to rotation appears in autumn when the spatial structure of a few circulation modes changes considerably with different numbers of rotated components. However, here we attempt to attribute the real differences in modes, which are not artifacts of the analysis method, to deficiencies known to exist in reanalyses.

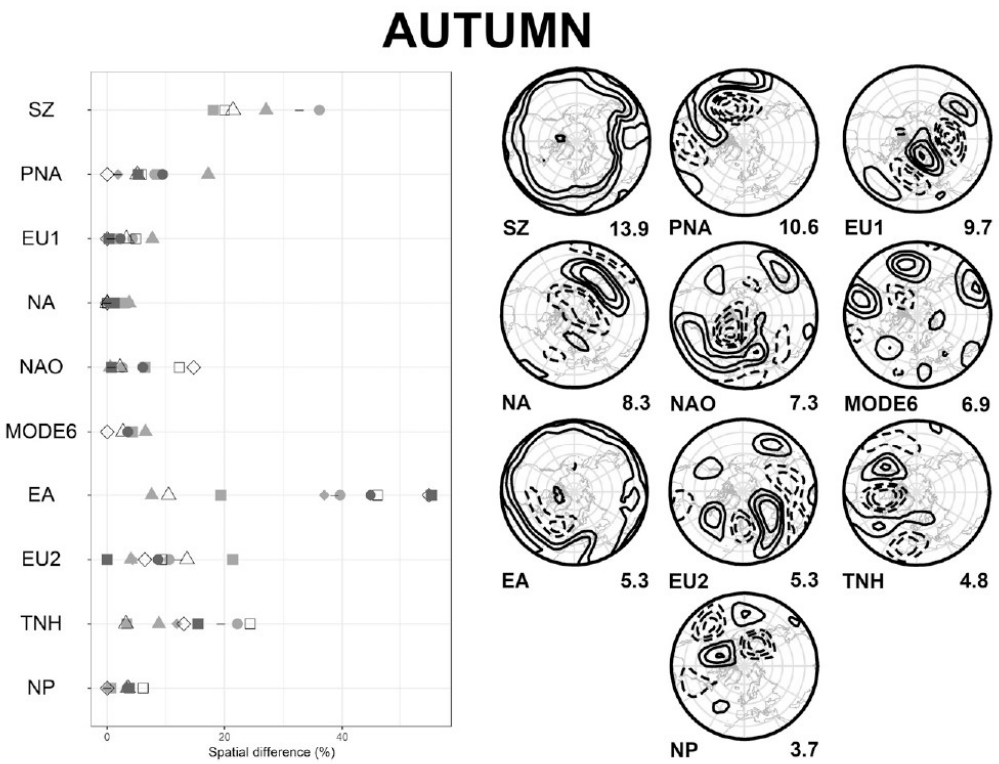

FIG. 11. As in the center and right top part of Fig. 3, but for autumn, with the exception of SZ, which is taken from ERA-20C because it is not identified in ERA-40. For the explanation of symbols in the left graph, see the bottom part of Fig. 3.

a. 20CRv2c

Previous studies (van den Besselaar et al. 2011; Lindsay et al. 2014; Stryhal and Huth 2017; Rohrer et al. 2018) reported positive sea level pressure biases in 20CRv2(c) over Eurasia and Europe, mainly over its northeast, while larger agreement with NCEP-1 was found over oceans (Wang et al. 2013). However, we do not reveal any substantial differences in circulation modes over Europe. Our results localize possible biases in 500-hPa heights to southern half of Asia where both PCA and autocorrelation maps (Figs. 4 and 7) point to different shapes of, for example, EU1 in winter, WPO in spring, and SZ in autumn, summer, and spring in 20CRv2c. In spring, the peculiarities of 20CRv2c give rise to the mode centered over southern Asia that does not appear in any other reanalysis (third mode in the order of explained variance; denoted as "xxx" in Fig. S1).

Furthermore, the behavior of some circulation modes in spring (NAO and mode 6) and summer (e.g., NP, PT) in 20CRv2c suggests a different orientation of spatial autocorrelations over and near North America: 20CRv2c seems to have stronger autocorrelations across the continent, resulting, for example, in the merger of NAO with PNA in spring (Fig. 8b). This points to additional possible biases over the subtropical eastern Pacific and adjacent North America. To investigate whether these biases really occur and where exactly they are located, Pearson correlations of 500-hPa anomalies between 20CRv2c and full-input reanalyses are calculated; results are presented here for ERA-40 only (Fig. 13, left), which are very similar to all other reanalyses. Correlations tend to be lower in spring and summer and in low latitudes especially over southern half of Asia, northern Africa, and the eastern Pacific. This coincides with what the spatial structure of modes suggests: discrepancies over southern and central Asia between 20CRv2c and other reanalyses appear for EU1 in winter and partly also in summer and for SZ in spring, summer, and autumn; moreover, the third spring mode not appearing in any other reanalysis is located there. The low correlations over the subtropical eastern Pacific and southwestern North America correspond to a different behavior of NAO and mode 6 in spring and several Pacific circulation modes in summer.

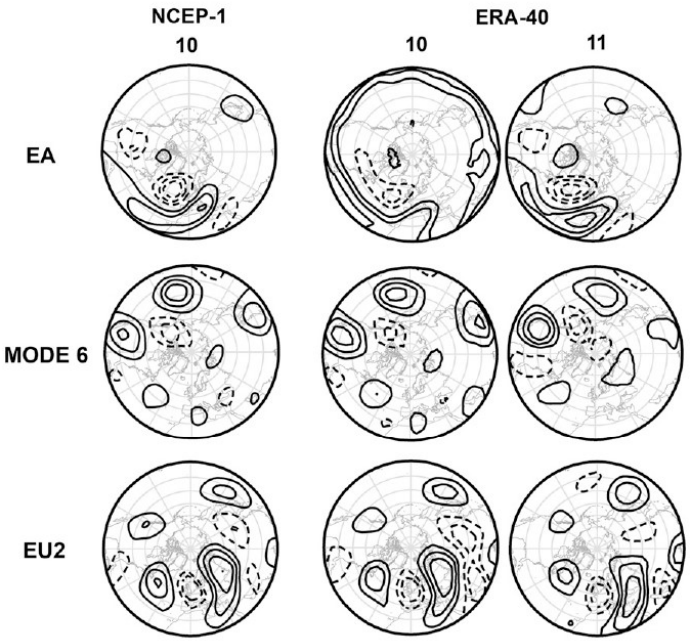

FIG. 12. EA, mode 6, and EU2 in autumn in ERA-40 and NCEP-1 for 10 and 11 rotated components.

The number of assimilated surface pressure observations in 20CRv2c over ''problematic'' areas has increased since the 1970s (Cram et al. 2015). Hence, we calculated differences in correlations between ERA-40 and 20CRv2c separately for periods 1957–79 and 1980–2002 to examine whether the reported biases predominantly result from the shortage of assimilated data in the former period in 20CRv2c. The larger agreement of both reanalyses in the later period (Fig. 13, right) seems to reflect the increased amount of surface data in 20CRv2c, although one can find small areas with worse correspondence (e.g., over low latitudes of the Pacific Ocean in summer). Furthermore, we visualize time series of anomalies in 20CRv2c and ERA-40 at three grid points with low correlations (Fig. 14) located in southern Asia and Pacific. All of them share a similar feature: differences between the time series tend to be larger prior to 1980. After 1980, the convergence of both reanalyses is confirmed by an increase in correlations. Thus, we demonstrate that a peculiar behavior of several modes over southern half of Asia and in the eastern Pacific/southwestern North America domain in 20CRv2c is real, due to a different behavior of the 500-hPa height data, in particular before 1980.

The location of disagreement between 20CRv2c and other reanalyses in data-sparse regions suggests that insufficient assimilated data (only surface pressure, sea ice distribution, and sea surface temperature), and hence a little constraint of the reanalysis output by observations, are the likely cause of the discrepancies that we identified. This is supported by the fact that the correspondence of 20CRv2c with other reanalyses (as illustrated in Fig. 13 for ERA-40) has increased since the 1970s, which coincides with the period when the number of assimilated surface pressure (Cram et al. 2015) and also sea surface temperature observations (Woodruff et al. 2011) has increased.

b. *ERA-20C*

Interestingly, the other century-long reanalysis, ERA-20C, exhibits a better congruity with the other reanalyses than 20CRv2c, despite also assimilating surface observed data only. In fact, there is just one occasion when and where modes in ERA-20C differ from the rest of reanalyses: it is in spring over the northern North Pacific and eastern Asia where northern centers of WPO and NP are weaker in ERA-20C (Fig. 7 and Fig. S2). The different structure of WPO is also confirmed in autocorrelation maps (Fig. 7b); therefore, this discrepancy results from the reanalysis itself and is not a statistical artifact of PCA. An overall better correspondence of ERA-20C with full-input reanalyses (also Stryhal and Huth 2017) might be caused by assimilation of surface

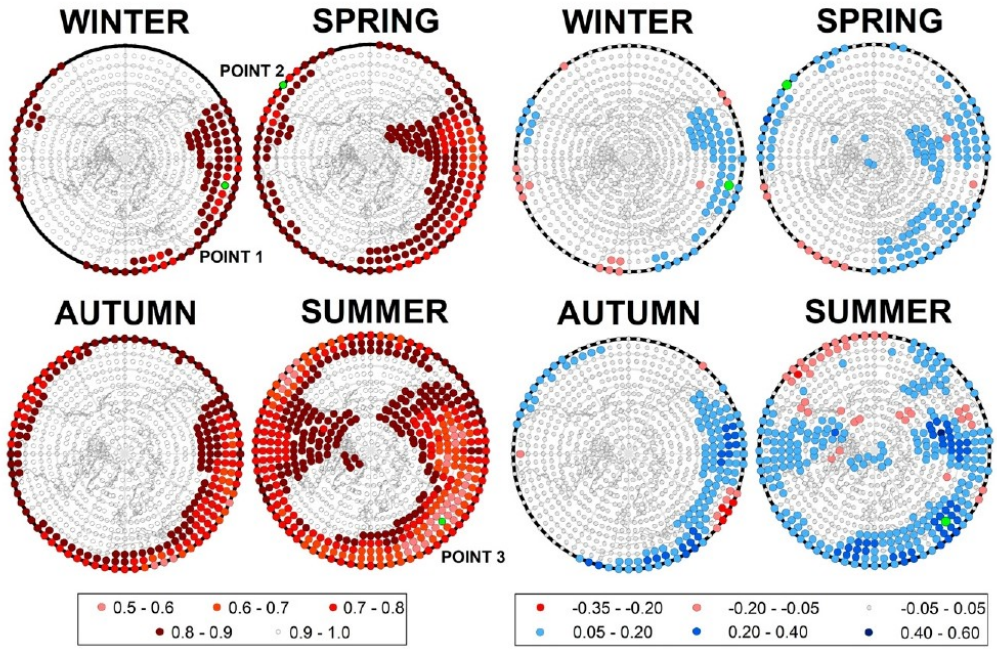

FIG. 13. (left) Pearson correlations of long-term (1957–2002) monthly 500-hPa anomalies between 20CRv2c and ERA-40 and (right) differences in the correlations between 20CRv2c and ERA-40 before and after 1980. Green dots indicate points for which time series are displayed in Fig. 14.

winds, which are lacking in 20CRv2c (Befort et al. 2016), or simply by another model used.

c. Full-input reanalyses

The mutual agreement of full-input reanalyses is fairly good, mainly between ERA-40 and JRA-55, although some spatial differences are detected. The most prominent is a different representation of SZ in summer in NCEP-1 (Fig. 10), which responds to errors detected in 500-hPa heights over Asia and partly northern Africa (Zhao and Fu 2009). These errors, which manifest also in the spatial structure of the EA mode (Fig. S9), result in an artificial increasing trend in 500-hPa heights prior to mid-1970s, accompanied by a sudden increase in sea level pressure in mid-1960s and early 1970s over eastern Asia (Inoue and Matsumoto 2004). The errors are manifestations of incorrect encoding of sea level pressure between 1948 and 1967 (Kistler et al. 2001); they are also reported by Wu et al. (2005), Yang et al. (2002), and Greatbatch and Rong (2006), the latter extending the area affected by the errors toward northern Africa.

d. Circulation modes before and after 1979

One would expect a better agreement of reanalyses after 1979 when satellite observations were introduced into full-input reanalyses, and the amount of pressure and sea surface temperature observations increased in surface-input reanalyses (section 4a). Hence, spatial differences between reanalyses are also computed separately for periods 1957–78 and 1979–2002. EU1 is not detected in the earlier period in any reanalysis and we do not find any support for its absence before 1979 in literature; therefore it is likely that its absence is a manifestation of sampling uncertainty due to a rather short analysis period.

Figure 15 clearly demonstrates a better correspondence of the majority of circulation modes in the later period, mainly between full-input reanalyses, in which the inclusion of satellite data results in their improved accuracy. Nevertheless, spatial structures of Eurasian modes NA and EU1 are different in surface-input reanalyses in the later period. The most likely explanation is again the uncertainty due to a short analysis period, although the biases in 20CRv2c over Eurasia may still affect circulation modes despite the higher congruence with ERA-40 after 1980 (section 4a).

In the period after 1979, several more recent reanalyses are available (CFSR; Saha et al. 2010; MERRA-2; Gelaro et al. 2017; ERA5; Hersbach et al. 2020). They assimilate larger amounts of data, and also additional data types (e.g., aerosol observations); therefore, a better agreement among them in representation of the modes may be expected. The

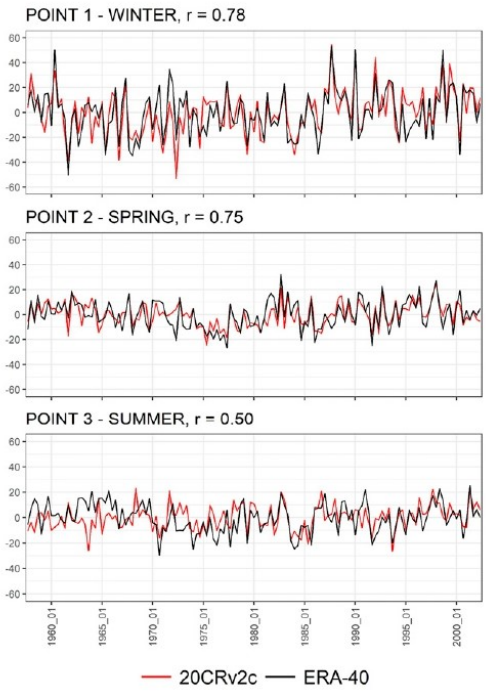

FIG. 14. Time series of 500-hPa anomalies in 20CRv2c and ERA-40 at three points denoted by green dots in the left panel of Fig. 13; r is the Pearson correlation coefficient.

comparison of circulation modes with those additional reanalyses may be a subject of a future research but only speculatively, we would expect large congruity with full-input reanalyses since all the reanalyses assimilate free atmosphere and satellite data.

5. Conclusions

Atmospheric reanalyses are often considered as almost perfect representations of a three-dimensional state of the atmosphere. However, they differ one from another in how they describe important atmospheric features, phenomena, and processes. This applies to atmospheric circulation as well. Here we analyze modes of atmospheric low-frequency variability, which have not been compared between reanalyses so far.

Circulation modes in the Northern Hemisphere extratropics are identified by rotated PCA of 500-hPa heights in individual seasons. A careful analysis is needed to distinguish real differences in the modes between reanalyses, reflecting differences in underlying autocorrelation structures, from differences caused by a particular application of PCA, most notably due to the sensitivity to the number of principal components rotated. The spatial structure of the modes appears, fortunately, to be fairly little sensitive to the particular choice of the number of components. In a few cases, however, the rotation of fewer or more principal components leads to a noticeable change in the spatial representation of the modes. A comparison of the spatial representation of the modes with correlation maps and a comparison of modes obtained for various numbers of components rotated are tools sufficient for distinguishing real differences in the modes between reanalyses from differences stemming from the PCA method.

We quantify the differences between reanalyses by the normalized percentage of grid points (which approximates the percentage of area) where component loadings significantly differ between reanalyses. The differences concentrate to a few modes in each season. The comparison shows that differences between surface-input reanalyses assimilating only surface observations (20CRv2c and ERA-20C) and full-input reanalyses (ERA-40, JRA-55, and NCEP-1) are mostly higher than differences within both groups. The only exception is autumn when the differences between reanalyses are more due to the PCA methodology (i.e., the sensitivity to the number of rotated components) than to their deficiencies. The reanalysis differing most from the remaining ones throughout the year is 20CRv2c.

Differences in spatial structure of circulation modes may point to biases in reanalyses. This is predominantly the case of 20CRv2c, in which biases are located mainly over southern half of Asia and subtropical eastern Pacific. These biases are larger prior to 1980, while getting substantially smaller afterward, which reflects mainly increases in the number of assimilated pressure observations there. On the contrary, the other surface-input reanalysis, ERA-20C, exhibits only minor differences from other reanalyses and has a higher resemblance with full-input reanalyses, all of which we consider, due to much more data assimilated, as more reliable.

Although differences between reanalyses are minor for most of the modes, the representation of some modes in some seasons is considerably sensitive to the choice of a reanalysis. Therefore, the use of a single reanalysis in climatological studies involving modes, such as studies of effects of atmospheric circulation on surface climate conditions and interpretation of climate model outputs (whether their validation or studies of future climate conditions), may be misleading. The use of multiple reanalyses is highly recommended. If there is a necessity for using a reanalysis covering the entire twentieth century, ERA-20C rather than 20CRv2c is recommended to be the first choice since it appears to be in a closer agreement with standard, full-input reanalyses. Nonetheless, full-input reanalyses should be preferred whenever it is possible.

Acknowledgments. This research was supported by the Czech Science Foundation, project 17-07043S. Martin Hynčica was also supported by the Grant Agency of the Charles University, student project 426216. We further acknowledge the following organizations for providing the reanalysis data: NOAA/OAR/ESRL PSD, Boulder, Colorado, United States for NCEP-1 and

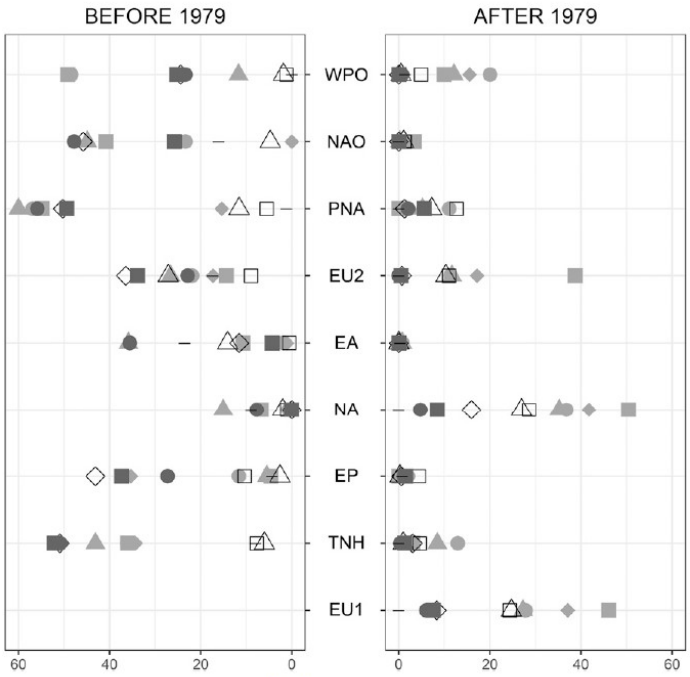

FIG. 15. As in the center top panel in Fig. 3, but for (left) 1957–78 and (right) 1979–2002. EU1 is not detected in the first period.

20CRv2c; ECMWF, Reading, United Kingdom for ERA-40 and ERA-20C; and JMA, Tokyo, Japan for JRA-55.

REFERENCES

Araneo, D. C., and R. H. Compagnucci, 2004: Removal of systematic biases in S-mode principal components arising from unequal grid spacing. *J. Climate*, **17**, 394–400, https://doi.org/10.1175/1520-0442(2004)017<0394:ROSBIS>2.0.CO;2.

Barnston, A. G., and R. E. Livezey, 1987: Classification, seasonality and persistence of low-frequency atmospheric circulation patterns. *Mon. Wea. Rev.*, **115**, 1083–1126, https://doi.org/10.1175/1520-0493(1987)115<1083:CSAPOL>2.0.CO;2.

Befort, D. J., S. Wild, T. Kruschke, U. Ulbrich, and G. C. Leckebusch, 2016: Different long-term trends of extra-tropical cyclones and windstorms in ERA-20C and NOAA-20CR reanalyses. *Atmos. Sci. Lett.*, **17**, 586–595, https://doi.org/10.1002/asl.694.

Belleflamme, A., X. Fettweis, C. Lang, and M. Erpicum, 2013: Current and future atmospheric circulation at 500 hPa over Greenland simulated by the CMIP3 and CMIP5 global models. *Climate Dyn.*, **41**, 2061–2080, https://doi.org/10.1007/s00382-012-1538-2.

Bromwich, D. H., R. L. Fogt, K. I. Hodges, and J. E. Walsh, 2007: A tropospheric assessment of the ERA-40, NCEP, and JRA-25 global reanalyses in the polar regions. *J. Geophys. Res.*, **112**, D10111, https://doi.org/10.1029/2006JD007859.

Butler, A. H., J. P. Sjoberg, D. J. Seidel, and K. H. Rosenlof, 2017: A sudden stratospheric warming compendium. *Earth Syst. Sci. Data*, **9**, 63–76, https://doi.org/10.5194/essd-9-63-2017.

Chang, E. K., and A. M. Yau, 2016: Northern Hemisphere winter storm track trends since 1959 derived from multiple reanalysis datasets. *Climate Dyn.*, **47**, 1435–1454, https://doi.org/10.1007/s00382-015-2911-8.

Christiansen, B., 2005: The shortcomings of nonlinear principal component analysis in identifying circulation regimes. *J. Climate*, **18**, 4814–4823, https://doi.org/10.1175/JCLI3569.1.

Compagnucci, R. H., and M. B. Richman, 2008: Can principal component analysis provide atmospheric circulation or teleconnection patterns? *Int. J. Climatol.*, **28**, 703–726, https://doi.org/10.1002/joc.1574.

Compo, G. P., and Coauthors, 2011: The Twentieth Century Reanalysis Project. *Quart. J. Roy. Meteor. Soc.*, **137**, 1–28, https://doi.org/10.1002/qj.776.

Cram, T. A., and Coauthors, 2015: The International Surface Pressure Databank version 2. *Geosci. Data J.*, **2**, 31–46, https://doi.org/10.1002/gdj3.25.

Dee, D. P., and S. M. Uppala, 2009: Variational bias correction of satellite radiance data in the ERA-Interim reanalysis. *Quart. J. Roy. Meteor. Soc.*, **135**, 1830–1841, https://doi.org/10.1002/qj.493.

——, and Coauthors, 2011: The ERA-Interim reanalysis: Configuration and performance of the data assimilation system. *Quart. J. Roy. Meteor. Soc.*, **137**, 553–597, https://doi.org/10.1002/qj.828.

Folland, C. K., J. Knight, H. W. Linderholm, D. Fereday, S. Ineson, and J. W. Hurrell, 2009: The summer North Atlantic

Oscillation: Past, present, future. *J. Climate*, **22**, 1082–1103, https://doi.org/10.1175/2008JCLI2459.1.

Fujiwara, M., T. Hibino, S. K. Mehta, L. Gray, D. Mitchell, and J. Anstey, 2015: Global temperature response to the major volcanic eruptions in multiple reanalysis data sets. *Atmos. Chem. Phys.*, **15**, 13 507–13 518, https://doi.org/10.5194/acp-15-13507-2015.

——, and Coauthors, 2017: Introduction to the SPARC Reanalysis Intercomparison Project (S-RIP) and overview of the reanalysis systems. *Atmos. Chem. Phys.*, **17**, 1417–1452, https://doi.org/10.5194/acp-17-1417-2017.

Gelaro, R., and Coauthors, 2017: The Modern-Era Retrospective Analysis for Research and Applications, version 2 (MERRA-2). *J. Climate*, **30**, 5419–5454, https://doi.org/10.1175/JCLI-D-16-0758.1.

Greatbatch, R. J., and P. P. Rong, 2006: Discrepancies between different Northern Hemisphere summer atmospheric data products. *J. Climate*, **19**, 1261–1273, https://doi.org/10.1175/JCLI3643.1.

Harnik, N., and E. K. Chang, 2004: The effects of variations in jet width on the growth of baroclinic waves: Implications for midwinter Pacific storm track variability. *J. Atmos. Sci.*, **61**, 23–40, https://doi.org/10.1175/1520-0469(2004)061<0023:TEOVIJ>2.0.CO;2.

Hersbach, H., and Coauthors, 2020: The ERA5 global reanalysis. *Quart. J. Roy. Meteor. Soc.*, **146**, 1999–2049, https://doi.org/10.1002/qj.3803.

Hodges, K. I., R. W. Lee, and L. Bengtsson, 2011: A comparison of extratropical cyclones in recent reanalyses ERA-Interim, NASA MERRA, NCEP CFSR, and JRA-25. *J. Climate*, **24**, 4888–4906, https://doi.org/10.1175/2011JCLI4097.1.

Horel, J. D., 1981: A rotated principal component analysis of the interannual variability of the Northern Hemisphere 500 mb height field. *Mon. Wea. Rev.*, **109**, 2080–2092, https://doi.org/10.1175/1520-0493(1981)109<2080:ARPCAO>2.0.CO;2.

Hsieh, W. W., 2004: Nonlinear multivariate and time series analysis by neural network methods. *Rev. Geophys.*, **42**, RG1003, https://doi.org/10.1029/2002RG000112.

Huth, R., 2006: The effect of various methodological options on the detection of leading modes of sea level pressure variability. *Tellus*, **58A**, 121–130, https://doi.org/10.1111/j.1600-0870.2006.00158.x.

——, L. Pokorná, J. Bochníček, and P. Hejda, 2006: Solar cycle effects on modes of low-frequency circulation variability. *J. Geophys. Res.*, **111**, D22107, https://doi.org/10.1029/2005JD006813.

Inoue, T., and J. Matsumoto, 2004: A comparison of summer sea level pressure over east Eurasia between NCEP-NCAR reanalysis and ERA-40 for the period 1960–99. *J. Meteor. Soc. Japan*, **82**, 951–958, https://doi.org/10.2151/jmsj.2004.951.

Kalnay, E., and Coauthors, 1996: The NCEP/NCAR 40-Year Reanalysis Project. *Bull. Amer. Meteor. Soc.*, **77**, 437–471, https://doi.org/10.1175/1520-0477(1996)077<0437:TNYRP>2.0.CO;2.

Kistler, R., and Coauthors, 2001: The NCEP–NCAR 50-Year Reanalysis: Monthly means CD-ROM and documentation. *Bull. Amer. Meteor. Soc.*, **82**, 247–268, https://doi.org/10.1175/1520-0477(2001)082<0247:TNNYRM>2.3.CO;2.

Kobayashi, S., and Coauthors, 2015: The JRA-55 reanalysis: General specifications and basic characteristics. *J. Meteor. Soc. Japan*, **93**, 5–48, https://doi.org/10.2151/jmsj.2015-001.

Kohyama, T., and D. L. Hartmann, 2016: Antarctic sea ice response to weather and climate modes of variability. *J. Climate*, **29**, 721–741, https://doi.org/10.1175/JCLI-D-15-0301.1.

Lian, T., and D. Chen, 2012: An evaluation of rotated EOF analysis and its application to tropical Pacific SST variability. *J. Climate*, **25**, 5361–5373, https://doi.org/10.1175/JCLI-D-11-00663.1.

Lin, Z., 2014: Intercomparison of the impacts of four summer teleconnections over Eurasia on East Asian rainfall. *Adv. Atmos. Sci.*, **31**, 1366–1376, https://doi.org/10.1007/s00376-014-3171-y.

Linderholm, H. W., T. Ou, J. H. Jeong, C. K. Folland, D. Gong, H. Liu, Y. Liu, and D. Chen, 2011: Interannual teleconnections between the summer North Atlantic Oscillation and the East Asian summer monsoon. *J. Geophys. Res.*, **116**, D13107, https://doi.org/10.1029/2010JD015235.

Lindsay, R., M. Wensnahan, A. Schweiger, and J. Zhang, 2014: Evaluation of seven different atmospheric reanalysis products in the Arctic. *J. Climate*, **27**, 2588–2606, https://doi.org/10.1175/JCLI-D-13-00014.1.

Long, C. S., M. Fujiwara, S. Davis, D. M. Mitchell, and C. J. Wright, 2017: Climatology and interannual variability of dynamic variables in multiple reanalyses evaluated by the SPARC Reanalysis Intercomparison Project (S-RIP). *Atmos. Chem. Phys.*, **17**, 14 593–14 629, https://doi.org/10.5194/acp-17-14593-2017.

Monahan, A. H., 2000: Nonlinear principal component analysis by neural networks: Theory and application to the Lorenz system. *J. Climate*, **13**, 821–835, https://doi.org/10.1175/1520-0442(2000)013<0821:NPCABN>2.0.CO;2.

O'Lenic, E. A., and R. E. Livezey, 1988: Practical considerations in the use of rotated principal component analysis (RPCA): In diagnostic studies of upper-air height fields. *Mon. Wea. Rev.*, **116**, 1682–1689, https://doi.org/10.1175/1520-0493(1988)116<1682:PCITUO>2.0.CO;2.

Pepler, A. S., A. Di Luca, and J. P. Evans, 2018: Independently assessing the representation of midlatitude cyclones in high-resolution reanalyses using satellite observed winds. *Int. J. Climatol.*, **38**, 1314–1327, https://doi.org/10.1002/joc.5245.

Pingree-Shippee, K. A., F. W. Zwiers, and D. E. Atkinson, 2018: Representation of mid-latitude North American coastal storm activity by six global reanalyses. *Int. J. Climatol.*, **38**, 1041–1059, https://doi.org/10.1002/joc.5235.

Pišoft, P., E. Holtanová, P. Huszár, J. Kalvová, J. Mikšovský, A. Raidl, K. Zemánková, and M. Žák, 2013: Manifestation of reanalyzed QBO and SSC signals. *Theor. Appl. Climatol.*, **112**, 637–646, https://doi.org/10.1007/s00704-012-0752-5.

Pokorná, L., and R. Huth, 2015: Climate impacts of the NAO are sensitive to how the NAO is defined. *Theor. Appl. Climatol.*, **119**, 639–652, https://doi.org/10.1007/s00704-014-1116-0.

Poli, P., and Coauthors, 2016: ERA-20C: An atmospheric reanalysis of the twentieth century. *J. Climate*, **29**, 4083–4097, https://doi.org/10.1175/JCLI-D-15-0556.1.

Richman, M. B., 1986: Rotation of principal components. *J. Climatol.*, **6**, 293–335, https://doi.org/10.1002/joc.3370060305.

Rogers, J. C., 1981: Spatial variability of seasonal sea level pressure and 500 mb height anomalies. *Mon. Wea. Rev.*, **109**, 2093–2106, https://doi.org/10.1175/1520-0493(1981)109<2093:SVOSSL>2.0.CO;2.

Rohrer, M., S. Brönnimann, O. Martius, C. C. Raible, M. Wild, and G. P. Compo, 2018: Representation of extratropical cyclones, blocking anticyclones, and Alpine circulation types in multiple reanalyses and model simulations. *J. Climate*, **31**, 3009–3031, https://doi.org/10.1175/JCLI-D-17-0350.1.

Saha, S., and Coauthors, 2010: The NCEP Climate Forecast System Reanalysis. *Bull. Amer. Meteor. Soc.*, **91**, 1015–1058, https://doi.org/10.1175/2010BAMS3001.1.

Serrano, A., J. A. García, V. L. Mateos, M. L. Cancillo, and J. Garrido, 1999: Monthly modes of variation of precipitation over the Iberian Peninsula. *J. Climate*, **12**, 2894–2919, https://doi.org/10.1175/1520-0442(1999)012<2894:MMOVOP>2.0.CO;2.

Soulard, N., and H. Lin, 2017: The spring relationship between the Pacific–North American pattern and the North Atlantic Oscillation. *Climate Dyn.*, **48**, 619–629, https://doi.org/10.1007/s00382-016-3098-3.

Spensberger, C., M. J. Reeder, T. Spengler, and M. Patterson, 2020: The connection between the southern annular mode and a feature-based perspective on Southern Hemisphere midlatitude winter variability. *J. Climate*, **33**, 115–129, https://doi.org/10.1175/JCLI-D-19-0224.1.

Stryhal, J., and R. Huth, 2017: Classifications of winter Euro-Atlantic circulation patterns: An intercomparison of five atmospheric reanalyses. *J. Climate*, **30**, 7847–7861, https://doi.org/10.1175/JCLI-D-17-0059.1.

Sturaro, G., 2003: Patterns of variability in the satellite Microwave Sounding Unit temperature record: Comparison with surface and reanalysis data. *Int. J. Climatol.*, **23**, 1799–1820, https://doi.org/10.1002/joc.975.

Sun, J., and H. Wang, 2012: Changes of the connection between the summer North Atlantic Oscillation and the East Asian summer rainfall. *J. Geophys. Res.*, **117**, D08110, https://doi.org/10.1029/2012JD017482.

Teng, Q., J. C. Fyfe, and A. H. Monahan, 2007: Northern Hemisphere circulation regimes: Observed, simulated and predicted. *Climate Dyn.*, **28**, 867–879, https://doi.org/10.1007/s00382-006-0220-y.

Thompson, D. W. J., and J. M. Wallace, 2000: Annular modes in the extratropical circulation. Part I: Month-to-month variability. *J. Climate*, **13**, 1000–1016, https://doi.org/10.1175/1520-0442(2000)013<1000:AMITEC>2.0.CO;2.

Tilinina, N., S. K. Gulev, I. Rudeva, and P. Koltermann, 2013: Comparing cyclone life cycle characteristics and their interannual variability in different reanalyses. *J. Climate*, **26**, 6419–6438, https://doi.org/10.1175/JCLI-D-12-00777.1.

Trigo, I. F., 2006: Climatology and interannual variability of storm-tracks in the Euro-Atlantic sector: A comparison between ERA-40 and NCEP/NCAR reanalyses. *Climate Dyn.*, **26**, 127–143, https://doi.org/10.1007/s00382-005-0065-9.

Ulbrich, U., G. C. Leckebusch, and J. G. Pinto, 2009: Extra-tropical cyclones in the present and future climate: A review. *Theor. Appl. Climatol.*, **96**, 117–131, https://doi.org/10.1007/s00704-008-0083-8.

Uppala, S. M., and Coauthors, 2005: The ERA-40 reanalysis. *Quart. J. Roy. Meteor. Soc.*, **131**, 2961–3012, https://doi.org/10.1256/qj.04.176.

van den Besselaar, E. J. M., M. R. Haylock, G. van der Schrier, and A. M. G. Klein Tank, 2011: A European daily high-resolution observational gridded data set of sea level pressure. *J. Geophys. Res.*, **116**, D11110, https://doi.org/10.1029/2010JD015468.

Wallace, J. M., and D. S. Gutzler, 1981: Teleconnections in the geopotential height field during the Northern Hemisphere winter. *Mon. Wea. Rev.*, **109**, 784–812, https://doi.org/10.1175/1520-0493(1981)109<0784:TITGHF>2.0.CO;2.

Wang, X. L., V. R. Swail, and F. W. Zwiers, 2006: Climatology and changes of extratropical cyclone activity: Comparison of ERA-40 with NCEP–NCAR reanalysis for 1958–2001. *J. Climate*, **19**, 3145–3166, https://doi.org/10.1175/JCLI3781.1.

——, Y. Feng, G. P. Compo, V. R. Swail, F. W. Zwiers, R. J. Allan, and P. D. Sardeshmukh, 2013: Trends and low frequency variability of extra-tropical cyclone activity in the ensemble of twentieth century reanalysis. *Climate Dyn.*, **40**, 2775–2800, https://doi.org/10.1007/s00382-012-1450-9.

——, ——, R. Chan, and V. Isaac, 2016: Inter-comparison of extra-tropical cyclone activity in nine reanalysis datasets. *Atmos. Res.*, **181**, 133–153, https://doi.org/10.1016/j.atmosres.2016.06.010.

Woodruff, S. D., and Coauthors, 2011: ICOADS Release 2.5: Extensions and enhancements to the surface marine meteorological archive. *Int. J. Climatol.*, **31**, 951–967, https://doi.org/10.1002/joc.2103.

Woollings, T., and Coauthors, 2018: Blocking and its response to climate change. *Curr. Climate Change Rep.*, **4**, 287–300, https://doi.org/10.1007/s40641-018-0108-z.

Wu, R., J. L. Kinter Iii, and B. P. Kirtman, 2005: Discrepancy of interdecadal changes in the Asian region among the NCEP–NCAR reanalysis, objective analyses, and observations. *J. Climate*, **18**, 3048–3067, https://doi.org/10.1175/JCLI3465.1.

Yang, S., K. M. Lau, and K. M. Kim, 2002: Variations of the East Asian jet stream and Asian–Pacific–American winter climate anomalies. *J. Climate*, **15**, 306–325, https://doi.org/10.1175/1520-0442(2002)015<0306:VOTEAJ>2.0.CO;2.

Zahn, M., M. Akperov, A. Rinke, F. Feser, and I. I. Mokhov, 2018: Trends of cyclone characteristics in the Arctic and their patterns from different reanalysis data. *J. Geophys. Res. Atmos.*, **123**, 2737–2751, https://doi.org/10.1002/2017JD027439.

Zhao, T., and C. Fu, 2009: Intercomparison of the summertime subtropical high from the ERA-40 and NCEP/NCAR reanalysis over east Eurasia and the western North Pacific. *Adv. Atmos. Sci.*, **26**, 119–131, https://doi.org/10.1007/s00376-009-0119-8.

2.2 Comparing relationships with circulation modes between reanalyses

Paper II: Hynčica, M., Huth, R. (2021). Temporal evolution of relationships between temperature and circulation modes in five reanalyses. *International Journal of Climatology*, 42, 4391-4404.

Received: 1 September 2021 | Revised: 22 November 2021 | Accepted: 29 November 2021
DOI: 10.1002/joc.7474

RESEARCH ARTICLE

International Journal of Climatology RMetS

Temporal evolution of relationships between temperature and circulation modes in five reanalyses

Martin Hynčica[1,2] | **Radan Huth**[1,3]

[1]Department of Physical Geography and Geoecology, Faculty of Science, Charles University, Prague, Czechia
[2]Czech Hydrometeorological Institute, Ústí nad Labem, Czechia
[3]Institute of Atmospheric Physics, Czech Academy of Sciences, Prague, Czechia

Correspondence
Martin Hynčica, Department of Physical Geography and Geoecology, Faculty of Science, Charles University, Albertov 6, 128 43 Prague, Czechia.
Email: martin.hyncica@natur.cuni.cz

Funding information
Akademie Věd České Republiky, Grant/Award Number: 17-07043S; Grantová Agentura, Univerzita Karlova, Grant/Award Number: 426216; Charles University; Czech Science Foundation, Grant/Award Number: 07043S

Abstract

Temporal evolution of relationships between surface temperature and modes of low-frequency circulation variability is compared between five reanalyses (20CRv3, 20CRv2c, ERA-20C, JRA-55, and NCEP-1) in winter from 1958 to 2010 over the northern Extratropics. The relationships are evaluated using 15-year running correlations between temperature anomalies (from the CRU TS v. 4.03 data set) and the intensity of circulation modes (detected in 500 hPa heights by rotated principal component analysis). The analysis, utilizing mean absolute differences between time series of running correlations, points to the large agreement between ERA-20C, JRA-55, and NCEP-1. Circulation modes in those reanalyses are highly similar, which in turn lead to the agreement in temporal development of correlations. In contrast, relationships of some circulation modes with temperature in 20CRv3 and 20CRv2c differ due to differences in the position, strength, and shape of the action centres. This concerns circulation modes located over Eurasia and the Atlantic, mainly North Atlantic Oscillation and Eurasian mode type 1 (EU1). Composite maps, calculated for all running periods, indicate dissimilar temporal evolution of action centres in both 20CR reanalyses. Increased differences in correlations occur mainly during periods when the position and strength of action centres diverge the most. Relationships of circulation modes located over North America and the Pacific with temperature share large resemblance between all reanalyses, including those from the 20CR family. Differences appear to be smaller in 20CRv3 compared to the preceding version, 20CRv2(c), suggesting that the development of the 20CR reanalysis has succeeded in correcting and diminishing biases.

KEYWORDS
circulation modes, reanalyses, running correlations, teleconnections

1 | INTRODUCTION

Modes of atmospheric circulation variability (also called "teleconnections" in literature and referred to as "circulation modes" or only "modes" here for brevity) are composed of typically two or more action centres, between which sea-level pressure, geopotential heights, or other quantities describing atmospheric circulation are highly correlated (e.g., Barnston and Livezey, 1987). Such interconnections manifest in simultaneous strengthening or weakening of action centres, an example of which is the behaviour of two main centres of the North Atlantic Oscillation (NAO), the Azores high and Icelandic low: The pressure difference between them modulates the

strength of westerlies blowing into Eurasia (e.g., Hurrell, 1995; Pokorná and Huth, 2015; Iles and Hegerl, 2017). Circulation modes affect various climate and environmental variables, such as temperature, precipitation, wind, snow cover, floods, and droughts, often far away from their action centres.

Relationships between circulation modes and climate variables (e.g., surface temperature, precipitation, wind) are not stable in time; they undergo periods of strengthening and weakening. This non-stationarity may be illustrated on the amplified impact (i.e., strengthened correlations) of NAO on temperature and precipitation over most of Eurasia roughly between 1960 and 1990 (Jung *et al.*, 2003; Peterson *et al.*, 2003; Polyakova *et al.*, 2006; Beranová and Huth, 2007; Beranová and Huth, 2008; Sun *et al.*, 2008; Vicente-Serrano and López-Moreno, 2008; Sun and Wang, 2012; Filippi *et al.*, 2014; Xu *et al.*, 2016; Zuo *et al.*, 2016). Temporal non-stationarity of the relationship between NAO and climate variables was shown to be caused by a shift of its both action centres. In most of the second half of the 20th century, the centres of NAO are located more easterly, which causes stronger relationships with surface climate elements over most of Eurasia (Jung *et al.*, 2003; Luo and Gong, 2006; Beranová and Huth, 2008; Sun *et al.*, 2008; Vicente-Serrano and López-Moreno, 2008; Sun and Wang, 2012; Filippi *et al.*, 2014). More eastward positions of the centres also give rise to an additional weaker positive centre over Central Asia, resulting in a strengthening effect of NAO in the Far East (Xu *et al.*, 2016; Zuo *et al.*, 2016).

The other dominant winter circulation mode in the Northern Hemisphere Extratropics is the Pacific/North American teleconnection pattern (PNA), the four centres of which are located over North America and eastern North Pacific (e.g., Leathers *et al.*, 1991; Franzke *et al.*, 2011). The structure of the PNA pattern changes mainly due to the eastward shift of the Aleutian low and the Canadian positive centre after 1980, which may have been invoked by changes in El Niño–Southern oscillation (He *et al.*, 2013) or by a climate shift in the late 1970s (Lee *et al.*, 2012). However, we are not aware of any study directly analysing the influence of the spatial changes of PNA on the stationarity of its relationships with climate variables. Furthermore, changes in relationships of other circulation modes in the northern Extratropics with climate variables have only been reported rarely (Krichak and Alpert, 2005; Beranová and Huth, 2008).

Circulation modes are frequently identified by principal component analysis (PCA) of geopotential heights in mid- or lower troposphere with an atmospheric reanalysis as a data source. Depending on the type of assimilated data, reanalyses can be divided into two groups (Fujiwara *et al.*, 2017). *Full-input* reanalyses assimilate all available data including surface, satellite, and radiosonde data. *Surface-input* reanalyses are based solely on surface observations such as pressure, surface winds, and sea-ice distribution. Because the surface-input reanalyses utilize only a limited amount of surface observations, they can extend farther into the past and usually span more than century-long period (20CRv3 starts in 1836). On the other hand, free atmosphere is completely calculated by the model in the surface-input reanalyses, which may bring about inhomogeneities and imperfections or even errors in the data set.

Studies comparing reanalyses indicate that the agreement among full-input reanalyses (JRA-55, NCEP-1) is generally very good, while the reanalysis most different from the others is surface-input reanalyses 20CRv2(c), in which biases were found to be located over central and southern Eurasia and northern to north-eastern Europe (Wang *et al.*, 2016; Stryhal and Huth, 2017; Rohrer *et al.*, 2018; Hynčica and Huth, 2020b). These biases affect the shape and position of some circulation modes, most strongly Eurasian mode type 1 (EU1) in winter (Hynčica and Huth, 2020b). The newly issued version of the 20CR reanalysis, 20CRv3, is not expected to suffer from these errors any longer (Slivinski *et al.*, 2019; Slivinski *et al.*, 2021). The other widely used surface-input reanalysis, ERA-20C, shares a larger congruity with full-input reanalyses (Stryhal and Huth, 2017; Hynčica and Huth, 2020b).

Although the papers mentioned above compare various climate variables between reanalyses, no study has compared temporal variations in their relationships with circulation modes yet. The goal of this paper is therefore to evaluate differences in relationships between circulation modes and temperature in five reanalyses in winter. Our aim is the comparison and identification of possible causes of differences. We do not intend to describe mechanisms causing the temporal non-stationarity of relationships with circulation modes.

2 | DATA AND METHODS

We compare relationships of circulation modes with temperature from January 1958 to December 2010 in winter over the Northern Hemisphere Extratropics (delimited by 20°N). We analyse the longest period possible with respect to the temporal coverage of all reanalyses.

The analysis is conducted for monthly mean 500 hPa geopotential height anomalies on a 5×5 regular grid in three surface-input reanalyses (ERA-20C, 20CRv2c, and 20CRv3) and two full-input reanalyses (JRA-55 and NCEP-1; for more details, see Table 1). The original resolution of 20CRv2c is 2×2; therefore, it was interpolated to the requested resolution by bicubic splines.

TABLE 1 Reanalyses used in this study

Name	Abbreviation	Temporal coverage	Horizontal grid step	Category	References
NOAA-CIRES-DOE 20th Century Reanalysis version 2c	20CRv2c	1851–2014	2 × 2	Surface-input	Compo *et al.* (2011)
NOAA-CIRES-DOE 20th Century Reanalysis version 3	20CRv3	1836–2015	1 × 1	Surface-input	Slivinski *et al.* (2019)
The ECMWF Twentieth century reanalysis	ERA-20C	1900–2010	1.25 × 1.25	Surface-input	Poli *et al.* (2016)
The Japanese 55-year Reanalysis (JRA) Project	JRA-55	1958–present	1.25 × 1.25	Full-input	Kobayashi *et al.* (2015)
The NCEP/NCAR 40-Year Reanalysis Project	NCEP-1	1948–present	2.5 × 2.5	Full-input	Kalnay *et al.* (1996)

Furthermore, the convergence of meridians towards the pole, which may bring biases into the analysis (Huth, 2006), is accounted for by forming a quasi-equal-area grid, that is, by excluding some gridpoints, so that the mean area of a gridbox is kept approximately the same at all latitudes.

Circulation modes are calculated by rotated PCA in an S-mode (spatial locations are organized in rows and time realizations in columns of the data matrix) from the correlation matrix. For each principal component (PC), PCA determines a loading (a spatial representation, i.e., correlation with the original data field) and a score (time series of the intensity of the mode). The PCs are subject to orthogonal Varimax rotation, which improves the interpretability of components; that is, loadings are then more regionalized (Barnston and Livezey, 1987; O'Lenic and Livezey, 1988; Lian and Chen, 2012). There are many options of how to determine the number of PCs to rotate (e.g., Richman, 1986); here, we employ the approach based on a scree plot. The scree plot is a graph showing the dependence of explained variance on the order of PCs, which are arranged on the *x*-axis in a descending order (O'Lenic and Livezey, 1988). There are usually drops on the scree plot; the rightmost drop typically indicates the number of components to rotate. However, the drop may not always represent the optimal value for rotation because some circulation modes might be located behind the drop and therefore would be lacking in the analysis; thus, it is sometimes better to rotate one additional component (Hynčica and Huth, 2020b). For example, the drop is localized to the 10th component in all reanalyses but 20CRv3, in which it occurs at the ninth component. Nevertheless, we prefer to keep 10 rotated components also in 20CRv3 because the additional (10th) mode is recognized in all other reanalyses.

Surface temperature data are obtained from the Climatic Research Unit gridded Time Series Dataset v 4.03 (Harris *et al.*, 2020, the CRU data set in further text) in its original 0.5 × 0.5 resolution. Monthly temperature anomaly from the long-term average is computed at each gridpoint. Since relationships with atmospheric circulation are mostly similar at stations and their nearest gridpoints in the CRU data set (Hynčica and Huth, 2020a), we use the gridded data set here because it provides data in a regularly distributed form, which is more suitable for spatial analysis.

Temporal evolution of relationships is evaluated by running correlations between all circulation modes in all reanalyses and temperature anomalies at all gridpoints. A moving 45 months (i.e., 15 winters) window (running period) with 1-month shift is employed; the value of running correlation is labelled to the central month of the window. Hence, time series of running correlations (116 values starting in 1965 and ending in 2003) between each circulation mode in five reanalyses and temperature anomaly at every gridpoint is created. Differences between running correlations for all pairs of reanalyses are quantified by the absolute value of the average difference between time series (mean absolute differences; MAD) for each circulation mode and each gridpoint in the CRU data set.

3 | GENERAL EVALUATION

Ten circulation modes explaining around 70% of total variance are identified in all reanalyses. Circulation modes in JRA-55 are displayed with their respective abbreviations in Figure 1 (circulation modes in other reanalyses are shown in Figures S1–S4). The appearance of nine circulation modes is largely similar to other hemispheric studies (Barnston and Livezey, 1987; Clinet and Martin, 1992; Huth *et al.*, 2006; Hynčica and Huth, 2020b). However, one of the modes, denoted as "Mode5" here, does not occur in most analyses. It is only listed in Huth *et al.* (2006) as "Mediterranean mode," which appears solely in maxima of solar activity when it seems to represent detached eastern parts of

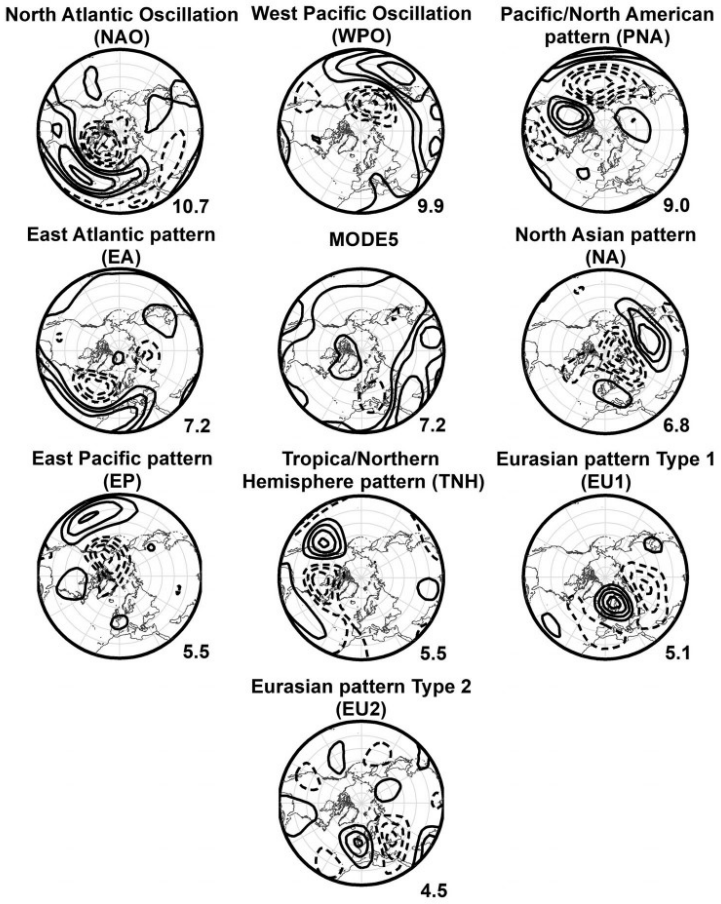

FIGURE 1 Circulation modes in the JRA-55 reanalysis, their abbreviations, and explained variance. Contour interval is 0.2, and zero contour is omitted. Positive contours are solid and negative are dashed

NAO. On the other hand, Mode5 is attached to EU2 in some reanalyses for a different period 1957–2002 (Hynčica and Huth, 2020b). The realism of the mode is supported by autocorrelation maps for its centres, which closely resemble the loading pattern (not shown). Interestingly, EU2 is not identified as a separate mode in 20CRv3 even when various numbers of components are rotated.

Figure 2 shows running correlations with selected circulation modes at a gridpoint in southern Greenland as an example. One can see a considerable temporal variability of running correlations for all modes in all reanalyses. Even this single example shows that 20CRv2c is outlying from other reanalyses, which is particularly evident for NAO and EU1. The relative behaviour of the time courses of correlations is varied: At this gridpoint, the differences between reanalyses tend to be smaller for some modes (TNH), time courses may tend to be parallel to each other, that is, differences between reanalyses tend to be constant over time (NAO), while for some other modes, differences tend to vary over time for most pairs of reanalyses (Mode5, EU1). Differences between running correlations at this gridpoint are summarized in Table 2. Smaller MADs correspond to similar time courses of running correlations in a pair of reanalyses (e.g., all the four circulation modes between JRA-55 and NCEP-1). One can see that differences are largest for 20CRv2c.

MADs are then aggregated over all gridpoints and displayed in boxplots in Figure 3 for each circulation mode (aggregating also over all reanalysis pairs) and for each reanalysis pair (aggregating also over all modes). Larger values of MADs indicate larger differences of time series of running correlations between reanalyses. The largest differences occur for Mode5, EU1, and NAO, while the

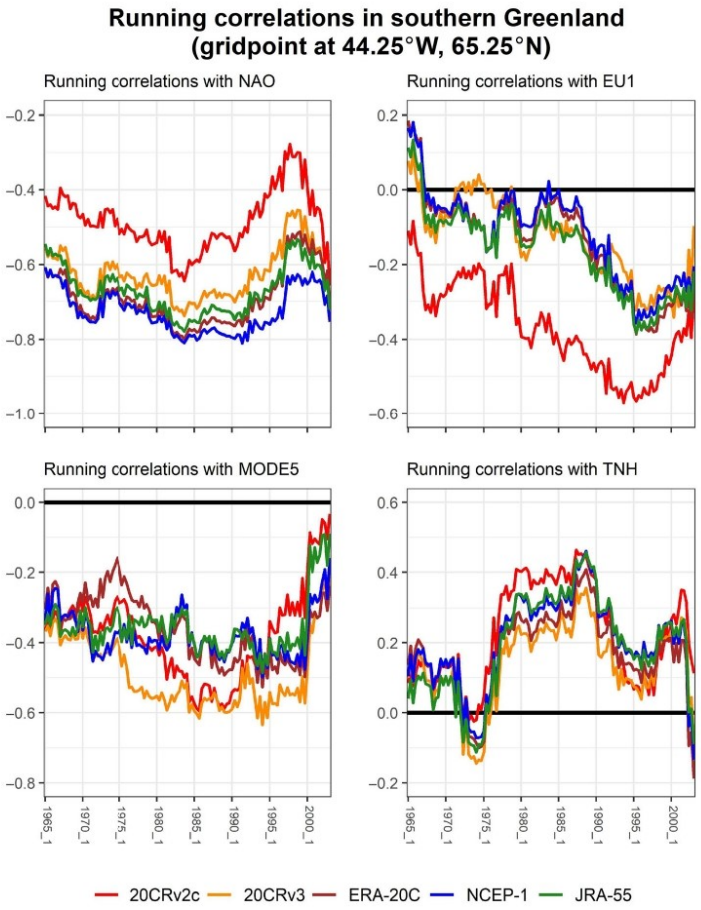

FIGURE 2 Running correlations between temperature anomaly at 65.25°N, 44.25°W (gridpoint located in southern Greenland) and four circulation modes in five reanalyses (distinguished by colour)

TABLE 2 MADs between running correlations displayed in Figure 2

Reanalyses pair	NAO	EU1	MODE5	TNH
20CRv2c–20CRv3	0.14	0.24	0.11	0.09
20CRv2c–ERA-20C	0.20	0.23	0.10	0.07
20CRv2c–JRA-55	0.18	0.21	0.08	0.06
20CRv2c–NCEP-1	0.24	0.25	0.09	0.06
20CRv3–ERA-20C	0.06	0.06	0.13	0.04
20CRv3–JRA-55	0.04	0.04	0.13	0.06
20CRv3–NCEP-1	0.10	0.06	0.11	0.07
ERA-20C–JRA-55	0.03	0.03	0.07	0.05
ERA-20C–NCEP-1	0.04	0.02	0.06	0.04
JRA-55–NCEP-1	0.06	0.04	0.04	0.02

time series of relationships are most similar for PNA and EP (Figure 3, top). If we focus on pairs of reanalyses, both 20CR reanalyses differ the most from the rest of reanalyses, and this is particularly so for the older version (20CRv2c), making it the most outlying reanalysis. NCEP-1, JRA-55, and ERA-20C exhibit a large congruity with each other (Figure 3, bottom). A more detailed insight is offered by Figure 4, which displays the median of MADs for each circulation mode and pair of reanalyses. It is evident that larger discrepancies in running correlations occur mainly for Mode5 in all reanalyses, NAO in 20CRv2c, and EU1 in both 20CR reanalyses.

We also display maps of MADs for two modes (NA and EA) and three pairs of reanalyses (Figure 5) as an example. Maps are organized so that MAD increases

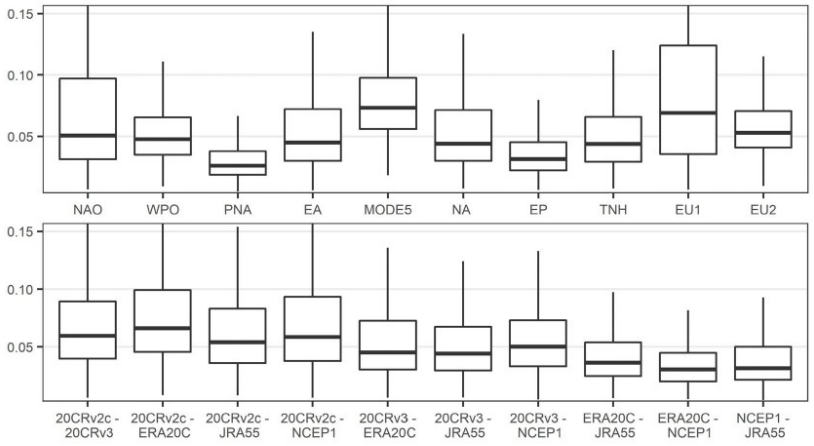

FIGURE 3 Boxplots of MADs of running correlations aggregated over all gridpoints with respect to (top) circulation modes and (bottom) pairs of reanalyses. The central line of the boxplot is the median; its lower and upper edges denote the lower and upper quartile. The upper and lower whiskers extend to 1.5 times the interquartile range from the respective edges

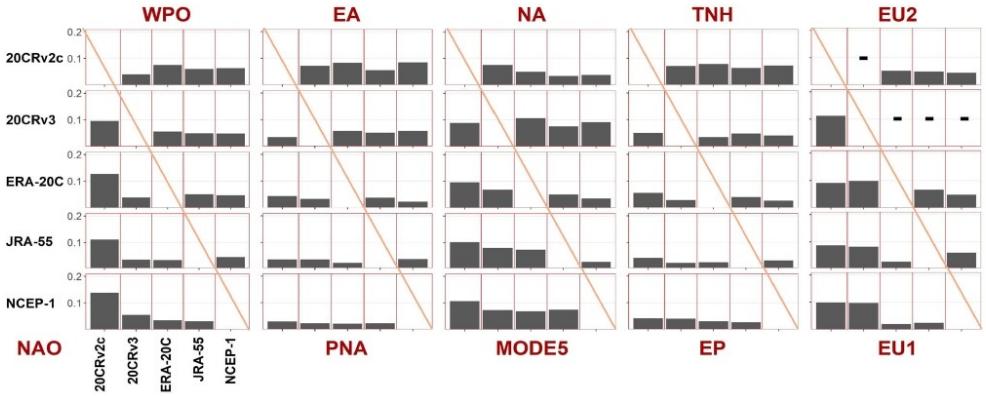

FIGURE 4 Medians of mean absolute differences (MADs) in running correlations with circulation modes between pairs of reanalyses, over all gridpoints, displayed for all 10 reanalysis pairs and 10 circulation modes. EU2 is not identified in 20CRv3

from top to bottom. The magnitude of MAD is primarily determined by the spatial similarity of circulation modes between reanalyses: a large spatial resemblance of the modes leads to a low or even negligible MAD (Figure 5, top row). In contrast, a spatial shift of the circulation mode between reanalyses leads to regionally increased MADs, as exemplified for NA in 20CRv3 and EA in 20CRv2c (Figure 5, bottom row). The relative shift of both modes (see Figures S1 and S2) subsequently results in a regionally enhanced dissimilarity of relationships and hence larger MADs. Additionally, correlations of scores (displayed in brackets on the top of each map in Figure 5) tend to relate proportionally to the similarity of relationships. This is, however, not always true as illustrated for the EA mode between 20CRv2c and NCEP-1 (Figure 5, bottom row, right): Large MADs appear despite high correlation of scores (0.95). The scores of EA in 20CRv2c are similar to other reanalyses (correlations exceeding 0.93; Table 3) although its spatial pattern is shifted (Figure S1). A comparison of medians of MADs

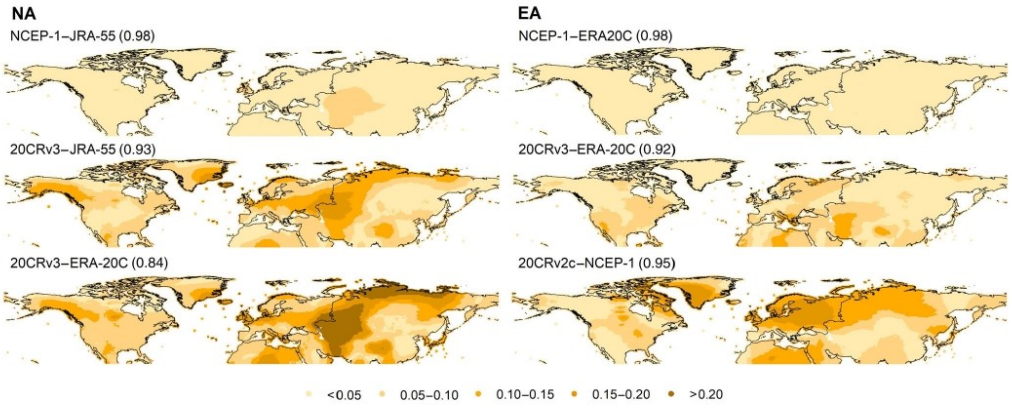

FIGURE 5 Spatial distribution of MADs for selected pairs of reanalyses for the NA (left) and EA (right) modes. Pearson correlation between the scores of modes is shown in brackets

TABLE 3 Correlations of scores (temporal intensity of circulation modes) between all pairs of reanalyses

Reanalyses pair	NAO	WPO	PNA	EA	MODE5	NA	EP	TNH	EU1	EU2
20CRv2c–20CRv3	0.93	0.95	0.98	0.93	0.82	0.91	0.95	0.90	0.73	—
20CRv2c–ERA-20C	0.88	0.88	0.97	0.95	0.81	0.95	0.94	0.89	0.84	0.94
20CRv2c–JRA-55	0.91	0.93	0.98	0.97	0.81	0.98	0.97	0.91	0.87	0.93
20CRv2c–NCEP-1	0.86	0.89	0.98	0.95	0.73	0.96	0.96	0.90	0.84	0.96
20CRv3–ERA-20C	0.98	0.96	0.98	0.92	0.94	0.84	0.98	0.97	0.76	—
20CRv3–JRA-55	0.98	0.95	0.97	0.92	0.87	0.93	0.99	0.94	0.83	—
20CRv3–NCEP-1	0.96	0.94	0.99	0.92	0.89	0.88	0.97	0.96	0.76	—
ERA-20C–JRA-55	0.98	0.94	0.99	0.98	0.89	0.94	0.98	0.96	0.98	0.91
ERA-20C–NCEP-1	0.98	0.95	0.99	0.98	0.88	0.96	0.98	0.99	0.99	0.95
NCEP-1–JRA-55	0.99	0.94	0.98	0.98	0.86	0.98	0.99	0.98	0.99	0.92

(Figure 4) and correlations of scores for all reanalyses (Table 3) indicates that this applies also to NAO in 20CRv2c and NA in 20CRv3.

4 | ANALYSIS OF DIFFERENCES IN 20CR REANALYSES

The comparison of reanalyses reveals that differences of relationships of temperature with circulation modes are largest for NAO and EU1 in 20CRv2c, for EU1 in 20CRv3, and for Mode5 in all reanalyses. Mode5 has a zonal orientation with a circumglobal belt located in low latitudes with little pronounced anomaly circulation related to it (see Figure 1); such circulation modes tend to have a lower agreement among reanalyses (this also applies, e.g., to the subtropical zonal pattern in spring, summer, and autumn; Hynčica and Huth, 2020b). Differences related to Mode5 are likely to result in only small discrepancies in correlations with temperature in mid-latitudes since the correlations themselves are small there (not shown); a detailed analysis of Mode5 is, therefore, of little potential interest. That is why we mainly focus on the 20CRv2c reanalysis in the investigation and interpretation of specific differences.

4.1 | Example 1: EU1 in 20CRv2c and NCEP-1

Now we look at differences in running correlations between reanalyses in more detail. We take mode EU1 and the 20CRv2c and NCEP-1 reanalyses as the first example. Results are representative for differences between the

20CR family and the rest of reanalyses; that is, they are qualitatively similar if 20CRv3 is taken instead of 20CRv2c and JRA-55 or ERA-20C instead of NCEP-1.

The positions of both major action centres of EU1 (the positive centre in northern Europe and the negative centre over Central Asia) differ between the two reanalyses (Figure 6, top). This leads to a different evolution of running correlations in two compact areas: Central, Northern, and north-eastern Europe, and a belt across north-eastern Africa and south-western Asia (marked as A and B in Figure 6, respectively). A more westward position of the northern centre in 20CRv2c leads to a potential for a stronger intrusion of cold air into Europe when EU1 is in its positive phase, implying more negative correlations. The negative centre over Asia is weaker and smaller in 20CRv2c, which leads to weaker anomaly circulation and correlations closer to zero over South-west Asia and North-east Africa (Figure 6, middle). A notable feature is that the magnitude of differences between correlations in the two reanalyses varies in time, peaking around 1985 in both areas (Figure 6, bottom).

In order to identify causes of the time variation of differences between reanalyses, composite maps of EU1 are calculated for all running periods in both reanalyses. For each running period, the composite map contains differences of 500 hPa anomalies between months with the score of EU1 higher than +1 and months with the score lower than −1. We define the position of action centres in the composite maps by the gridpoints with the largest or lowest anomaly in two longitudinally limited domains (75°W–40°E for the European centre and 42.5°W–145°E for the Asian centre). Then, the time series of strength, latitude, and longitude of both centres are compared between reanalyses.

The composites and composite differences in Figure 7a show that the two centres of EU1 move differently in the

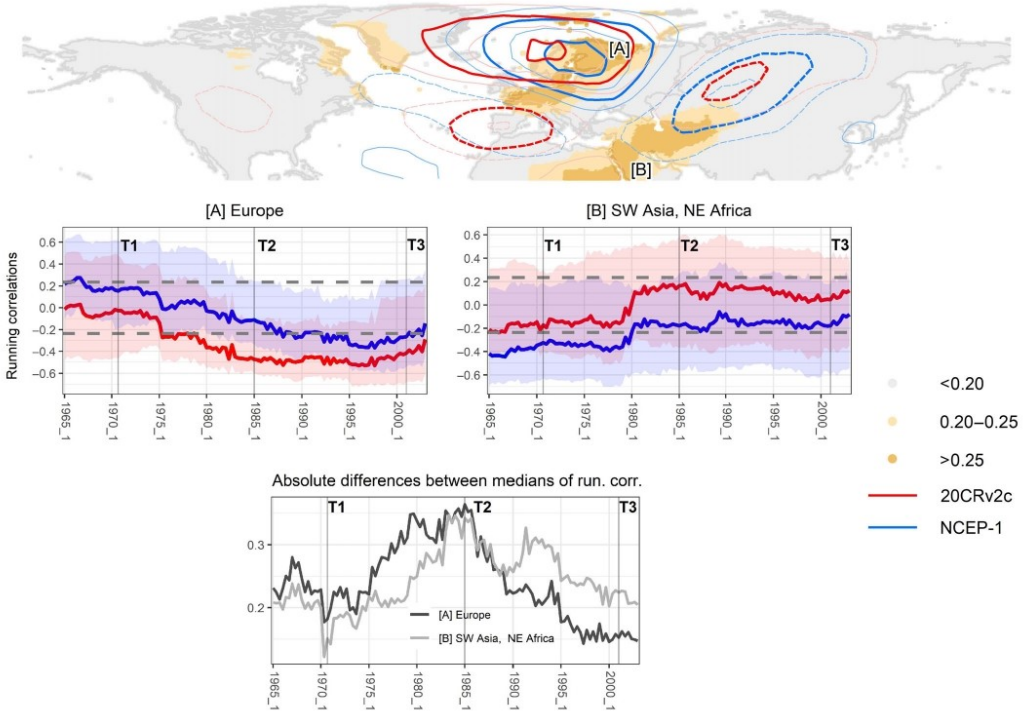

FIGURE 6 (Top) EU1 in 20CRv2c (red lines) and NCEP-1 (blue lines). Contour interval is 0.2, positive/negative values are indicated by solid/dashed lines; every other contour is highlighted, and zero line is omitted. Brown shades highlight regions where MAD is large (over 0.20 in light brown and over 0.25 in dark brown). (Middle) time series of spatial medians (thick lines) of running correlations in areas with MAD > 0.2 (highlighted by brown shading and a letter in the top map) with fifth and 95th percentiles indicated by shading. Grey dashed lines delimit statistical significance at the 5% level. T1, T2, and T3 indicate periods that are further analysed in Figure 7. (Bottom) absolute differences in spatial medians of running correlations over areas analysed in detail (i.e., differences between thick red and blue lines in the middle graphs)

two reanalyses and that their relative position varies in time. The European centre is located more westerly in 20CRv2c in almost all running periods (Figure 7b, top left). It starts moving westward earlier (in 1979) in 20CRv2c than in NCEP-1 (in 1986), resulting in the largest longitudinal difference to occur in 1985 (marked as T2).

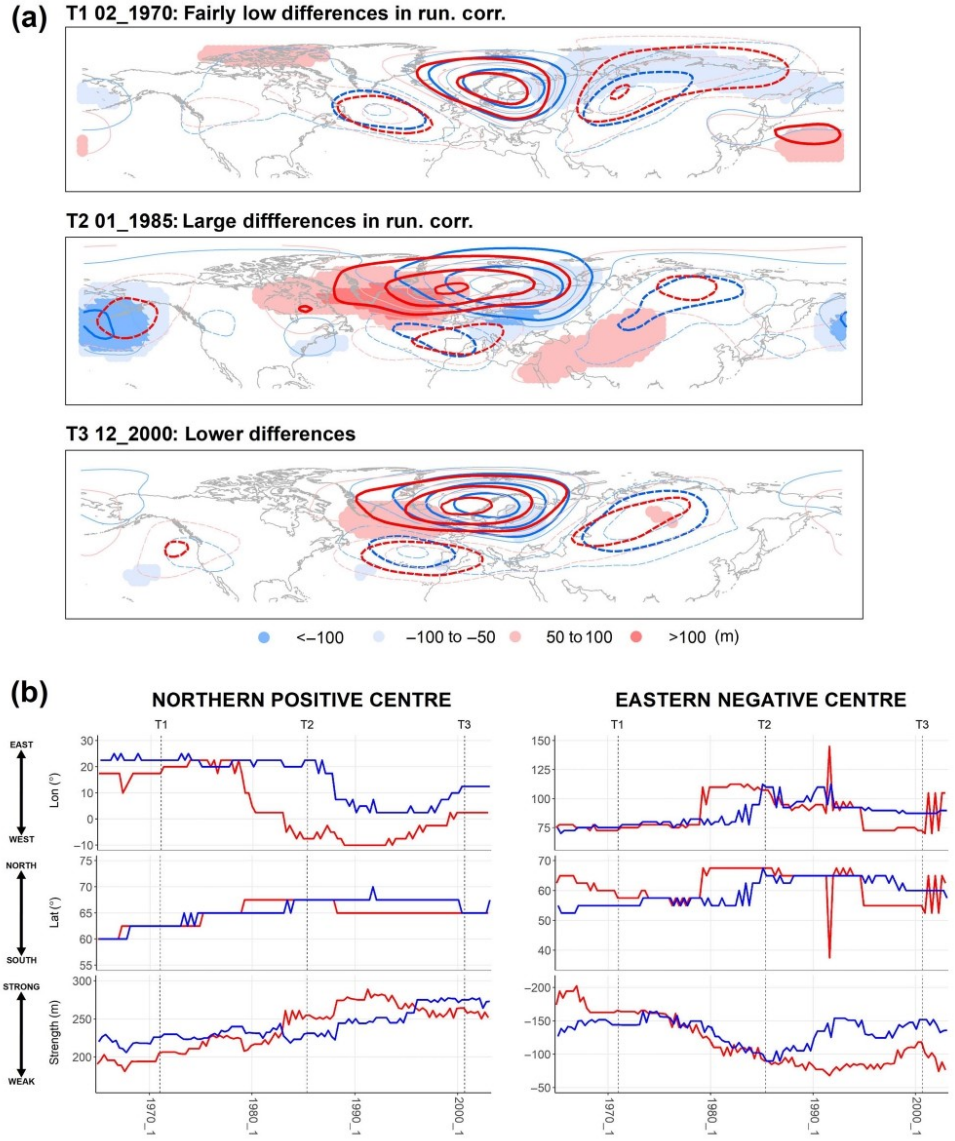

FIGURE 7 (a) Composite maps of EU1 in periods T1, T2, and T3 (see Figure 6). 20CRv2c in red, NCEP-1 in blue; positive contours are solid and negative are dashed; contour interval is 40 m. The sign and magnitude of differences between composites for NCEP-1 and 20CRv2c are displayed by colour shading: Bluish/pinkish for NCEP-1/20CRv2 larger. (b) Time series of the longitude (top), latitude (middle), and strength (bottom) of action centres of EU1: 20CRv2c in red and NCEP-1 in blue

Later, the centre moves back eastwards, again earlier in 20CRv2c, resulting in a diminished longitudinal difference between the reanalyses near the end of the analysed period (running period T3). The northward move of the centre is similar in both reanalyses (Figure 7b, middle left); its overall strengthening is less synchronized between the reanalyses, the centre being stronger in 20CRv2c from 1983 to 1995 (Figure 7b, bottom left). The similarity of the position of the European centre and its spatial structure between the reanalyses near the beginning and end of the analysed period (including running periods T1 and T3) are the reasons for small differences in correlations of EU1 with temperature in Europe (Area A in Figure 6). On the other hand, the potential for an inflow of cold air from north-west and north into most of Europe under the positive phase of EU1 is particularly effective in the mid-1980s (Period T2) in 20CRv2c, thanks to the European centre being stronger and located more westward. This is reflected by more negative correlations in 20CRv2c compared to NCEP-1.

The differential position and intensity are not sufficient for the explanation of different running correlations near the Asian centre. Although the correlations in the area affected by it (north-eastern Africa and south-western Asia, B in Figure 6) differ between the two reanalyses in Running Period T2 as much as in Area A, the position and intensity of the Asian centre are fairly similar in both reanalyses (Figure 7b, right). The reason for the difference in correlations appears to consist in the shape of the Asian centre: In 20CRv2c, it lacks the south-westward extension across Central Asia towards Iran, which is rather strong in NCEP-1. As a consequence, the positive phase of EU1 supports the intrusion of cold air from the north into Area B in NCEP-1, whereas this effect is absent in 20CRv2c. This explains negative correlations in Area B in period T2 in NCEP-1 and less negative/more positive correlations in 20CRv2c.

4.2 | Example 2: NAO in 20CRv2c and NCEP-1

Spatial representation of NAO is also slightly different in the two reanalyses: Both the major centres of NAO are

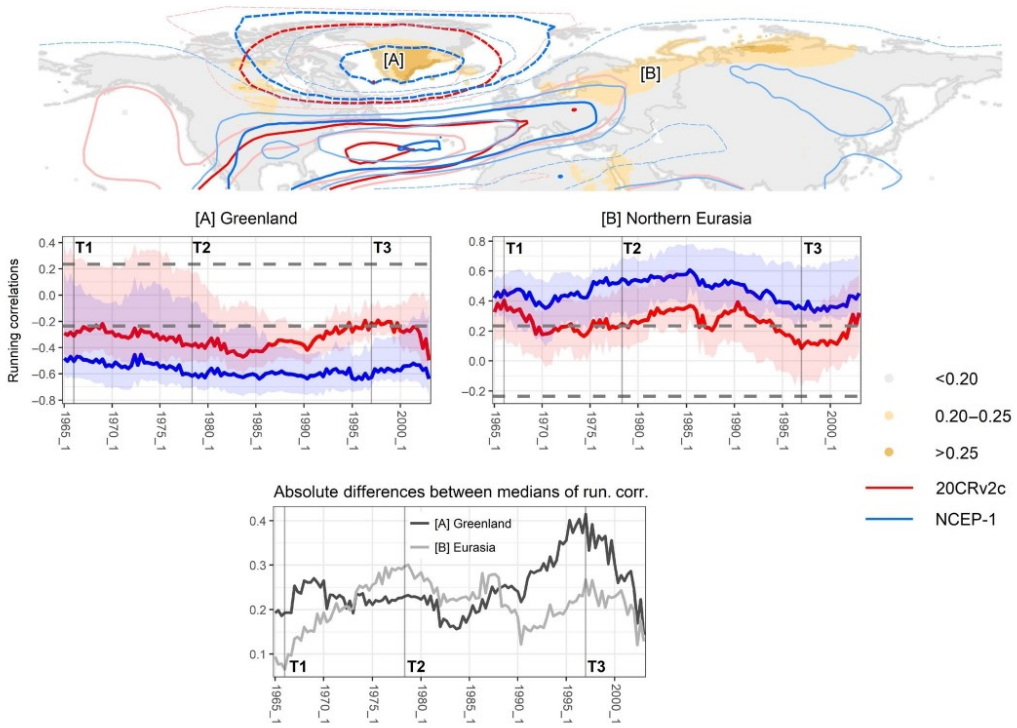

FIGURE 8 As in Figure 6 but for NAO

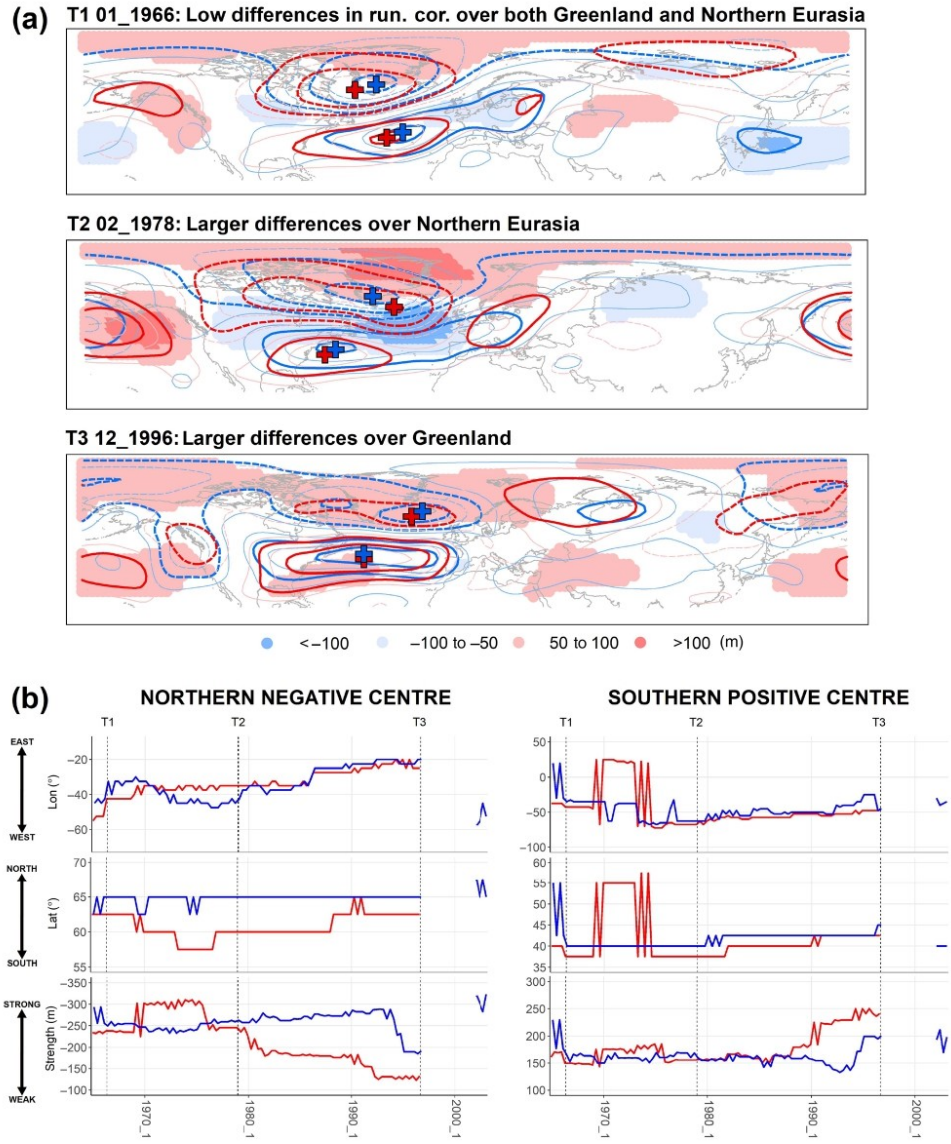

FIGURE 9 As in Figure 7 but for NAO

shifted westward to south-westward, and the northern negative centre is considerably weaker in 20CRv2c (Figure 8, top). Such spatial setting consequently induces weaker (less negative and less positive, respectively) running correlations (and larger MADs) in 20CRv2c over the southern half of Greenland and in a long belt over northern Eurasia (Areas A and B, respectively, in Figure 8, middle).

Over northern Eurasia, the correlations are closest in the two reanalyses at the beginning of the studied period, followed by the increase of differences until the late 1970s. On the contrary, differences culminate in the

1990s over southern Greenland (Figure 8, bottom). Composite maps are calculated in the same way as for EU1; positions of the centres are detected between 100°W and 70°E. Figure 9a shows composite maps in the three selected periods: T1 is a period with small differences in running correlations, particularly in northern Eurasia, while the other two periods correspond to increased differences over northern Eurasia (T2) and southern Greenland (T3) (Figure 8). Time series of the position and strength of the NAO centres in both reanalyses are shown in Figure 9b. Note that composites could not be calculated between 1997 and 2002 because of missing negative phase: There are no months with the score of NAO below −1 in the corresponding periods.

The positive relationship between temperature and NAO over large parts of Eurasia is determined by the intensity of westerlies, which is modified by the position, strength, and shape of the NAO centres: A strong positive NAO induces strong westerlies, which bring warm air into most of Europe, which results in positive correlations of the intensity of NAO with temperature. Over northern Eurasia, running correlations started to differ after 1965 with the differences peaking before 1980 (T2; Figure 8, middle). In spite of the similar position and strength of the southern positive centre in both reanalyses in T2 (Figure 9a, middle; Figure 9b, right), its spatial appearance differs between the reanalyses: the extension towards Eurasia is weaker and less pronounced in 20CRv2c. The centre spreads far into northern Siberia in NCEP-1, which together with a more poleward located northern centre account for stronger westerlies penetrating deeper into Eurasia, and therefore stronger correlations compared to 20CRv2c.

In T1, a closer agreement in the position and intensity of both centres and consequent lower composite differences over Atlantic and Europe (Figure 9a, top) result in similar relationships over Northern Eurasia. Despite the centres being fairly similar also after 1990 (T3, Figure 9a, bottom), relationships differ (Figure 8). The reason is in the positive centre over Northern Eurasia (Figure 9a, bottom), which is responsible for weaker relationships with NAO due to stronger meridional circulation. This centre is stronger and more extensive in 20CRv2, which elicits stronger anomaly circulation and hence more pronounced decrease in correlations.

Relationships between NAO and temperature in Greenland are driven by the northern centre, which controls advection of cold northerly/north-easterly air into the region. The centre is permanently placed more southward in 20CRv2c (Figure 9b, left), which results in weaker advection of cold air into southern Greenland under the positive phase of NAO and subsequent less negative correlations. The weakening of the northern centre in 20CRv2c during the late 1970s and early 1980s (Figure 9b, left) was not accompanied by a change in relationships with temperature. However, correlations became less negative in 20CRv2c after 1990 (Figure 8a, bottom) without a prominent change in the position and intensity of the centre. Differences in the shape of the centre are a probable cause of differences in correlations.

5 | CONCLUSIONS

Temporal evolution of relationships between circulation modes and temperature in the northern Extratropics in winter was compared between five reanalyses. Relationships are defined by running correlations calculated for 45-month windows (corresponding to 15 winter seasons) between the intensity of circulation modes (provided by rotated PCA) and temperature anomalies from 1958 to 2010. Running correlations with all circulation modes are in high accordance with the full-input reanalyses (NCEP-1 and JRA-55) and ERA-20C; this is in accord with Hynčica and Huth (2020b) where a high congruity of spatial patterns of circulation modes between these reanalyses is reported especially for winter. Both versions of the 20CR reanalysis differ from other reanalyses more substantially, which is particularly so for the older version, 20CRv2c. The modes located over Eurasia and the North Atlantic have different positions and differ in correlations or even are not detected at all. This concerns EU1 (in both 20CR reanalyses), NAO (in 20CRv2c), EU2 (not identified in 20CRv3), and to a lesser extent EA in 20CRv2c and NA in 20CRv3. The other circulation modes and related correlations with temperature in 20CRv2c and 20CRv3 are largely consistent with other reanalyses; this applies mainly to those over the Pacific and North America (PNA, WPO, TNH, and EP). Overall, 20CRv3 is closer to other reanalyses than 20CRv2c, suggesting that the development of the 20CR reanalysis is successful in the reduction of its errors and biases. The large congruity of the other surface-input reanalysis, ERA-20C, with the full-input reanalyses, indicates that even the surface-input reanalyses have the potential to accurately reproduce atmospheric circulation in mid-troposphere, at least in periods when surface data are sufficiently dense and reliable. This concerns mainly the second half of the 20th century when the amount of the input data substantially increased, while the lack of data in the preceding period is responsible for a lower reliability of reanalyses.

The differences between reanalyses in correlations of the modes with temperature, their spatial distribution, and development in time are attributed to differences in the position and strength of the action centres of the modes, uncovered by the composite analysis. The different patterns of the modes induce different anomaly circulations, which in turn leads to a different temperature

response to the intensity of the mode and different correlations of the intensity of the mode with temperature.

ACKNOWLEDGEMENTS

This research was supported by the Czech Science Foundation, project 17-07043S. Martin Hynčica was also supported by the Grant Agency of the Charles University, student project 426216. We further acknowledge the following organizations for providing the reanalysis data: NOAA/OAR/ESRL PSL, Boulder, Colorado, USA, for 20CRv3, 20CRv2c, and NCEP-1; ECMWF, Reading, United Kingdom, for ERA-40 and ERA-20C; and JMA, Tokyo, Japan, for JRA-55. We also acknowledge CRU for providing the CRU TS v 4.03 gridded data set.

AUTHOR CONTRIBUTIONS

Martin Hynčica: Conceptualization; data curation; formal analysis; investigation; methodology; software; validation; visualization; writing – original draft. **Radan Huth:** Conceptualization; formal analysis; funding acquisition; methodology; project administration; resources; supervision; writing – review and editing.

ORCID

Martin Hynčica https://orcid.org/0000-0003-4537-7736

REFERENCES

Barnston, A.G. and Livezey, R.E. (1987) Classification, seasonality and persistence of low-frequency atmospheric circulation patterns. *Monthly Weather Review*, 115, 1083–1126.

Beranová, R. and Huth, R. (2007) Time variations of the relationships between the North Atlantic oscillation and European winter temperature and precipitation. *Studia Geophysica et Geodaetica*, 51, 575–590.

Beranová, R. and Huth, R. (2008) Time variations of the effects of circulation variability modes on European temperature and precipitation in winter. *International Journal of Climatology*, 28, 139–158.

Clinet, S. and Martin, S. (1992) 700-HPA geopotential height anomalies from a statistical analysis of the French Hemis data set. *International Journal of Climatology*, 12, 229–256.

Compo, G.P., Whitaker, J.S., Sardeshmukh, P.D., Matsui, N., Allan, R.J., Yin, X., Gleason, B.E., Vose, R.S., Rutledge, G., Bessemoulin, P., Brönnimann, S., Brunet, M., Crouthamel, R.I., Grant, A.N., Groisman, P.Y., Jones, P.D., Kruk, M.C., Kruger, A. C., Marshall, G.J., Maugeri, M., Mok, H.Y., Nordli, Ø., Ross, T.F., Trigo, R.M., Wang, X.L., Woodruff, S.D. and Worley, S.J. (2011) The twentieth century reanalysis project. *Quarterly Journal of the Royal Meteorological Society*, 137, 1–28.

Filippi, L., Palazzi, E., von Hardenberg, J. and Provenzale, A. (2014) Multidecadal variations in the relationship between the NAO and winter precipitation in the Hindu Kush–Karakoram. *Journal of Climate*, 27, 7890–7902.

Franzke, C., Feldstein, S.B. and Lee, S. (2011) Synoptic analysis of the Pacific–North American teleconnection pattern. *Quarterly Journal of the Royal Meteorological Society*, 137, 329–346.

Fujiwara, M., Wright, J.S., Manney, G.L., Gray, L.J., Anstey, J., Birner, T., Davis, S., Gerber, E.P., Harvey, V.L., Hegglin, M.I., Homeyer, C.R., Knox, J.A., Krüger, K., Lambert, A., Long, C.S., Martineau, P., Molod, A., Monge-Sanz, B.M., Santee, M.L., Tegtmeier, S., Chabrillat, S., Tan, D.G.H., Jackson, D.R., Polavarapu, S., Compo, G.P., Dragani, R., Ebisuzaki, W., Harada, Y., Kobayashi, C., McCarty, W., Onogi, K., Pawson, S., Simmons, A., Wargan, K., Whitaker, J.S. and Zou, C.Z. (2017) Introduction to the SPARC reanalysis Intercomparison project (S-RIP) and overview of the reanalysis systems. *Atmospheric Chemistry and Physics*, 17, 1417–1452.

Harris, I., Osborn, T.J., Jones, P. and Lister, D. (2020) Version 4 of the CRU TS monthly high-resolution gridded multivariate climate dataset. *Scientific Data*, 7, 1–18.

He, S., Wang, H. and Liu, J. (2013) Changes in the relationship between ENSO and Asia–Pacific midlatitude winter atmospheric circulation. *Journal of Climate*, 26, 3377–3393.

Hurrell, J.W. (1995) Decadal trends in the North Atlantic oscillation: regional temperatures and precipitation. *Science*, 269, 676–679.

Huth, R. (2006) The effect of various methodological options on the detection of leading modes of sea level pressure variability. *Tellus A: Dynamic Meteorology and Oceanography*, 58, 121–130.

Huth, R., Pokorná, L., Bochníček, J. and Hejda, P. (2006) Solar cycle effects on modes of low-frequency circulation variability. *Journal of Geophysical Research: Atmospheres*, 111, D22107.

Hynčica, M. and Huth, R. (2020a) Gridded versus station temperatures: time evolution of relationships with atmospheric circulation. *Journal of Geophysical Research: Atmospheres*, 125, e2020JD033254.

Hynčica, M. and Huth, R. (2020b) Modes of atmospheric circulation variability in the northern Extratropics: a comparison of five reanalyses. *Journal of Climate*, 33, 10707–10726.

Iles, C. and Hegerl, G. (2017) Role of the North Atlantic oscillation in decadal temperature trends. *Environmental Research Letters*, 12, 114010.

Jung, T., Hilmer, M., Ruprecht, E., Kleppek, S., Gulev, S.K. and Zolina, O. (2003) Characteristics of the recent eastward shift of interannual NAO variability. *Journal of Climate*, 16, 3371–3382.

Kalnay, E., Kanamitsu, M., Kistler, R., Collins, W., Deaven, D., Gandin, L., Iredell, M., Saha, S., White, G., Woollen, J., Zhu, Y., Leetmaa, A., Reynolds, R., Chelliah, M., Ebisuzaki, W., Higgins, W., Janowiak, J., Mo, K.C., Ropelewski, C., Wang, J., Jenne, R. and Joseph, D. (1996) The NCEP/NCAR 40-year reanalysis project. *Bulletin of the American Meteorological Society*, 77, 437–471.

Kobayashi, S., Ota, Y., Harada, Y., Ebita, A., Moriya, M., Onoda, H., Onogi, K., Kamahori, H., Kobayashi, C., Endo, H., Miyaoka, K. and Takahashi, K. (2015) The JRA-55 reanalysis: general specifications and basic characteristics. *Journal of the Meteorological Society of Japan. Ser. I*, 93, 5–48.

Krichak, S.O. and Alpert, P. (2005) Decadal trends in the East Atlantic–West Russia pattern and Mediterranean precipitation. *International Journal of Climatology*, 25, 183–192.

Leathers, D.J., Yarnal, B. and Palecki, M.A. (1991) The Pacific/North American teleconnection pattern and United States climate. Part I: regional temperature and precipitation associations. *Journal of Climate*, 4, 517–528.

Lee, Y.Y., Kug, J.S., Lim, G.H. and Watanabe, M. (2012) Eastward shift of the Pacific/North American pattern on an interdecadal

time scale and an associated synoptic eddy feedback. *International Journal of Climatology*, 32, 1128–1134.

Lian, T. and Chen, D. (2012) An evaluation of rotated EOF analysis and its application to tropical Pacific SST variability. *Journal of Climate*, 25, 5361–5373.

Luo, D. and Gong, T. (2006) A possible mechanism for the eastward shift of interannual NAO action centers in last three decades. *Geophysical Research Letters*, 33, L24815.

O'Lenic, E.A. and Livezey, R.E. (1988) Practical considerations in the use of rotated principal component analysis (RPCA): in diagnostic studies of upper-air height fields. *Monthly Weather Review*, 116, 1682–1689.

Peterson, K.A., Lu, J. and Greatbatch, R.J. (2003) Evidence of nonlinear dynamics in the eastward shift of the NAO. *Geophysical Research Letters*, 30, 1030.

Pokorná, L. and Huth, R. (2015) Climate impacts of the NAO are sensitive to how the NAO is defined. *Theoretical and Applied Climatology*, 119, 639–652.

Poli, P., Hersbach, H., Dee, D.P., Berrisford, P., Simmons, A.J., Vitart, F., Laloyaux, P., Tan, D.G.H., Peubey, C., Thépaut, J.N., Trémolet, Y., Hólm, E.V., Bonavita, M., Isaksen, L. and Fisher, M. (2016) ERA-20C: An atmospheric reanalysis of the twentieth century. *Journal of Climate*, 29, 4083–4097.

Polyakova, E.I., Journel, A.G., Polyakov, I.V. and Bhatt, U.S. (2006) Changing relationship between the North Atlantic oscillation and key North Atlantic climate parameters. *Geophysical Research Letters*, 33, L03711.

Richman, M.B. (1986) Rotation of principal components. *Journal of Climatology*, 6, 293–335.

Rohrer, M., Brönnimann, S., Martius, O., Raible, C.C., Wild, M. and Compo, G.P. (2018) Representation of extratropical cyclones, blocking anticyclones, and alpine circulation types in multiple reanalyses and model simulations. *Journal of Climate*, 31, 3009–3031.

Slivinski, L.C., Compo, G.P., Sardeshmukh, P.D., Whitaker, J.S., McColl, C., Allan, R.J., Brohan, P., Yin, X., Smith, C.A., Spencer, L.J., Vose, R.S., Rohrer, M., Conroy, R.P., Schuster, D.C., Kennedy, J.J., Ashcroft, L., Brönnimann, S., Brunet, M., Camuffo, D., Cornes, R., Cram, T.A., Domínguez-Castro, F., Freeman, J.E., Gergis, J., Hawkins, E., Jones, P.D., Kubota, H., Lee, T.C., Lorrey, A.M., Luterbacher, J., Mock, C.J., Przybylak, R.K., Pudmenzky, C., Slonosky, V.C., Tinz, B., Trewin, B., Wang, X.L., Wilkinson, C., Wood, K. and Wyszyński, P. (2021) An evaluation of the performance of the twentieth century reanalysis version 3. *Journal of Climate*, 34, 1417–1438.

Slivinski, L.C., Compo, G.P., Whitaker, J.S., Sardeshmukh, P.D., Giese, B.S., McColl, C., Allan, R., Yin, X., Vose, R., Titchner, H., Kennedy, J., Spencer, L.J., Ashcroft, L., Brönnimann, S., Brunet, M., Camuffo, D., Cornes, R., Cram, T. A., Crouthamel, R., Domínguez-Castro, F., Freeman, J.E., Gergis, J., Hawkins, E., Jones, P.D., Jourdain, S., Kaplan, A., Kubota, H., Blancq, F.L., Lee, T.C., Lorrey, A., Luterbacher, J., Maugeri, M., Mock, C.J., Moore, G.W.K., Przybylak, R., Pudmenzky, C., Reason, C., Slonosky, V.C., Smith, C.A., Tinz, B., Trewin, B., Valente, M.A., Wang, X.L., Wilkinson, C., Wood, K. and Wyszyński, P. (2019) Towards a more reliable historical reanalysis: improvements for version 3 of the twentieth century reanalysis system. *Quarterly Journal of the Royal Meteorological Society*, 145, 2876–2908.

Stryhal, J. and Huth, R. (2017) Classifications of winter Euro-Atlantic circulation patterns: an intercomparison of five atmospheric reanalyses. *Journal of Climate*, 30, 7847–7786.

Sun, J. and Wang, H. (2012) Changes of the connection between the summer North Atlantic oscillation and the east Asian summer rainfall. *Journal of Geophysical Research: Atmospheres*, 117, D08110.

Sun, J., Wang, H. and Yuan, W. (2008) Decadal variations of the relationship between the summer North Atlantic oscillation and middle east Asian air temperature. *Journal of Geophysical Research: Atmospheres*, 113, D15107.

Vicente-Serrano, S.M. and López-Moreno, J.I. (2008) Nonstationary influence of the North Atlantic oscillation on European precipitation. *Journal of Geophysical Research: Atmospheres*, 113, D20120.

Wang, X.L., Feng, Y., Chan, R. and Isaac, V. (2016) Intercomparison of extra-tropical cyclone activity in nine reanalysis datasets. *Atmospheric Research*, 181, 133–153.

Xu, T., Shi, Z., Wang, H. and An, Z. (2016) Nonstationary impact of the winter North Atlantic oscillation and the response of mid-latitude Eurasian climate. *Theoretical and Applied Climatology*, 124, 1–14.

Zuo, J., Ren, H.L., Li, W. and Wang, L. (2016) Interdecadal variations in the relationship between the winter North Atlantic oscillation and temperature in south-Central China. *Journal of Climate*, 29, 7477–7493.

SUPPORTING INFORMATION

Additional supporting information may be found in the online version of the article at the publisher's website.

How to cite this article: Hynčica, M., & Huth, R. (2021). Temporal evolution of relationships between temperature and circulation modes in five reanalyses. *International Journal of Climatology*, 1–14. https://doi.org/10.1002/joc.7474

3. Comparing relationships with circulation modes at gridpoints and nearest stations

Here, the evaluation of the CRU dataset is conducted by comparison of relationships between circulation modes and temperature at stations and their nearest gridpoints. A large agreement between the CRU dataset and observations is evident, only regional biases in the CRU dataset appear mostly in orographically complex areas, such as eastern Asia or Rocky Mountains, and isolated locations, e.g. islands.

Paper III: Hynčica, M., Huth, R. (2020). Gridded versus station temperatures: Time evolution of relationships with atmospheric circulation. *Journal of Geophysical Research: Atmospheres*, 125, e2020JD033254.

JGR Atmospheres

RESEARCH ARTICLE
10.1029/2020JD033254

Gridded Versus Station Temperatures: Time Evolution of Relationships With Atmospheric Circulation

Martin Hynčica[1,2] and Radan Huth[1,3]

[1]Department of Physical Geography and Geoecology, Faculty of Science, Charles University, Prague, Czechia, [2]Czech Hydrometeorological Institute, Ústí nad Labem, Czechia, [3]Institute of Atmospheric Physics, Czech Academy of Sciences, Prague, Czechia

Key Points:
- Relationships of temperature with atmospheric circulation are mostly similar at stations and gridpoints nearest to them
- Differences are found mainly over southeastern Asia, the Black Sea, the Iberian Peninsula, foothills of the Alps, and western North America
- Differences occur where station network is spatially heterogeneous or there is climatic contrast near the station

Correspondence to:
M. Hynčica,
martin.hyncica@natur.cuni.cz

Citation:
Hynčica, M., & Huth, R. (2020). Gridded versus station temperatures: Time evolution of relationships with atmospheric circulation. *Journal of Geophysical Research: Atmospheres, 125*, e2020JD033254. https://doi.org/10.1029/2020JD033254

Received 10 JUN 2020
Accepted 10 SEP 2020
Accepted article online 18 OCT 2020

Abstract Interpolated data sets are often considered to be a reliable source of information on a variety of meteorological variables, such as temperature and precipitation. Users expect the interpolated data to be rather similar to those directly observed at stations, which is not always true: well documented is the influence of interpolation on, e.g., extremes. Here another kind of discrepancy between gridpoints and station observations is presented: the time evolution of relationships between temperature and atmospheric circulation. One of the most widely utilized gridded temperature data sets, CRU TS (Climatic Research Unit gridded Time Series), is compared with 634 station time series from GHCN (Global Historical Climatology Network) in the Northern Extratropics. We analyze running correlations (calculated for 15-year windows) of monthly values between modes of atmospheric circulation variability (identified in the ERA-40 reanalysis) and temperature anomalies in winter from 1957 to 2002. The smallest differences in the running correlations are found in Europe and North America due to a dense station network. On the other hand, the sites with considerable differences are located mainly in mountainous regions or in isolated locations. In order to uncover causes of these differences, we analyze two sites in more detail. Mike (the North Sea) is an isolated site where the gridpoint temperature is affected by rather distant Scandinavian stations. At Songpan (central China; 2,852 m a.s.l), the terrain configuration in mountainous region influences the gridpoint value, in which the effect of stations with much lower altitude and different climate conditions is dominant.

1. Introduction

Atmospheric circulation may be analyzed with various approaches, one of which is the detection of modes of low-frequency variability (referred to as "circulation modes" hereafter). Circulation modes mostly consist of several distant centers, between which pressure or geopotential heights are highly correlated. Circulation modes can be identified by two major approaches: one-point correlation maps (e.g., Li & Ruan, 2018; Raible et al., 2014; Wallace & Gutzler, 1981) or principal component analysis (e.g., Barnston & Livezey, 1987; Huth et al., 2006; Yu et al., 2018). Circulation modes affect surface climate elements, such as temperature and precipitation; many studies have looked into it, e.g., Bueh and Nakamura (2007), Iles and Hegerl (2017), Lim (2015), Linkin and Nigam (2008), Liu et al. (2014), Moore and Renfrew (2012), Piper et al. (2019), Pokorná and Huth (2015), and Wang and Zhang (2015). However, the relationships of circulation modes with surface climate elements change in space and time (Beranová & Huth, 2008; Jacobeit et al., 2001; Polyakova et al., 2006; Slonosky et al., 2001; Zuo et al., 2016). One of the first studies describing such a nonstationarity (Chen & Hellström, 1999) shows the high temporal variability of the relationship of the North Atlantic oscillation (NAO) with temperature in Sweden where the gradually decreasing correlations between NAO and temperature from the beginning of the 20th century to the early 1920s followed by its strengthening were revealed. Increasing correlations of NAO with temperature are detected for the last quarter of the 20th century in western, central, and southeastern Europe, while the opposing tendency is observed in Iceland and Norway (Beranová & Huth, 2008, where also the nonstationarity of other circulation modes is examined over Europe). The nonstationarity has been suggested to be caused by the shift of the action centers of circulation modes (Jung et al., 2003): for instance, the eastward shift of the NAO centers during the second half of the 20th century may cause the strengthening of the relationships with temperature over large parts of Europe (Beranová & Huth, 2008).

All the aforementioned studies use station data only. Yet gridded data sets provide regularly spaced surface data which may be utilized for the description of the changing relationships with circulation modes over large areas and in a longer temporal perspective. Gridded data sets are mostly produced by interpolating station data to a regular grid by various interpolation methods, such as natural neighbor, kriging, triangulation, cubic spline, and angular distance weighting: their description is given in, e.g., Avila et al. (2015), Hofstra and New (2009), New et al. (2000), and Willmott and Robeson (1995). The gridded data sets, however, have limitations given by the interpolation process and changes in station data, spatiotemporal changes in the density of stations entering the interpolation in particular (e.g., van der Schrier et al., 2013). The station time series are corrected (homogenized) before entering the interpolation process, therefore the influence of other factors such as, e.g., the change of observational site and increasing effect of urbanization is suppressed.

In general, gridded data sets maintain well the values around the mean state of input data, while the temporal variations are typically oversmoothed, which leads to an underestimation of variance and extreme values in gridded data (Beguería et al., 2016; Gervais et al., 2014; Herold et al., 2016; Hofstra et al., 2009, 2010). The density of the station network is crucial in the appearance of oversmoothing: it manifests stronger at gridpoints computed over sparse station network (e.g., less populated areas, higher elevations) where distant stations outside a grid-box, which share less similarity with near-to-gridpoint stations, contribute to the interpolation (Herrera et al., 2019; Hofstra et al., 2010). Thus, the gridded data have to be treated with caution when analyzing changes in extremes, mainly over the areas with low-density station network. Gridding affects also trends (Beier et al., 2012; Donat et al., 2014; Krauskopf & Huth, 2020) and a shape of underlying statistical distribution, including higher-order statistical moments (Cavanaugh & Shen, 2015; Director & Bornn, 2015; Gross et al., 2018; Rhines et al., 2017).

Nevertheless, the number of stations entering the interpolation affects the output even in an area with a dense station network, as is shown by comparing the Climatic Research Unit (CRU) data set (where approximately 400 stations are used) with the high-resolution national data set (incorporating about 2,400 stations) over China (Xu et al., 2020). Differences in seasonal temperature trends reach up to 0.13°C/decade there. The CRU data set also produces lower precipitation sums in higher elevations (above 1,500 m a.s.l.), indicating that the accuracy of the data set decreases with increasing elevation (Shi et al., 2017; Zhu et al., 2015). Generally, precipitation sums provided by interpolated data sets are lower than observed while the bias increases with altitude (Fallah et al., 2020).

As we have just demonstrated, gridded data sets have been evaluated and compared with station data for a variety of characteristics. However, the sensitivity of relationships with atmospheric circulation to the type of surface climate data has not been studied yet. Here we compare the temporal evolution of relationships of circulation modes detected in ERA-40 reanalysis and temperature between stations and their nearest gridpoints in the CRU data set (Harris et al., 2020). A particular attention is paid to the pairs of the station and gridpoint data, for which the time series exhibit substantial discrepancies. The goal of the paper is solely the comparison of gridded and observed data, and subsequent seek for the causes of differences between both data types. It is not our intention to improve or modify the interpolation procedure used for the creation of gridded data.

2. Materials and Methods

Monthly temperature at 634 stations (obtained from the Global Historical Climatology Network-version 3, GHCN; Lawrimore et al., 2011) and at the gridpoints in Climate Research Unit gridded Time Series v 4.01 (Harris et al., 2020, further named as the CRU data set) nearest to the stations is used. Two types of station series are available in GHCN: unadjusted (i.e., data are not homogenized by the authors of GHCN but they may have been modified before by, e.g., national meteorological services) and adjusted (data are homogenized by the authors of GHCN). We employ unadjusted data; nevertheless, both types of series provide fairly similar results.

The studied area covers continents in the Northern Extratropics, approximately north of 20°N. At all gridpoints and stations, monthly long-term temperature anomalies from 1957 to 2002 as a reference period (or shorter if a station time series ends earlier) in winter months (December, January, and February) are calculated. It should be stressed that the station data are retrieved independently of the CRU data set, thus only some of the GHCN stations were incorporated in the gridding process of the CRU data set.

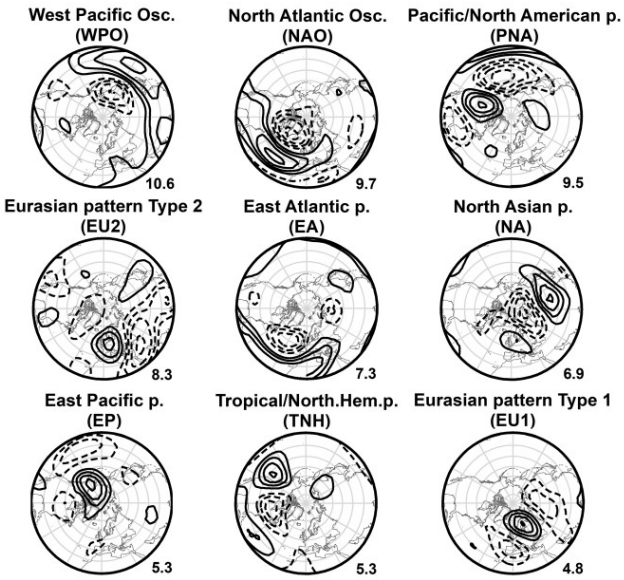

Figure 1. Circulation modes in winter in the ERA-40 reanalysis and their explained variance (in %). Names and abbreviations are adopted from Barnston and Livezey (1987).

Atmospheric circulation is described by circulation modes, which are detected with the use of rotated principal component analysis (PCA), based on the correlation matrix of monthly 500 hPa height anomalies north of 20°N inclusive (excluding the North Pole) in the ERA-40 reanalysis (DJF, 1957–2002; Uppala et al., 2005). Circulation modes in ERA-40 are the most similar (i.e., having the lowest differences) to other reanalyses (Hynčica & Huth, 2020), which is the reason why we opt for it. Correlations of time series between "traditional" reanalyses (ERA-40, JRA-55, and NCEP-1) exceed 0.95 for the majority of circulation modes in winter (Hynčica & Huth, 2020). The utilization of another reanalysis would therefore not change our results.

The data are available on a 2.5° × 2.5° grid. We use the double spacing (5° × 5°), which is sufficient given the large spatial autocorrelation in the data. The decreasing area of gridboxes toward the pole is eliminated by using a quasi-equal-area grid, in which individual gridpoints are omitted at individual latitudes so that an average gridbox area is roughly the same in all latitudes and approximates that on the Equator (Barnston & Livezey, 1987; Huth, 2006). Ten principal components are rotated, resulting in 10 circulation modes, of which nine that correspond to those described already by Barnston and Livezey (1987) are considered for further analysis and interpretation (Figure 1).

For the description of the time evolution of relationships of temperature with atmospheric circulation, running Pearson correlations are computed between the scores (i.e., the time series of intensity) of all the nine circulation modes and monthly temperature anomalies at all 634 stations and gridpoints. Running correlations are calculated for the moving 45-month (15 winters) windows with a one-month shift; the running correlation of each window is assigned to its central month. Hence, time series of running correlations with nine circulation modes are produced for all 634 stations and their nearest gridpoints. Finally, the maximum difference between the time series of running correlations at every pair is determined for all circulation modes.

For the examination of differences between the two data sets, we apply the same procedure that is used in the creation of the CRU data set, namely, the Angular Distance Weighting interpolation method (ADW; Hofstra & New, 2009; New et al., 2000; Shepard, 1968). ADW is a combination of two components. The first one weighs each station by its distance in the radius of 1,200 km (for temperature) from the gridpoint. It

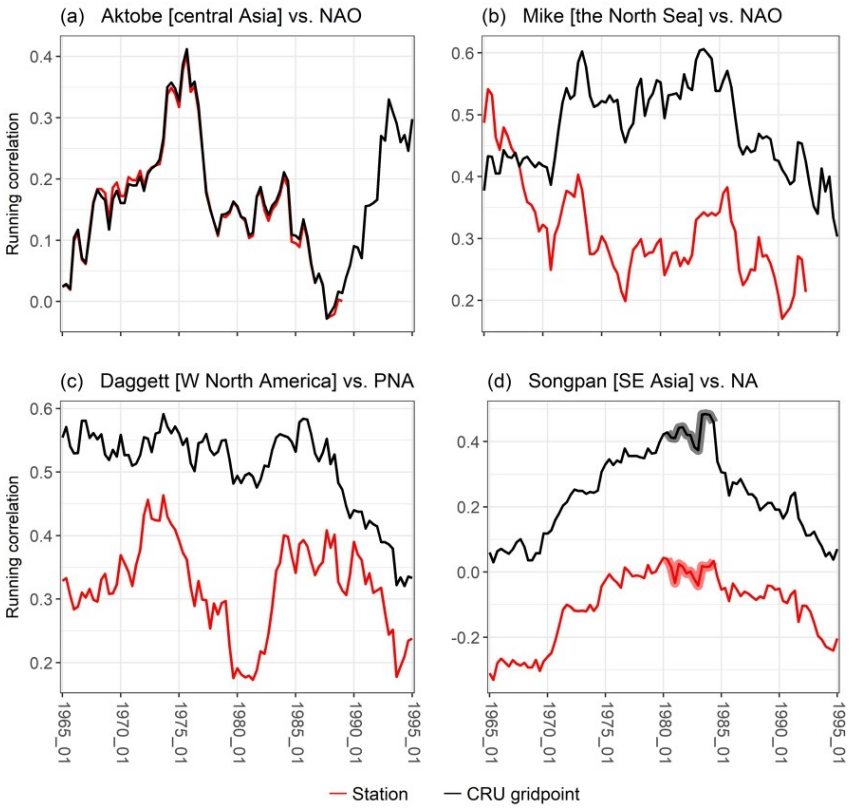

Figure 2. Running correlations (1957–2002) of temperature at four (a, b, c, d) selected stations (red) and their nearest CRU gridpoints (black) with the indicated circulation modes. The locations of stations are depicted in Figure 3. Time series in bold refer to periods with significant differences between running correlations at the 5% level.

controls the contribution of stations to the gridpoint by the exponential function. The second component evaluates the directional isolation of each station and ensures that isolated stations gain more weight (Caesar et al., 2006; Harris et al., 2014; Hofstra & New, 2009; New et al., 2000; Shepard, 1968). ADW thus assigns the largest weight to the stations nearest to the gridpoint and to those being most isolated, the latter preventing the gridpoint to be heavily affected by a region with a high density of observations. We perform ADW to the selected group of stations used for the creation of the CRU data set to explore whether a station network used for gridding may explain differences between station and the nearest gridpoint. The stations contributing to the calculation of a given gridpoint in the CRU data set are found out using a freely available utility in Google Earth (which is maintained by the team around CRU; Harris et al., 2020). Then, temperature anomalies at eight or less selected stations (this condition is also used in the CRU data set) are interpolated in each time step.

3. Results

3.1. Overall Evaluation

Figure 2 displays running correlations for four station-gridpoint pairs. In Figure 2a, the situation one would normally expect is shown: running correlations at the station and the gridpoint almost coincide. The

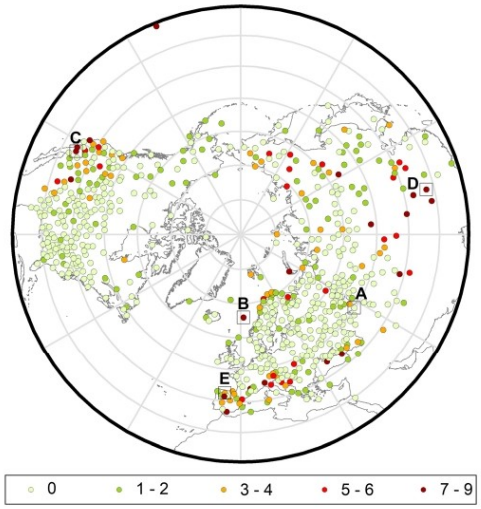

Figure 3. The number of circulation modes with the maximum difference between running correlations at the station and at the closest gridpoint exceeding 0.15. Locations of the sites from Figures 2 and 12 are highlighted by a square and letter (A = Aktobe; B = Mike; C = Daggett; D = Songpan; E = León).

gridpoint almost perfectly represents the relationship with the atmospheric circulation at the nearby station. As we show later, such a high congruity of both time series prevails at most locations. However, there are sites with rather large differences in the time course of circulation-to-temperature relationships between the station and the closest gridpoint, of which we show and discuss several examples. The correlations may run almost in parallel with approximately the same difference through the analysis period as in Songpan for the NA mode (Figure 2d) or the difference of correlations may vary in time as for Mike and NAO (Figure 2b), and Daggett and PNA (Figure 2c). Although the interpolation method contributes to this disagreement as it brings a little smoothing to gridded time series, its effect cannot explain such large differences; there must be other factors causing the discrepancies between the gridded and station data. Differences between running correlations are mostly not statistically significant at the 5% level (after applying the Fisher transformation, see, e.g., Hynčica & Huth, 2020, for the formula and testing details). Nevertheless, their magnitudes often oscillate around 0.3, which is fairly close to being significant (the significance is detected for differences around 0.4). Our intention is to determine the causes responsible for the differences at gridpoint-station pairs; for that purpose, we consider the differences in running correlations large enough to be inspected in more detail regardless of their (in)significance.

The number of circulation modes, for which the maximum difference in running correlations between the station and gridpoint exceeds 0.15, is shown in Figure 3 for all sites. Running correlations are in a high agreement at the majority of station-gridpoint pairs where the large differences are detected for two or fewer circulation modes only. On the other hand, running correlations differ more for the sites located over the southeastern and southern Asia, around the Black Sea, in the Alps, the Iberian Peninsula, locally over Siberia, and in western North America (Figure 3). There are locations where correlations at the station and at the nearest gridpoint differ by more than 0.15 for all the nine modes. In order to identify plausible causes of this disagreement, a deeper analysis of two locations is carried out in the following sections.

3.2. Example 1: Mike

Station Mike (in operation from 1949 to 1999) was an isolated ship station located in the North Sea at 66°N, 2°E. Four gridpoints are located around it at the same distance; we analyze that at 65.75°N, 2.25°E (this choice does not have any effect on our results). Station Mike was utilized in the gridding of the CRU data set and station series in the CRU station database almost perfectly matches that in GHCN. Figure 4 depicts monthly temperature anomalies at the station and the gridpoint, and their running correlations with all circulation modes. Somewhat counterintuitively, anomalies at the gridpoint exhibit larger variability than at the station, although one expects the opposite as the interpolation suppresses local variance (Beguería et al., 2016; Gervais et al., 2014). Considerable differences between running correlations at the station and at the gridpoint occur for all circulation modes, the largest being detected for EU1 (0.46), NA (0.33), and NAO (0.27). Three circulation modes significantly affect temperature at Mike, i.e., their running correlations stay outside the significance bounds for most of time (Figure 4): NAO, EU1, and EU2. Since NAO and EU1 exhibit substantial differences in running correlations during most of the studied period and the differences for the latter mode are significant for a considerable time, both are inspected in more detail. Correlations at the gridpoint are higher than at the station for NAO, while the opposite holds for EU1.

Correlations with NAO and EU1 at all stations that have contributed to the calculation of temperature at the gridpoint closest to Mike at any time during 1901–2016 are shown in Figure 5a. A stronger relationship with NAO and a weaker relationship with EU1 are evident for stations in Scandinavia; this is in accord with how the gridpoint behaves (Figure 4). Figure 5b identifies stations incorporated in the calculation of the gridpoint temperature from 1957 to 2002 (left) and their availability (right). Seven of eight stations that were used for

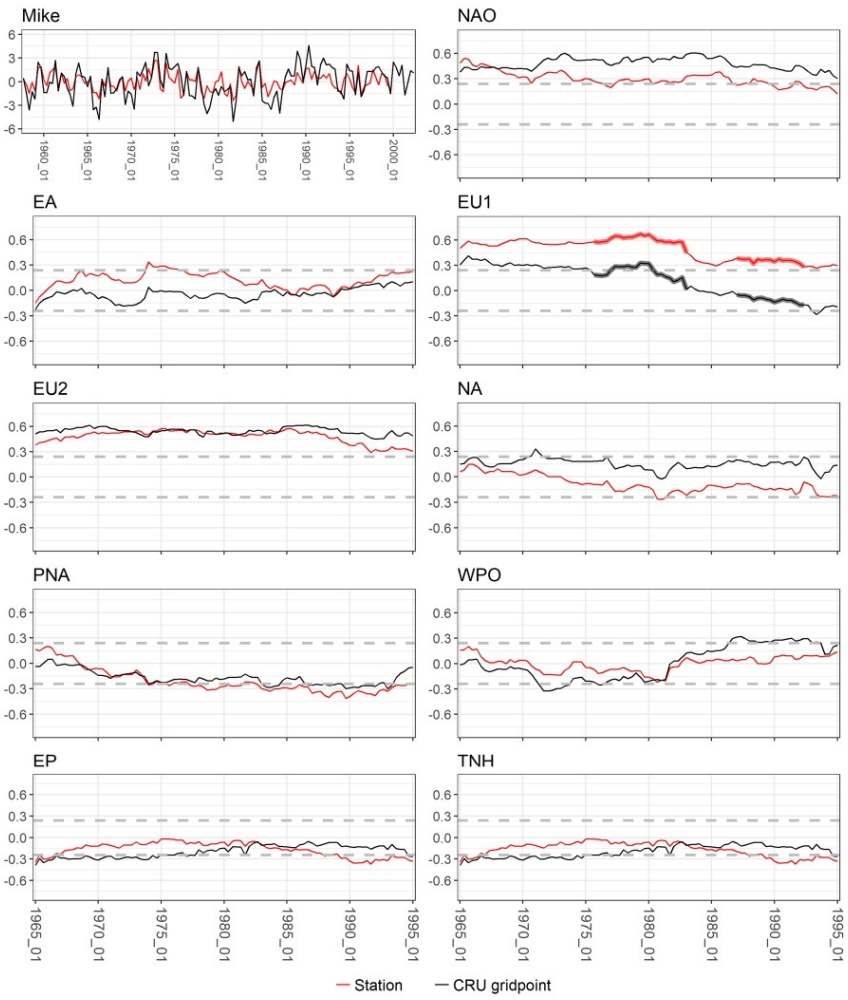

Figure 4. Monthly temperature anomalies (top left) and their running correlations with the circulation modes at station Mike (red) and its closest CRU gridpoint (black). Gray dashed lines show statistical significance at the 5% level, time series in bold refer to periods when differences between running correlations are significant at the 5% level as well.

interpolation to the gridpoint until December 1999, when most of the time series (including Mike) terminate, are situated in Scandinavia where the relationships with atmospheric circulation are different from Mike; the eighth station is Mike itself. Hence, the gridpoint in the CRU data set appears to be heavily affected by Scandinavian stations and the contribution of the nearest station Mike is thus suppressed. This may explain the discrepancy of correlations between the Mike station and the gridpoint.

To verify this hypothesis, we use a selection of stations for reinterpolation of temperature to the CRU gridpoint. We refer to temperature at the gridpoint constructed this way as "reinterpolated temperature" (RIT),

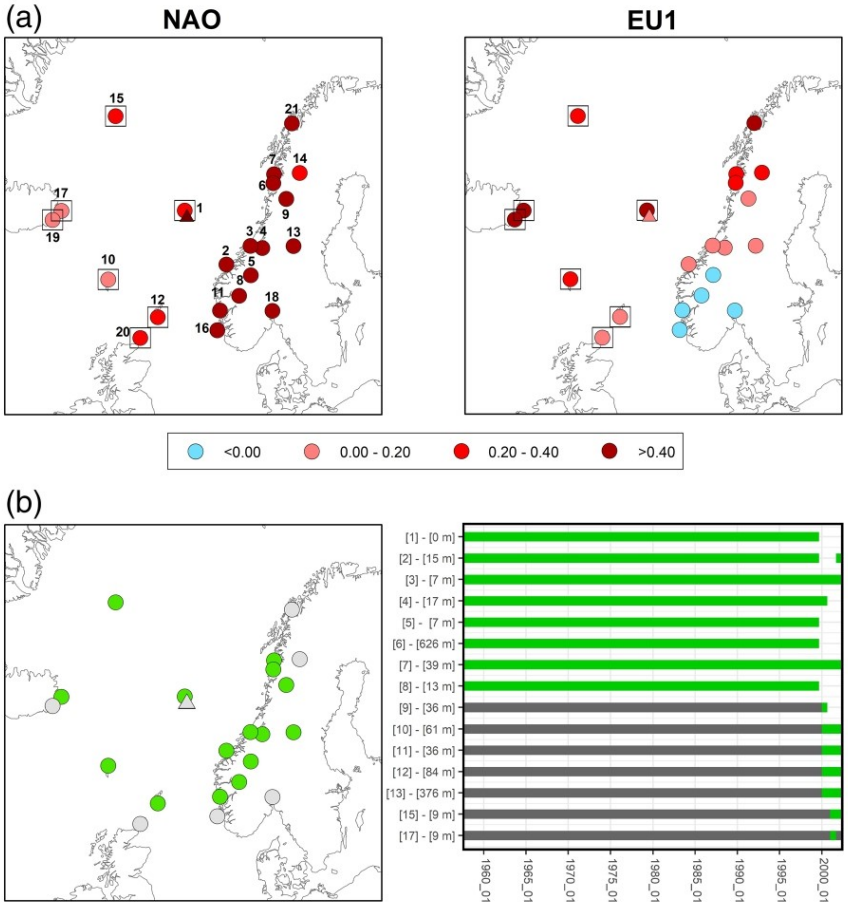

Figure 5. (a) Correlations of stations contributing to the calculation of temperature at the CRU gridpoint closest to Mike (triangle) with NAO (left) and EU1 (right). For station names see Figure 7. Stations highlighted with square are used in reinterpolation. (b) Stations contributing to the CRU gridpoint between 1957 and 2002 (left, in green) and their altitude and availability; with green color highlighting the period when the station contributed to the CRU gridpoint (right). Stations are ordered by the distance, with the nearest station on the top.

while the original temperature at the CRU gridpoint is called "CRU temperature" (CRUT). Only Mike and stations west of it (on Iceland, Jan Mayen, the Faroe Islands, and Shetlands; marked by squares in Figure 5a) are used in reinterpolation. Figure 6 (top) shows that running correlations of RIT with NAO and EU1 are similar to Mike. Dissimilar running correlations of CRUT confirm the high impact of Scandinavian stations, which overweigh the influence of the nearest station, Mike, despite more than double weight assigned to it by ADW compared to other stations. Moreover, a rather high temperature variability of Scandinavian stations is transferred to the gridpoint (Figure 4, top left) where temperature variance is substantially larger than at the station, although one would expect a lower temporal variability due to the influence of sea on local climate at Mike.

Running correlations of RIT and at Mike do not match perfectly, however (Figure 6, top): running correlations with NAO start deviating from each other after 1982, which is caused by decreasing correlations with

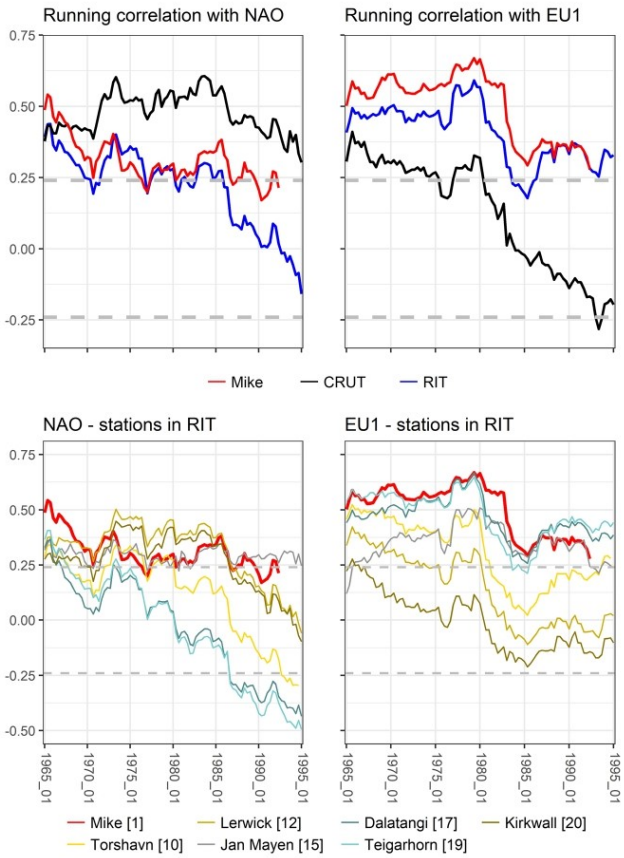

Figure 6. (top) Running correlations of NAO and EU1 with temperature at Mike, its nearest CRU gridpoint (CRUT), and reinterpolated temperature at the gridpoint (RIT); (bottom) running correlations with NAO and EU1 at the stations (numbers refer to the locations shown in Figure 5) used in reinterpolation. Gray dashed lines show statistical significance at the 5% level.

NAO at the majority (five out of seven) of contributing stations in approximately the last 20 years (Figure 6, bottom). That trend projects to RIT, while it is observed only marginally at the station. Running correlations of RIT with EU1 are lower than for Mike until 1987. Afterward, the stagnation or a slight decrease in running correlations at Mike are accompanied by their increases especially at southwestern stations (Dalatangi, Teigarhorn, and Torshavn, Figure 6), which in conclusion causes running correlations of RIT to approach station temperature at Mike.

Aggregated information on relationships with NAO and EU1 for all stations contributing to the CRU gridpoint is given in Figure 7. The correlation of RIT (blue dashed vertical line) is much closer to Mike in comparison with CRUT (black dashed vertical line) for both circulation modes. Mean absolute differences in running correlations between individual stations and CRUT/RIT (black/blue bar) indicate that CRUT shares large similarity with Scandinavian stations, mainly those located in central and southern Norwegian coast. On the other hand, most of the stations west of Mike, used for reinterpolation (shown

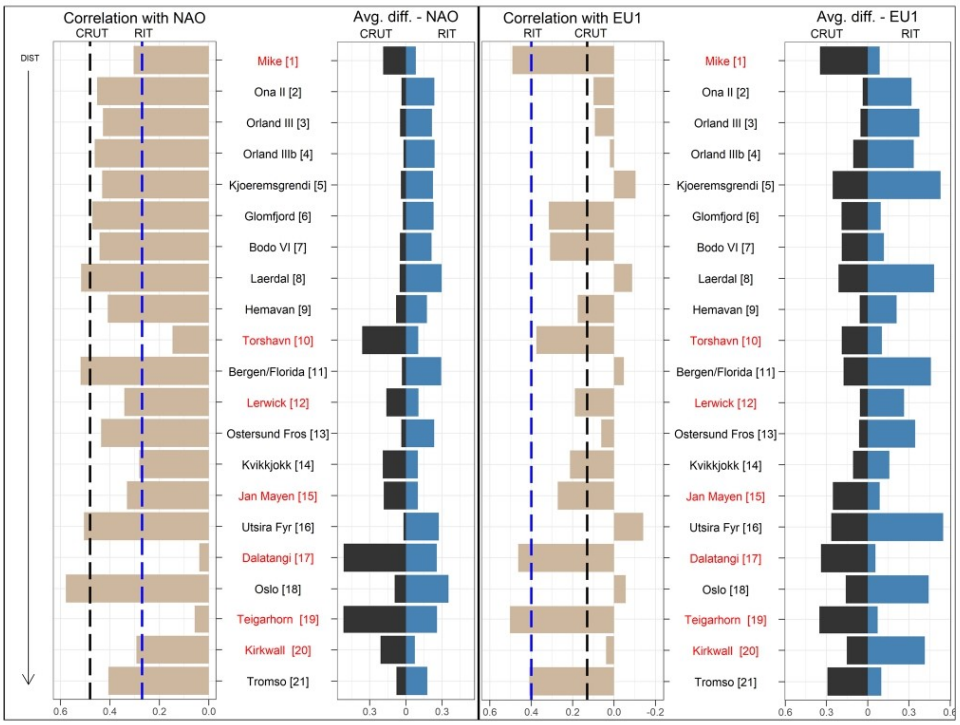

Figure 7. For stations contributing to interpolation to the gridpoint nearest to Mike are shown: correlations with temperature at stations (1957–2002, ordered by their distance from the gridpoint closest to Mike; gray bars in the left graph of each panel), and mean absolute differences in running correlations between stations and CRUT (black), and between stations and RIT (blue; right graph of each panel). Stations in red are used for reinterpolation. Correlations with temperature at the CRU gridpoint and reinterpolated temperature (RIT) are shown by black and blue dashed vertical line, respectively. Left panel is for NAO, right panel for EU1.

in red in Figure 7), exhibit a considerable dissimilarity from CRUT. CRUT is thus driven mainly by easterly located Scandinavian stations, the influence of which overweighs the contribution of the nearest station and results in a substantial discrepancy between the station and its nearest gridpoint in the running correlations with the circulation modes.

3.3. Example 2: Songpan

The other station analyzed in more detail is Songpan, central China (32.65°N, 103.57°E, 2,852 m a.s.l); the closest gridpoint is located at 32.75°N, 103.75°E. It is worthy to note that unlike Mike, Songpan is not included in the gridding of the CRU data set. The site exhibits considerable differences in running correlations for almost all circulation modes (Figure 8), the largest maximum differences being detected for NA (0.50), NAO (0.35), and EU1 (0.33). We present the analysis for the NA and EU1 modes because their running correlations with temperature are significantly different from zero for a considerable time. Running correlations with NA are systematically overestimated at the gridpoint; the opposite behavior is detected for EU1. The same approach as for Mike is applied to uncover causes behind the differences between the station and the closest gridpoint.

Figure 9a shows correlations with NA and EU1 at all stations contributing to the gridpoint closest to Songpan at any time during 1901–2016. Stations form two distinct groups: those located west, northwest,

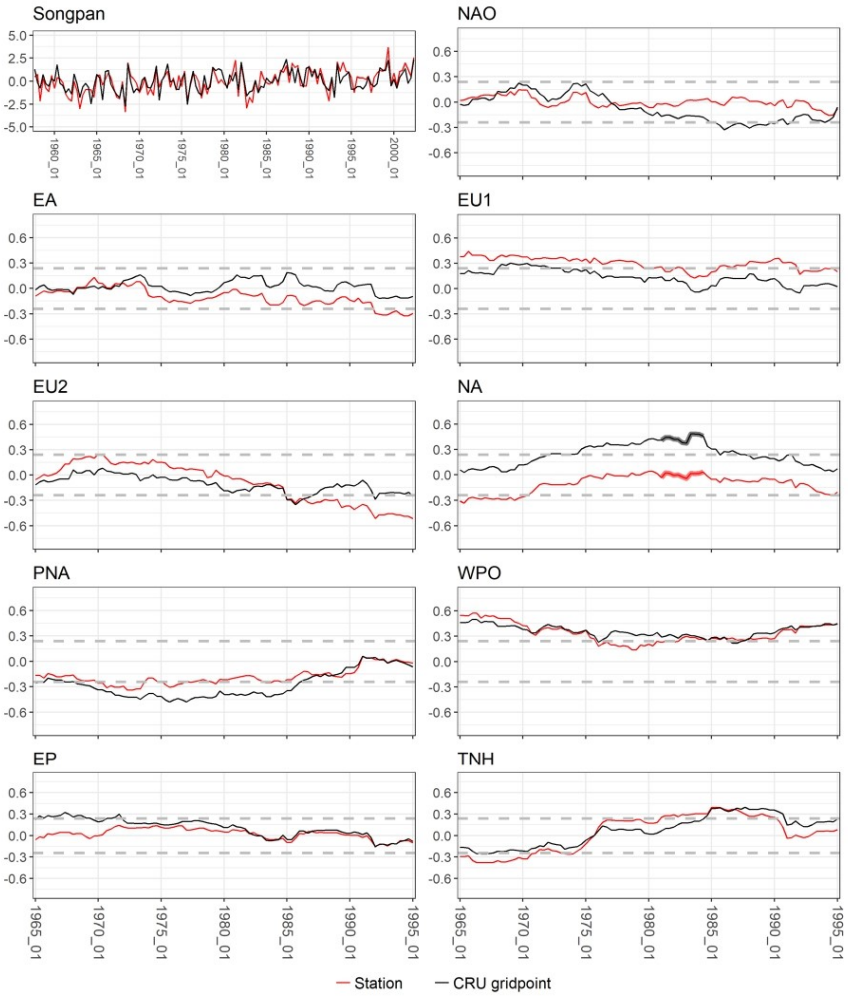

Figure 8. As in Figure 4, but for Songpan.

and south of Songpan correlate positively with EU1, while their correlations with NA are near zero or negative. Stations north, east, southeast, and far southwest of Songpan behave in an opposite way: they correlate positively with NA, but have near zero correlations with EU1. The difference between the two groups appears to be related to elevation (Figure 9b): stations at high elevations form the first group, while stations in the second group are low lying. The Songpan station is situated on the border between the two groups, but at a high elevation. The four stations with the largest influence on CRUT (2, 3, 4, and 5) belong to the second group; that is why the behavior of running correlations of CRUT follows them, although running correlations at the station are similar to the first group, likely because of a similar elevation.

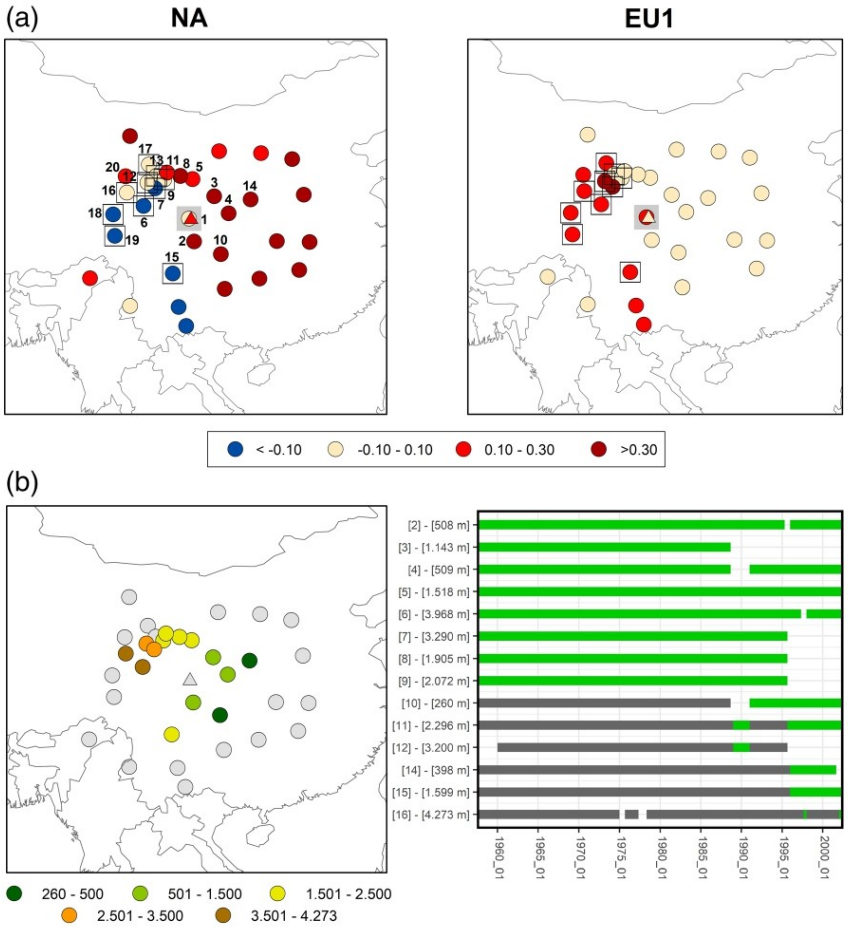

Figure 9. As in Figure 5, except for Songpan. The Songpan site is highlighted by gray square in (a). For station names see Figure 11. For stations contributing to interpolation to the CRU gridpoint in 1957–2002, the elevation is shown in color in (b) left.

The influence of stations in the second group is evaluated by reinterpolation, to which only selected stations from the first group enter (highlighted by squares in Figure 9a). The agreement of RIT with the time series at Songpan is substantially improved relative to CRUT for both modes (Figure 10, top). The match of the time series for NA is very close until 1993 when the decreasing correlation at Songpan is not captured by most stations incorporated in RIT (Figure 10, bottom). A stronger correlation of RIT than of station temperature with EU1 prior to 1982 is caused by the simple fact that most of the contributing stations have a stronger correlation with the mode which, however, decreases in the 1980s.

RIT has a larger similarity with Songpan station than CRUT in both the overall correlation and the average difference of running correlations (Figure 11). On the contrary, CRUT is obviously more similar to stations in the second group (mainly to stations 2, 3, and 4). Thus, the reinterpolation proves that CRUT is substantially affected by lowland stations east of Songpan, the absence of which in reinterpolation results in a better

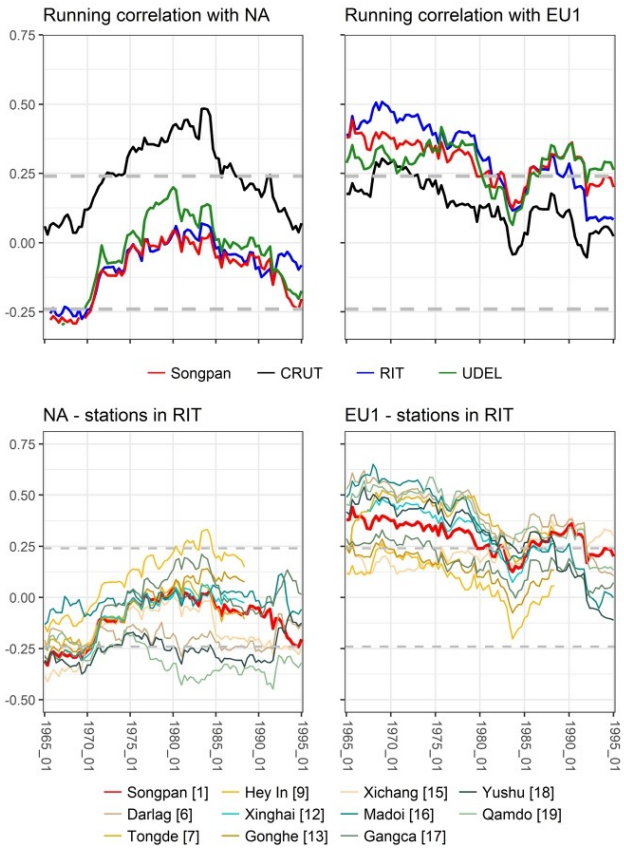

Figure 10. As in Figure 6, but for NA and EU1 at Songpan. UDEL stands for the University of Delaware data set. Numbers refer to locations shown in Figure 9.

congruence with the Songpan station. The influence of elevation is further examined with the use of the University of Delaware Air Temperature & Precipitation data set (UDEL; Willmott & Matsuura, 2001), which incorporates a combination of interpolation methods, including digital elevation model, so the data set is expected to better account for the effect of elevation. Running correlations with the gridpoint in UDEL (in the identical position as in the CRU data set) are fairly similar to the station (Figure 10), which may be caused by either different stations used for interpolation or the utilization of more complex interpolation methods including an elevation model. In any case, it proves that both elevation and inadequate amount of stations entering interpolation in the CRU data set may cause a different behavior of relationships with circulation modes between the station and gridpoint.

3.4. Other Examples

Some stations seem to have unique and very local relationships with atmospheric circulation, which are hard to capture even by interpolation of the close and most similar stations. For instance, the reinterpolation is conducted for various groups of selected stations for the gridpoints nearest to Daggett (western North

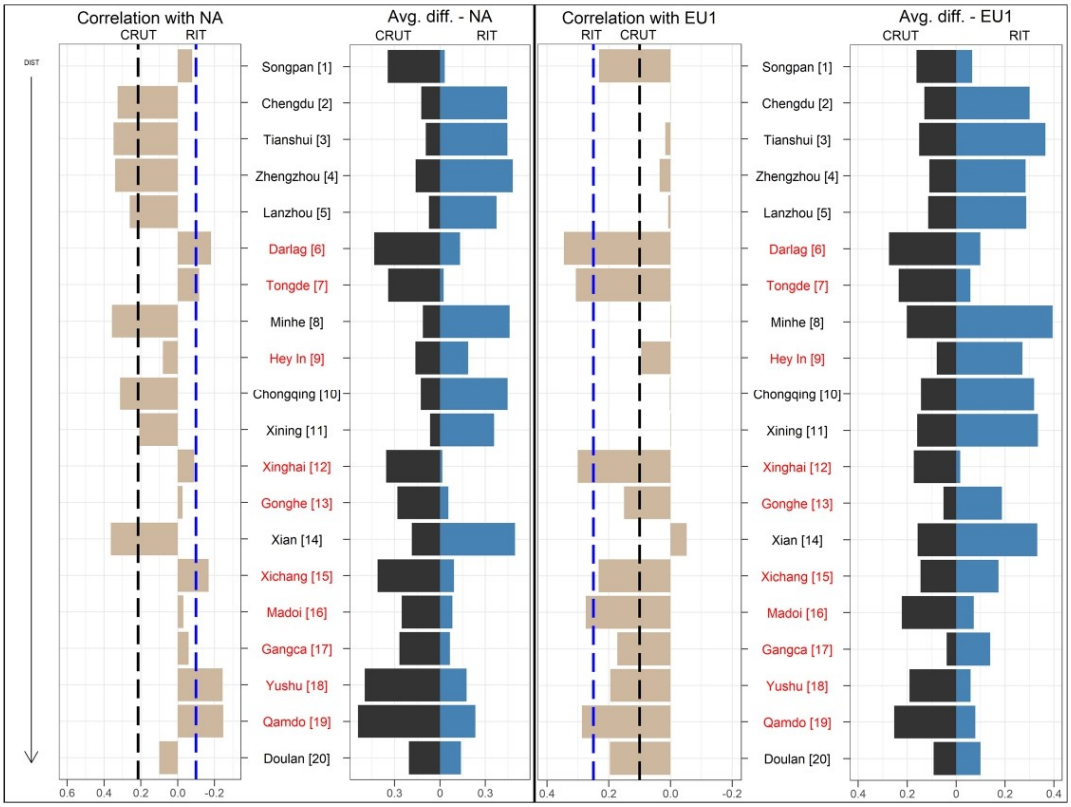

Figure 11. As in Figure 7, but for Songpan. Numbers refer to locations shown in Figure 9.

America) and León (northern Spain). At both gridpoints, only a partial improvement of relationships to circulation is achieved, as the bias between relationships with circulation modes is still present even after the reinterpolation (Figure 12). Thus, a strong signal of a specific local climate cannot be fully reproduced in a gridded data set on some occasions.

4. Discussion and Conclusions

We investigate relationships of temperature at 634 stations and at their closest gridpoints in the CRU data set with nine circulation modes in the Northern Hemisphere Extratropics using running correlations. At the majority of the station-gridpoint pairs, running correlations are in a high agreement; however, some notable exceptions occur mainly over southeastern Asia, the Black Sea, the Iberian Peninsula, foothills of the Alps, and western North America. Some station-gridpoint pairs in these regions exhibit a considerable discrepancy between running correlations for even five and more circulation modes.

We identify the cause of the discrepancy in local geographical and climate settings and illustrate it on two examples. One example is Mike, an isolated ship station in the North Sea. Temperature at the gridpoint nearest to Mike is strongly influenced by rather distant stations on the Scandinavian coast with different relationships with circulation, while the influence of the station itself is suppressed although ADW assigns more

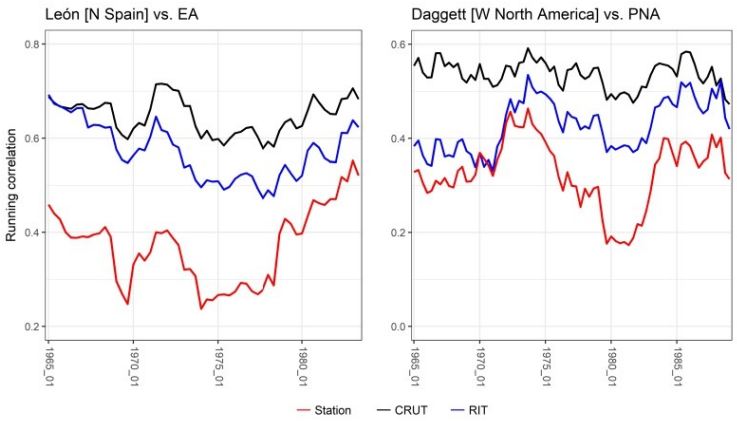

Figure 12. Running correlations of temperature at León (site E in Figure 3) and Daggett (site C in Figure 3), and of CRUT and RIT at the closest gridpoint, with EA and PNA, respectively. The time series are shorter due to the insufficient data needed for reinterpolation.

than double weight to it compared to other stations. The stations located to the west of Mike (on Iceland, the Faroe Islands, and Shetlands) do not enter the interpolation because of their larger distance, despite their similar relationship with circulation. The isolated island position results in rather large differences between the station and gridpoint also, e.g., in Honolulu (21.32°N, 157.93°W). However, the isolated position itself does not automatically imply a disagreement between station and gridded data: some island sites exhibit negligible differences in running correlations (e.g., Jan Mayen, 70.93°N, 8.67°W).

The bias at the other site, Songpan, is explained by the specific terrain setting. Although the station is located at a high elevation near the edge of a mountain plateau, close lowland stations with rather different climate conditions are used in the interpolation, while stations at high elevation and with climate conditions similar to the site are mainly excluded from the interpolation because of their larger distance from the gridpoint. Similar effects can be induced by other geographical barriers, such as mountain ridges (e.g., around the Alps, the Rocky Mountains, and the Scandinavian Mountains), large lakes or inland seas (such as near the Black Sea), or generally vast areas without station data (such as in less populated areas in northern and central Asia).

Gridpoints do not perfectly correspond to the nearest station because they represent spatial average created by interpolation of stations from or even outside the given radius. Interpolation brings some smoothing into gridpoint values, which causes the discrepancy between majority of gridpoints and station observations. Nonetheless, the influence of smoothing on relationships with atmospheric circulation is fairly small because the running correlations with circulation modes are in a high agreement at majority of the sites. For examples discussed above, the spatial setting of station network is more important, leading to overrepresentation of some stations due to either altitude or isolation of the site. In some cases, we cannot even acquire the relationship with atmospheric circulation similar to the nearest station, in spite of various groups of stations entering interpolation. Hypothetically speaking, one way how to improve gridpoint values (and consequently relationships with atmospheric circulation) is to increase the number of observations entering interpolation, which is, however, problematic given the strict quality control rules imposed on station data. The other way might be a modification of the ADW procedure, in which the distance is the only criterion for the selection of stations used for interpolation now. Other criteria might be included in the procedure, such as elevation, variable searching radius, and intercorrelations of station anomalies, all of which should prevent the overrepresentation of some region in a gridpoint. A different interpolation method brings different results: e.g., the interpolation method incorporating elevation in the UDEL data set results in a larger congruence of the Songpan gridpoint/station pair; on the contrary, the other issues may emerge in the data set

over other regions. Although our study uses a specific criterion for evaluation of the gridded data set, the results are relevant also to other gridded data sets, particularly to those created by ADW. Moreover, different issues may arise in a case of considering other climate variables (precipitation, humidity, etc.).

A high station density is supportive to the agreement in correlations with atmospheric circulation between stations and near gridpoints, but does not always guarantee this agreement, as examples from the Iberian Peninsula, northern Scandinavia, and western United States demonstrate. Our study suggests that although gridded data sets are generally a good proxy for station data when relationships with atmospheric circulation are analyzed, one must take the gridded data with caution and examine their suitability (i.e., their correspondence with station data in the analyzed region) before they are used.

Data Availability Statement

We acknowledge ECMWF for providing the ERA-40 reanalysis data, which were downloaded from https://apps.ecmwf.int/datasets/data/era40-moda/levtype=pl/ [downloaded 2016-10-18]. We further acknowledge CRU for providing the CRU TS gridded data set and station time series used for the creation of the data set (both acquired from https://crudata.uea.ac.uk/cru/data/hrg/cru_ts_4.01/ [downloaded 2017-09-08]). Google Earth interface of CRU TS can be accessed from https://crudata.uea.ac.uk/cru/data/hrg/cru_ts_4.04/ge/ [downloaded 2019-05-18] (the original interface for 4.01 is not available anymore). UDEL data are provided by the NOAA/OAR/ESRL PSL, Boulder, Colorado, United States, from https://psl.noaa.gov/data/gridded/data.UDel_AirT_Precip.html [downloaded 2020-08-03]. The GHCN station data (provided by NOAA) were obtained from https://www.ncdc.noaa.gov/data-access/land-based-station-data/land-based-datasets/global-historical-climatology-network-monthly-version-3 and https://gis.ncdc.noaa.gov/maps/ncei/summaries/monthly (in a map format) [downloaded between 2018-02-24 and 2018-03-02].

Acknowledgments
We would like to thank Phil Jones and Ian Harris, Climatic Research Unit at the University of East Anglia, for their helpful comments on the manuscript. This research was supported by the Czech Science Foundation, project 17-07043S. Martin Hynčica was also supported by the Grant Agency of the Charles University, student project 426216.

References

Avila, F. B., Dong, S., Menang, K. P., Rajczak, J., Renom, M., Donat, M. G., & Alexander, L. V. (2015). Systematic investigation of gridding-related scaling effects on annual statistics of daily temperature and precipitation maxima: A case study for south-east Australia. *Weather and Climate Extremes*, *9*, 6–16. https://doi.org/10.1016/j.wace.2015.06.003

Barnston, A. G., & Livezey, R. E. (1987). Classification, seasonality and persistence of low-frequency atmospheric circulation patterns. *Monthly Weather Review*, *115*(6), 1083–1126. https://doi.org/10.1175/1520-0493(1987)115<1083:CSAPOL>2.0.CO;2

Beguería, S., Vicente-Serrano, S. M., Tomás-Burguera, M., & Maneta, M. (2016). Bias in the variance of gridded data sets leads to misleading conclusions about changes in climate variability. *International Journal of Climatology*, *36*(9), 3413–3422.

Beier, C. M., Signell, S. A., Luttman, A., & DeGaetano, A. T. (2012). High-resolution climate change mapping with gridded historical climate products. *Landscape Ecology*, *27*(3), 327–342. https://doi.org/10.1007/s10980-011-9698-8

Beranová, R., & Huth, R. (2008). Time variations of the effects of circulation variability modes on European temperature and precipitation in winter. *International Journal of Climatology*, *28*(2), 139–158. https://doi.org/10.1002/joc.1516

Bueh, C., & Nakamura, H. (2007). Scandinavian pattern and its climatic impact. *Quarterly Journal of the Royal Meteorological Society*, *133*(629), 2117–2131. https://doi.org/10.1002/qj.173

Caesar, J., Alexander, L., & Vose, R. (2006). Large-scale changes in observed daily maximum and minimum temperatures: Creation and analysis of a new gridded data set. *Journal of Geophysical Research*, *111*, D05101. https://doi.org/10.1029/2005JD006280

Cavanaugh, N. R., & Shen, S. S. (2015). The effects of gridding algorithms on the statistical moments and their trends of daily surface air temperature. *Journal of Climate*, *28*(23), 9188–9205. https://doi.org/10.1175/JCLI-D-14-00668.1

Chen, D., & Hellström, C. (1999). The influence of the North Atlantic oscillation on the regional temperature variability in Sweden: Spatial and temporal variations. *Tellus A*, *51*(4), 505–516. https://doi.org/10.3402/tellusa.v51i4.14086

Director, H., & Bornn, L. (2015). Connecting point-level and gridded moments in the analysis of climate data. *Journal of Climate*, *28*(9), 3496–3510. https://doi.org/10.1175/JCLI-D-14-00571.1

Donat, M. G., Sillmann, J., Wild, S., Alexander, L. V., Lippmann, T., & Zwiers, F. W. (2014). Consistency of temperature and precipitation extremes across various global gridded in situ and reanalysis datasets. *Journal of Climate*, *27*(13), 5019–5035. https://doi.org/10.1175/JCLI-D-13-00405.1

Fallah, A., Rakhshandehroo, G. R., Berg, P., Sungmin, O., & Orth, R. (2020). Evaluation of precipitation datasets against local observations in southwestern Iran. *International Journal of Climatology*, *40*(9), 4102–4116. https://doi.org/10.1002/joc.6445

Gervais, M., Tremblay, L. B., Gyakum, J. R., & Atallah, E. (2014). Representing extremes in a daily gridded precipitation analysis over the United States: Impacts of station density, resolution, and gridding methods. *Journal of Climate*, *27*(14), 5201–5218. https://doi.org/10.1175/JCLI-D-13-00319.1

Gross, M. H., Donat, M. G., Alexander, L. V., & Sisson, S. A. (2018). The sensitivity of daily temperature variability and extremes to dataset choice. *Journal of Climate*, *31*(4), 1337–1359. https://doi.org/10.1175/JCLI-D-17-0243.1

Harris, I., Jones, P. D., Osborn, T. J., & Lister, D. H. (2014). Updated high-resolution grids of monthly climatic observations–the CRU TS3.10 dataset. *International Journal of Climatology*, *34*(3), 623–642. https://doi.org/10.1002/joc.3711

Harris, I., Osborn, T. J., Jones, P., & Lister, D. (2020). Version 4 of the CRU TS monthly high-resolution gridded multivariate climate dataset. *Scientific Data*, *7*(1), 1–18.

Herold, N., Alexander, L. V., Donat, M. G., Contractor, S., & Becker, A. (2016). How much does it rain over land? *Geophysical Research Letters*, *43*, 341–348. https://doi.org/10.1002/2015GL066615

Herrera, S., Kotlarski, S., Soares, P. M., Cardoso, R. M., Jaczewski, A., Gutiérrez, J. M., & Maraun, D. (2019). Uncertainty in gridded precipitation products: Influence of station density, interpolation method and grid resolution. *International Journal of Climatology*, *39*(9), 3717–3729. https://doi.org/10.1002/joc.5878

Hofstra, N., Haylock, M., New, M., & Jones, P. D. (2009). Testing E-OBS European high-resolution gridded data set of daily precipitation and surface temperature. *Journal of Geophysical Research*, *114*, D21101. https://doi.org/10.1029/2009JD011799

Hofstra, N., & New, M. (2009). Spatial variability in correlation decay distance and influence on angular-distance weighting interpolation of daily precipitation over Europe. *International Journal of Climatology*, *29*(12), 1872–1880. https://doi.org/10.1002/joc.1819

Hofstra, N., New, M., & McSweeney, C. (2010). The influence of interpolation and station network density on the distributions and trends of climate variables in gridded daily data. *Climate Dynamics*, *35*(5), 841–858. https://doi.org/10.1007/s00382-009-0698-1

Huth, R. (2006). The effect of various methodological options on the detection of leading modes of sea level pressure variability. *Tellus A: Dynamic Meteorology and Oceanography*, *58*(1), 121–130. https://doi.org/10.1111/j.1600-0870.2006.00158.x

Huth, R., Pokorná, L., Bochníček, J., & Hejda, P. (2006). Solar cycle effects on modes of low-frequency circulation variability. *Journal of Geophysical Research*, *111*, D22107. https://doi.org/10.1029/2005JD006813

Hynčica, M., & Huth, R. (2020). Modes of atmospheric circulation variability in the Northern Extratropics: A comparison of five reanalyses. *Journal of Climate*. https://doi.org/10.1175/JCLI-D-19-0904.1

Iles, C., & Hegerl, G. (2017). Role of the North Atlantic oscillation in decadal temperature trends. *Environmental Research Letters*, *12*(11), 114010. https://doi.org/10.1088/1748-9326/aa9152

Jacobeit, J., Jönsson, P., Bärring, L., Beck, C., & Ekström, M. (2001). Zonal indices for Europe 1780–1995 and running correlations with temperature. *Climatic Change*, *48*(1), 219–241. https://doi.org/10.1023/A:1005619023045

Jung, T., Hilmer, M., Ruprecht, E., Kleppek, S., Gulev, S. K., & Zolina, O. (2003). Characteristics of the recent eastward shift of interannual NAO variability. *Journal of Climate*, *16*(20), 3371–3382. https://doi.org/10.1175/1520-0442(2003)016<3371:COTRES>2.0.CO;2

Krauskopf, T., & Huth, R. (2020). Temperature trends in Europe: Comparison of different data sources. *Theoretical and Applied Climatology*, *139*(3–4), 1305–1316. https://doi.org/10.1007/s00704-019-03038-w

Lawrimore, J. H., Menne, M. J., Gleason, B. E., Williams, C. N., Wuertz, D. B., Vose, R. S., & Rennie, J. (2011). An overview of the Global Historical Climatology Network monthly mean temperature data set, version 3. *Journal of Geophysical Research*, *116*, D19121. https://doi.org/10.1029/2011JD016187

Li, J., & Ruan, C. (2018). The North Atlantic–Eurasian teleconnection in summer and its effects on Eurasian climates. *Environmental Research Letters*, *13*(2), 024007. https://doi.org/10.1088/1748-9326/aa9d33

Lim, Y. K. (2015). The East Atlantic/West Russia (EA/WR) teleconnection in the North Atlantic: Climate impact and relation to Rossby wave propagation. *Climate Dynamics*, *44*(11–12), 3211–3222. https://doi.org/10.1007/s00382-014-2381-4

Linkin, M. E., & Nigam, S. (2008). The North Pacific oscillation–west Pacific teleconnection pattern: Mature-phase structure and winter impacts. *Journal of Climate*, *21*(9), 1979–1997. https://doi.org/10.1175/2007JCLI2048.1

Liu, Y., Wang, L., Zhou, W., & Chen, W. (2014). Three Eurasian teleconnection patterns: Spatial structures, temporal variability, and associated winter climate anomalies. *Climate Dynamics*, *42*(11–12), 2817–2839.

Moore, G. W. K., & Renfrew, I. A. (2012). Cold European winters: Interplay between the NAO and the East Atlantic mode. *Atmospheric Science Letters*, *13*(1), 1–8. https://doi.org/10.1002/asl.356

New, M., Hulme, M., & Jones, P. (2000). Representing twentieth-century space–time climate variability. Part II: Development of 1901–96 monthly grids of terrestrial surface climate. *Journal of Climate*, *13*(13), 2217–2238. https://doi.org/10.1175/1520-0442(2000)013<2217:RTCSTC>2.0.CO;2

Piper, D. A., Kunz, M., Allen, J. T., & Mohr, S. (2019). Investigation of the temporal variability of thunderstorms in Central and Western Europe and the relation to large-scale flow and teleconnection patterns. *Quarterly Journal of the Royal Meteorological Society*, *145*(725), 3644–3666. https://doi.org/10.1002/qj.3647

Pokorná, L., & Huth, R. (2015). Climate impacts of the NAO are sensitive to how the NAO is defined. *Theoretical and Applied Climatology*, *119*(3–4), 639–652.

Polyakova, E. I., Journel, A. G., Polyakov, I. V., & Bhatt, U. S. (2006). Changing relationship between the North Atlantic oscillation and key North Atlantic climate parameters. *Geophysical Research Letters*, *33*, L03711. https://doi.org/10.1029/2005GL024573

Raible, C. C., Lehner, F., González Rouco, J. F., & Fernández Donado, L. (2014). Changing correlation structures of the Northern Hemisphere atmospheric circulation from 1000 to 2100 AD. *Climate of the Past*, *10*(2), 537–550. https://doi.org/10.5194/cp-10-537-2014

Rhines, A., McKinnon, K. A., Tingley, M. P., & Huybers, P. (2017). Seasonally resolved distributional trends of North American temperatures show contraction of winter variability. *Journal of Climate*, *30*(3), 1139–1157. https://doi.org/10.1175/JCLI-D-16-0363.1

Shepard, D. (1968). A two-dimensional interpolation function for irregularly-spaced data. In *Proceedings of the 1968 23rd ACM national Conference* (pp. 517–524). ACM.

Shi, H., Li, T., & Wei, J. (2017). Evaluation of the gridded CRU TS precipitation dataset with the point raingauge records over the Three-River Headwaters Region. *Journal of Hydrology*, *548*, 322–332. https://doi.org/10.1016/j.jhydrol.2017.03.017

Slonosky, V. C., Jones, P. D., & Davies, T. D. (2001). Atmospheric circulation and surface temperature in Europe from the 18th century to 1995. *International Journal of Climatology*, *21*(1), 63–75. https://doi.org/10.1002/joc.591

Uppala, S. M., Kållberg, P. W., Simmons, A. J., Andrae, U., da Costa Bechtold, V., Fiorino, M., et al. (2005). The ERA-40 re-analysis. *Quarterly Journal of the Royal Meteorological Society*, *131*(612), 2961–3012. https://doi.org/10.1256/qj.04.176

van der Schrier, G., van den Besselaar, E. M., Klein Tank, A. M. G., & Verver, G. (2013). Monitoring European average temperature based on the E-OBS gridded data set. *Journal of Geophysical Research: Atmospheres*, *118*, 5120–5135. https://doi.org/10.1002/jgrd.50444

Wallace, J. M., & Gutzler, D. S. (1981). Teleconnections in the geopotential height field during the Northern Hemisphere winter. *Monthly Weather Review*, *109*(4), 784–812. https://doi.org/10.1175/1520-0493(1981)109<0784:TITGHF>2.0.CO;2

Wang, N., & Zhang, Y. (2015). Evolution of Eurasian teleconnection pattern and its relationship to climate anomalies in China. *Climate Dynamics*, *44*(3–4), 1017–1028. https://doi.org/10.1007/s00382-014-2171-z

Willmott, C. J., & Matsuura, K. (2001). Terrestrial air temperature and precipitation: Monthly and annual time series (1900–2017) version 5.01. *Center for Climatic Research, University of Delaware, Newark*.

Willmott, C. J., & Robeson, S. M. (1995). Climatologically aided interpolation (CAI) of terrestrial air temperature. *International Journal of Climatology*, *15*(2), 221–229. https://doi.org/10.1002/joc.3370150207

Xu, Y., Zhao, P., Si, D., Cao, L., Wu, X., Zhao, Y., & Liu, N. (2020). Development and preliminary application of a gridded surface air temperature homogenized dataset for China. *Theoretical and Applied Climatology*, *139*(1–2), 505–516. https://doi.org/10.1007/s00704-019-02972-z

Yu, B., Lin, H., Wu, Z. W., & Merryfield, W. J. (2018). The Asian–Bering–North American teleconnection: Seasonality, maintenance, and climate impact on North America. *Climate Dynamics*, *50*(5–6), 2023–2038. https://doi.org/10.1007/s00382-017-3734-6

Zhu, X., Zhang, M., Wang, S., Qiang, F., Zeng, T., Ren, Z., & Dong, L. (2015). Comparison of monthly precipitation derived from high-resolution gridded datasets in arid Xinjiang, central Asia. *Quaternary International*, *358*, 160–170. https://doi.org/10.1016/j.quaint.2014.12.027

Zuo, J., Ren, H. L., Li, W., & Wang, L. (2016). Interdecadal variations in the relationship between the winter North Atlantic oscillation and temperature in south-Central China. *Journal of Climate*, *29*(20), 7477–7493. https://doi.org/10.1175/JCLI-D-15-0873.1

4. Temporal evolution of relationships between surface climatic variables and circulation modes

The ERA-20C reanalysis and the CRU dataset were shown to be appropriate datasets for purposes of this study. Hence, the temporal evolution of relationships between circulation modes (from ERA-20C) and surface temperature and precipitation (both from the CRU dataset) is determined by 15-year running correlations. The analysis is conducted for 1901-2010 for winter (DJF). Time series of running correlations are then clustered to determine regions where the behaviour of relationships with atmospheric circulation is similar. It is shown that changes in action centres, mainly their position, intensity, and shape, affect spatiotemporal impact of circulation modes on surface climatic variables.

Paper IV: Hynčica, M., Huth, R. (2022). Temporal variation of relationships between circulation modes and surface climatic variables in the 20th century in winter. *Journal of Climate*. In Review.

Temporal variation of relationships between circulation modes and surface climatic variables in the 20th century in winter

Martin Hynčica [1, 2], Radan Huth [1, 3]

[1] Dept. of Physical Geography and Geoecology, Faculty of Science, Charles University, Albertov 6, 128 43, Prague, Czechia

[2] Dept. of Environment, Faculty of Environment, Jan Evangelista Purkyně University, Pasteurova 15, 400 96, Ústí nad Labem, Czechia

[3] Institute of Atmospheric Physics, Czech Academy of Sciences, Boční II 1401, 141 31, Prague, Czechia

Corresponding author: **Martin Hynčica:** martin.hyncica@natur.cuni.cz

Abstract

Circulation modes undergo decadal variability, which also affects spatiotemporal impact of modes on climatic variables on long time scales. Previous studies focused either to one circulation mode or to limited geographical area. In this study, the topic is substantially extended as we provide an overview of long-term variations of nine circulation modes in winter and their impact on relationships with surface climatic variables, that is, temperature and precipitation, during the 20th century over the Northern Extratropics. Circulation modes are identified by rotated Principal Component Analysis of 500 hPa geopotential heights in the ERA-20C reanalysis; gridded surface climatic data are gained from the CRUTS dataset. Temporal variations of relationships are evaluated by 15-year running correlations between circulation modes and climatic variables at all land gridpoints. Time series of running correlations with all nine circulation modes at all gridpoints are clustered using the partitioning around medoids (PAM) method into 18 and 11 clusters for temperature and precipitation, respectively. Composite maps, displaying the modes during specific periods of strengthened, weakened, and normal relationships with climatic variables, are used for determination of mechanisms responsible for the variation of relationships. The main mechanisms are changes in the location, shape, and intensity of centres, and formation or split of centres. These mechanisms affect mainly the intensity and direction of advection, which translate into the magnitude of relationships. Possible causes of changes in circulation modes are linked with El Niño-Southern Oscillation (ENSO), shifts of the Pacific Decadal Oscillation (PDO), and long-term changes in the sea ice extent.

Keywords: atmospheric circulation, circulation modes, teleconnections, non-stationarity, temporal variation

1. Introduction

Modes of low-frequency variability of atmospheric circulation ('circulation modes' for brevity), also referred as teleconnections in literature, are composed of typically two or more mutually correlated centres, all of which simultaneously strengthen and/or weaken. The modes modify various climatic variables, such as temperature, winds, and precipitation. The most often studied circulation modes are the North Atlantic Oscillation (NAO) and the Pacific-North American pattern (PNA). Two centres of the former are located over the Atlantic Ocean and pressure gradient between them modulates the strength of westerlies into Eurasia, hence influencing climatic variables across much of the continent (e.g. Hurrell 1995; Wanner et al. 2001; Trigo et al. 2002). The PNA pattern consists of four centres over the Pacific Ocean and North America, regulates the undulation of zonal flow, and accounts for variation of climatic variables mainly in North America (Leathers et al. 1991; Soulard et al. 2019).

Circulation modes undergo spatiotemporal variability in a short-term (days, weeks, months) and long-term (years, decades) range. The decadal variability of circulation modes manifests in changes in position, intensity, and shapes of circulation modes, which subsequently lead to a strengthening or weakening of relationships with climatic variables on long time scales. An illustration of such a variability is the widely studied response of surface climatic variables to the eastward migration of NAO in the second half of the 20th century, which led to larger correlations with temperature and precipitation over Eurasia (Jung et al. 2003; Beranová and Huth 2008; Vicente-Serrano and López-Moreno 2008; Yadav et al. 2009; Filippi et al. 2014; Xu et al. 2016; Zuo et al. 2016; Marshall 2021). Yet, decadal changes in relationships between circulation modes and surface climatic variables have been studied rarely. Beranová and Huth (2008) analyse non-stationarity of precipitation and temperature linkage with four modes over Europe, whereas Krichak et al. (2002) study the decadal change in relationships with two circulation modes in the eastern Mediterranean. Marshall (2021) describes changing relationships with circulation modes over Northern Russia. Hertig et al. (2015) provide a review of non-stationarities in circulation modes in Europe and the North Atlantic.

All the studies mentioned above analyse station data in the second half of the 20th century. To our knowledge, however, no study has investigated changes in relationships with surface

climatic variables during the whole 20th century, for all circulation modes, and using surface gridded data. Hence, this study fills this gap by analysing decadal variation of relationships between circulation modes and temperature and precipitation data from a gridded dataset between 1901 and 2010 in winter.

2. Data and methodology

The analysis is conducted for winter (December, January, and February) between 1901 and 2010 for the northern Extratropics (delimited by 20° N). The analysed period is determined by the temporal availability of the utilized datasets.

2.1 Identification of circulation modes

The ERA-20C reanalysis (Poli et al. 2016) is employed for the detection of circulation modes. The common characteristic of reanalyses covering the entire 20th century is the assimilation of surface data only. Specifically, ERA-20C is computed with the use of surface pressure and marine winds only. Hynčica and Huth (2020a) show that circulation modes in ERA-20C are largely consistent with "traditional" full-input reanalyses, which are considered more reliable owing to the assimilation of much more data from radiosondes, satellites, and other sources, allowing the three-dimensional structure of atmosphere to be fully captured. Another reanalysis covering the 20th century, 20CRv2c (Compo et al. 2011), has been shown to contain biases over southern Asia, which result in a different spatial representation of some circulation modes (Hynčica and Huth, 2020a). These biases have been eliminated in its new version, 20CRv3 (Slivinski et al. 2019), which is confirmed by its comparison with four other reanalyses (Hynčica and Huth, 2022). Nevertheless, ERA-20C is preferred in this study because its circulation modes are largely consistent with other reanalyses in all seasons (Hynčica and Huth, 2020a), which adds more confidence to mid-troposphere pressure fields in ERA-20C.

Circulation modes are detected with the use of Principal Component Analysis (PCA) with correlation matrix. We utilize monthly anomalies of 500 hPa geopotential heights on the 5°x5° grid. The effect of converging meridians towards the pole, which negatively influences outputs of PCA, is eliminated by using a quasi-equal-area grid, that is, by omitting gridpoints so that the mean area of a grid box is approximately the same in all latitudes (Araneo and

Compagnucci 2004; Huth 2006; Hynčica and Huth 2020a). Varimax rotation is then applied to the selected number of components. The number of components to rotate is assessed with the use of a scree-plot (Fig. S1) where explained variance is plotted against the order of components; the rightmost drop on the plot indicates the number of components to rotate. Whereas the scree-plot indicates that ten components should be rotated (Fig. S1), we prefer to rotate nine components in order to make our study consistent with other studies (Barnston and Livezey 1987, Huth et al. 2006, Hynčica and Huth 2020a). All components correspond to well-known circulation modes. The outputs of PCA are loadings (spatial representation of modes giving correlations of modes with the original data field), scores (temporal intensity of modes), and explained variance of individual modes.

2.2 Running correlations

Temperature and precipitation data are obtained from the Climatic Research Unit Time Series v. 4.03 dataset (Harris et al. 2020), hereafter named as the CRU dataset. CRU data are available at land grid points only. Relationships with circulation modes in the CRU dataset are largely consistent with the station data (Hynčica and Huth, 2020b), hence, we consider it reliable for our purposes. The original resolution of the CRU dataset (0.5 x 0.5°) is lowered by omitting every second gridpoint, the amount of considered gridpoints being, therefore, 23.112 for temperature. However, some gridpoints with no precipitation data, mainly over Greenland and the Sahara, are left out; number of analysed gridpoints for precipitation is 22.193.

Running correlations with the window of 45 months and the one-month step are calculated between time series of the intensities (scores) of the nine circulation modes and temperature and precipitation anomalies from long-term averages at each gridpoint. The running windows are labelled by their central month. Hence, time series of running correlations start in February 1908 (corresponding to period January 1901 – December 1915) and end in February 2003 (corresponding to January 1996 – December 2010). They describe how the influence of modes on temperature and precipitation was changing during the 20th century at each gridpoint.

2.3 Cluster analysis

Having a huge number of time series of running correlations, which are difficult to handle, cluster analysis is utilized to aggregate information on the behaviour of running correlations over large geographical areas. Of many existing clustering methods, we opt for "partitioning around medoids" (PAM) with Euclidean distance, which is carried out in the R environment with the use of the *clara* package (Kaufman and Rousseeuw 1990). This method is relatively computationally inexpensive and fairly effective. The principle of PAM is the detection of representative objects (time series in our case), that is, medoids, around which clustering with Euclidean distance proceeds. All time series are assigned to the nearest medoid, which leads to formation of clusters. Euclidean distance represents square root of sum-of-squares of differences between medoids and individual objects. Other measures that were also tested (e.g. Manhattan distance, dynamic time wrapping, and Pearson correlation coefficient) brought either fairly similar results or solutions, in which clusters were highly geographically incoherent.

Before entering cluster analysis, time series of running correlations are multiplied by the absolute value of long-term correlation (that is, correlation over the entire analysis period). This approach allows strong correlations of either sign to have a larger weight in the clustering procedure as it amplifies running correlations with circulation modes holding strong relationships, that is, having large long-term correlation, while weak relationships are suppressed. This is appropriate since we are interested in time variations of really existing relationships and not in relationships with no effect on temperature and precipitation that lack statistical significance; it is also appropriate that strong relationships (i.e., higher correlations) have a stronger effect on the result of clustering than weak ones. The time series adjusted for the strength of correlation are concatenated, which results in one series of running correlations with all nine circulation modes at each gridpoint. These series are then clustered by the PAM method. The determination of the number of clusters is somewhat subjective. We estimate the number of clusters manually by comparing solutions from 10 to 20 clusters. Clusters should be as geographically coherent as possible; the best solution that we choose seems to be 18 clusters for temperature and 11 clusters for precipitation.

Time series in clusters are then filtered in two steps with the objective that information on time variation of relationships is conveyed in as clear way as possible. Firstly, there are time series weakly temporally correlated with some circulation modes. Therefore, for each cluster and circulation mode, time series with majority of running correlations close to zero, that is, with at least 66 % of values of running correlations being within ±0.3 (for temperature) or ±0.25 (for precipitation), are not considered in further analysis. In addition, for clusters in which the proportion of such removed time series exceeds 90 %, the relationship with a circulation mode is not analysed. Secondly, small groups of time series that substantially differ from the rest of time series for a specific mode and a specific cluster in terms of magnitude and/or temporal course, are not considered in further analysis. An example is the few time series with the most positive correlations with temperature for PNA in cluster 3 (second column and third row in Fig. S2). This applies mainly for time series assigned to geographically incoherent clusters (e.g. those containing island stations). The number of such removed time series is fairly small, usually not exceeding 20 for one cluster, so the impact on results is negligible. Both steps lead to the reduction of data analysed and displayed while bringing clearer results at the expense of losing little information only.

Some clusters contain two courses of running correlations with opposite signs. Those two courses can run nearly parallel (e.g. temperature and WPO in cluster 1; first column and first row in Fig. S2) or completely different (e.g. temperature and EA in cluster 9; sixth column and ninth row in Fig. S2). This feature is inherent to clustering because some clusters cover areas with opposite relationships with circulation modes. However, to keep the results clear, the displayed time series always represents the dominant branch, i.e. that containing more gridpoints.

Composite maps for all running periods are calculated as a difference of 500 hPa height composites when the intensity of a circulation mode is larger than +1 and lower than -1. They are utilized for the explanation of changes in relationships with climatic variables. Action centres are defined as the largest or lowest value in composite maps in all running periods, respectively to each circulation mode. We can therefore compile time series of the position and strength of action centres. Note that all years and periods in the following text correspond to 15-year running periods, not to exact dates.

3 Results

Fig. 1 displays nine circulation modes in ERA-20C with their respective explained variance and abbreviations adopted from Barnston and Livezey (1987). Note that Eurasian pattern type 1 is not identified even if other numbers of components are rotated. The pattern resembling the Eurasian pattern identified by Wallace and Gutzler (1981) and Liu et al. (2014) is detected instead and named here Eurasian pattern Type 3 (EU3).

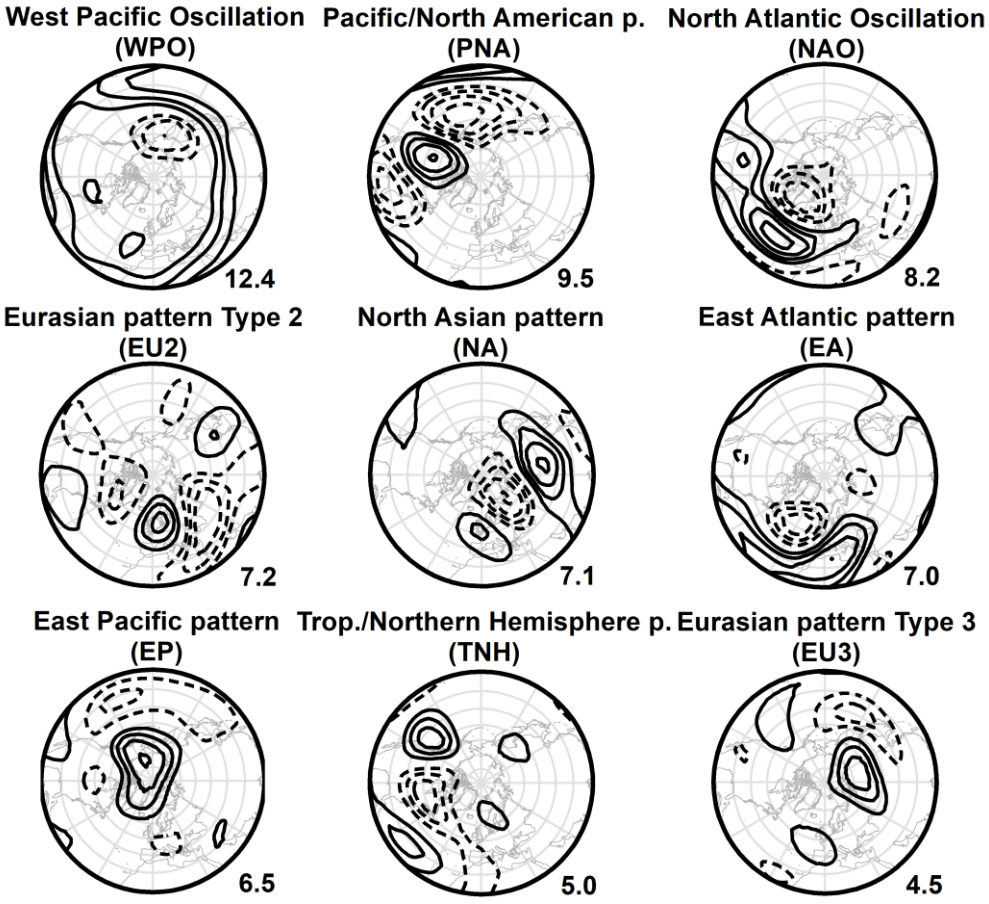

FIG. 1. Circulation modes in winter (1901-2010) in ERA-20C, their abbreviations, and explained variance (in %).

Analysed time series satisfying conditions presented in Sec. 2.3 and the average running correlations over all analysed gridpoints for each cluster and circulation mode are displayed in Figs. S2 and S3. Time series of corresponding anomalies from the long-term average correlation (that is, average of correlations for all running periods) for temperature and precipitation are shown in lower parts of Figs. 2 and 3, respectively. The running correlations

with a mode representative for the cluster are calculated only from the time series with a non-negligible relationship to a circulation mode, that is, with at least 34% of running correlations exceeding the threshold (±0.3 for temperature and ±0.25 for precipitation). The percentage of such time series for each cluster-mode pair is indicated by the width of a bar. Normal relationship is when running correlations are within ±0.1 around the long-term correlation. Anomalies of running correlations larger than 0.1 indicate periods of either strengthened (if approaching ±1) or weakened (if approaching 0) relationships. In the following sections, we do not mention references to Figs. 2 and 3 for each circulation mode due to length of the text.

Cluster analysis delimits large areas where temporal evolution of relationships with all nine circulation modes is approximately similar. However, some clusters are not spatially consistent; for example, some island stations belong to distant clusters (e.g. for temperature, parts of Ryukyu Islands belong to cluster 3 in North America; Fig. 2). An even more striking example is cluster 9 for temperature, which is divided into two geographically distant areas: southwestern US and southeastern Europe to western Siberia (Fig. 2). Discrepancies in the CRU dataset (Hynčica and Huth 2020b) may partly explain why cluster analysis merges distant areas into one cluster. Nevertheless, filtering of time series in clusters (Sec. 2.3.) minimizes the impact of such distant locations on the characteristic temporal course of correlation anomalies as shown in Figs. 2 and 3. This is exemplified for temperature in cluster 9: the impact of its minor part in North America is suppressed and the cluster therefore corresponds to the Eurasian climate. Because relationships of modes with precipitation are generally weaker and more regionalized, some clusters are divided into several distant areas (clusters 8 and 9, Fig. 3). The large blank cluster (Fig. 3) aggregates regions where only one or no circulation mode has non-negligible influence (as defined by the thresholds for running correlations introduced in Sec. 2.3) on precipitation (Fig. S4), which is why cluster analysis does not divide it into additional clusters.

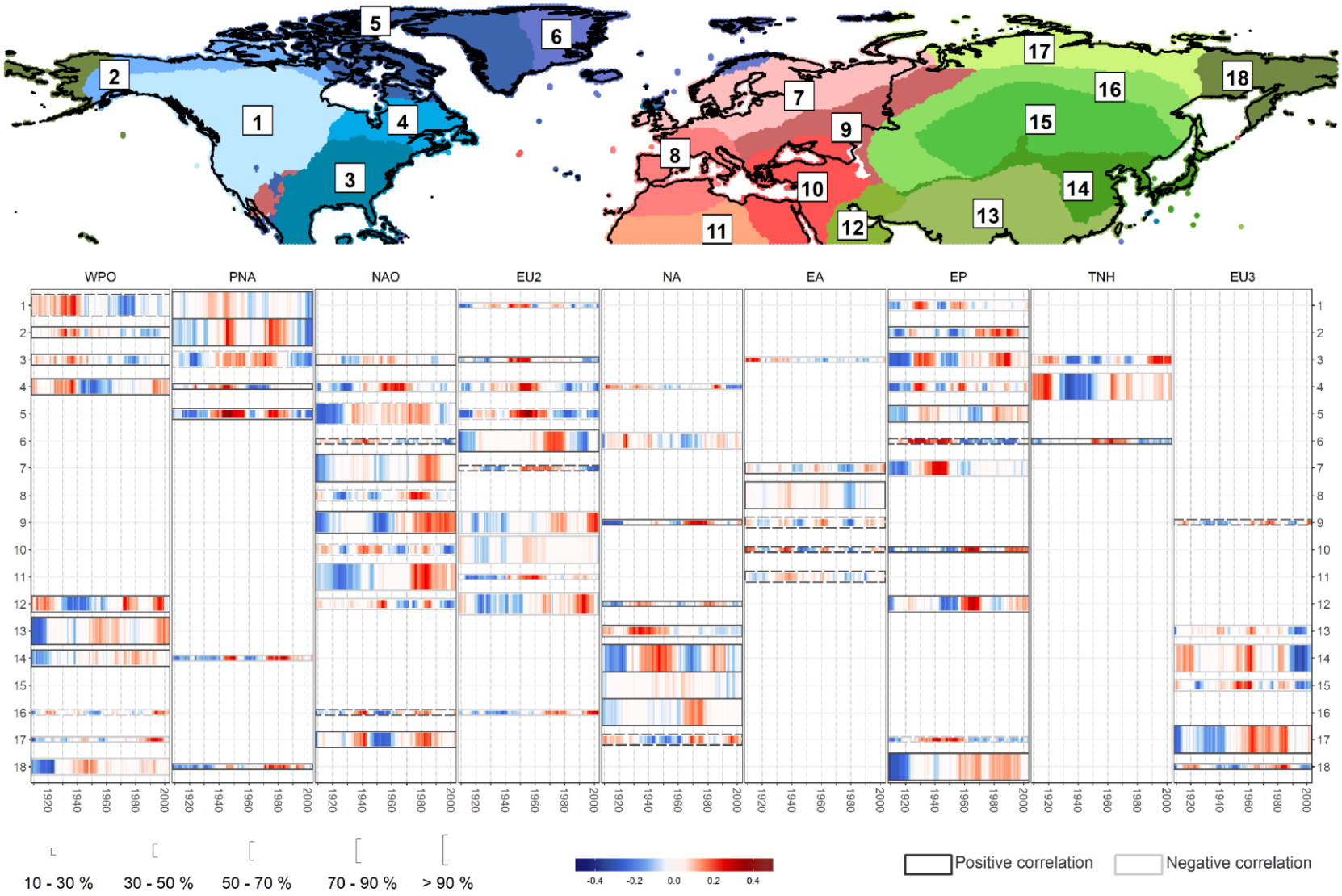
1
2
3
4
5
6
7
8
9
10
11
12
13
14
15
16
17
18
WPO
PNA
NAO
EU2
NA
EA
EP
TNH
EU3
1920
1940
1960
1980
2000
10 - 30 %
30 - 50 %
50 - 70 %
70 - 90 %
> 90 %
-0.4
-0.2
0.0
0.2
0.4
Positive correlation
Negative correlation

FIG. 2. Clusters with similar temporal evolution of relationships between surface temperature anomalies and intensity of circulation modes (1908 – 2003). Top: map of clusters. Bottom: temporal evolution of correlations in each cluster. Horizontal bars display anomalies of running correlations from their long-term average. Colours indicate deviations of running correlations from the long-term average correlation: strengthened relationships (i.e., correlations closer to ±1) are in red, weakened relationships (i.e., correlations closer to 0) are in blue, running correlations within ±0.1 (normal relationships) from the long-term average correlation are in white. The width of each bar represents the percentage of gridpoints in a cluster from which the temporal evolution of the cluster is calculated, that is, percentage of gridpoints with at least 34% of running correlations exceeding the threshold of ±0.3. Dark (light) grey frame of the bar denotes positive (negative) long-term correlation; cluster-mode pairs with two different branches of temporal courses of correlations are indicated by a dashed frame.

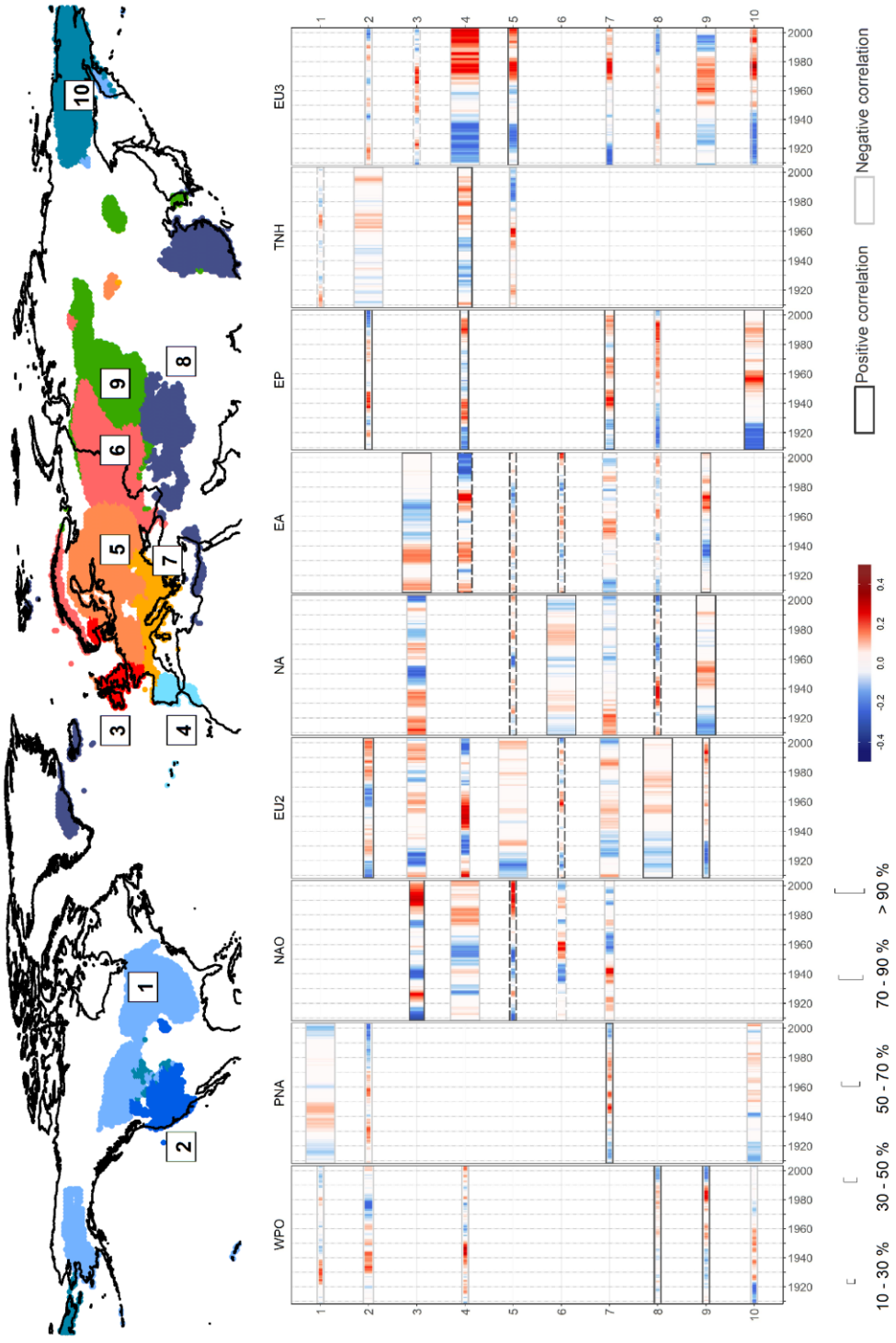

FIG. 3. As in Fig. 2, but for precipitation. The threshold value is 0.25. Please see Sec. 3 for the explanation of blank cluster.

Geographical distribution of relationships with circulation modes (Figs 2 and 3) shows that entire North America except northeastern Canada is affected by WPO, PNA, and EP. Its eastern and southeastern part is also affected by TNH and, somewhat marginally, also by Atlantic and Eurasian modes (NAO, EU2, EA, NA). Dominant circulation modes in Europe and northern Africa are NAO, EU2, and EA, smaller influence is found for NA, EP, and EU3. Interestingly, the Pacific modes (WPO, PNA, EP, and TNH) correlate with precipitation in the Mediterranean and the Iberian Peninsula. This linkage may be real since the linkage between precipitation in the Mediterranean and El Niño-Southern Oscillation has been documented by several studies (Pozo-Vázquez et al. 2005; Brönnimann et al. 2007; Zanchettin et al. 2008). For Asia, the most prominent circulation modes are WPO, NA, and EU3, while other circulation modes manifest in regional scale (PNA, NAO, EU2, and EP).

In further subsections, we analyse temporal variation of relationships with all nine circulation modes; the three most prominent modes, namely WPO, PNA and NAO, are investigated in more detail in separate subsections.

3.1 WPO

WPO consists of the negative centre residing in the Bering Sea and its positive counterpart, which occupies a zonally elongated belt along 30 to 35 ° parallels. The positive phase of WPO is associated with stronger zonal circulation over western North Pacific (Barnston and Livezey 1987; Linkin and Nigam 2008) and hence prevailing positive temperature correlations in North America (Fig. 4a). Positive correlations are found also in southern and southeastern Asia, while negative temperature response over northeastern Asia arises from a deeper negative centre strengthening cold advection to the area (Linkin and Nigam 2008; Xu and Fan 2020; Aru et al. 2021). Precipitation correlations are more patchy; they are negative in central and western North America and northeastern Asia, while positive correlations appear in central Asia and southeastern North America (Fig. 4a).

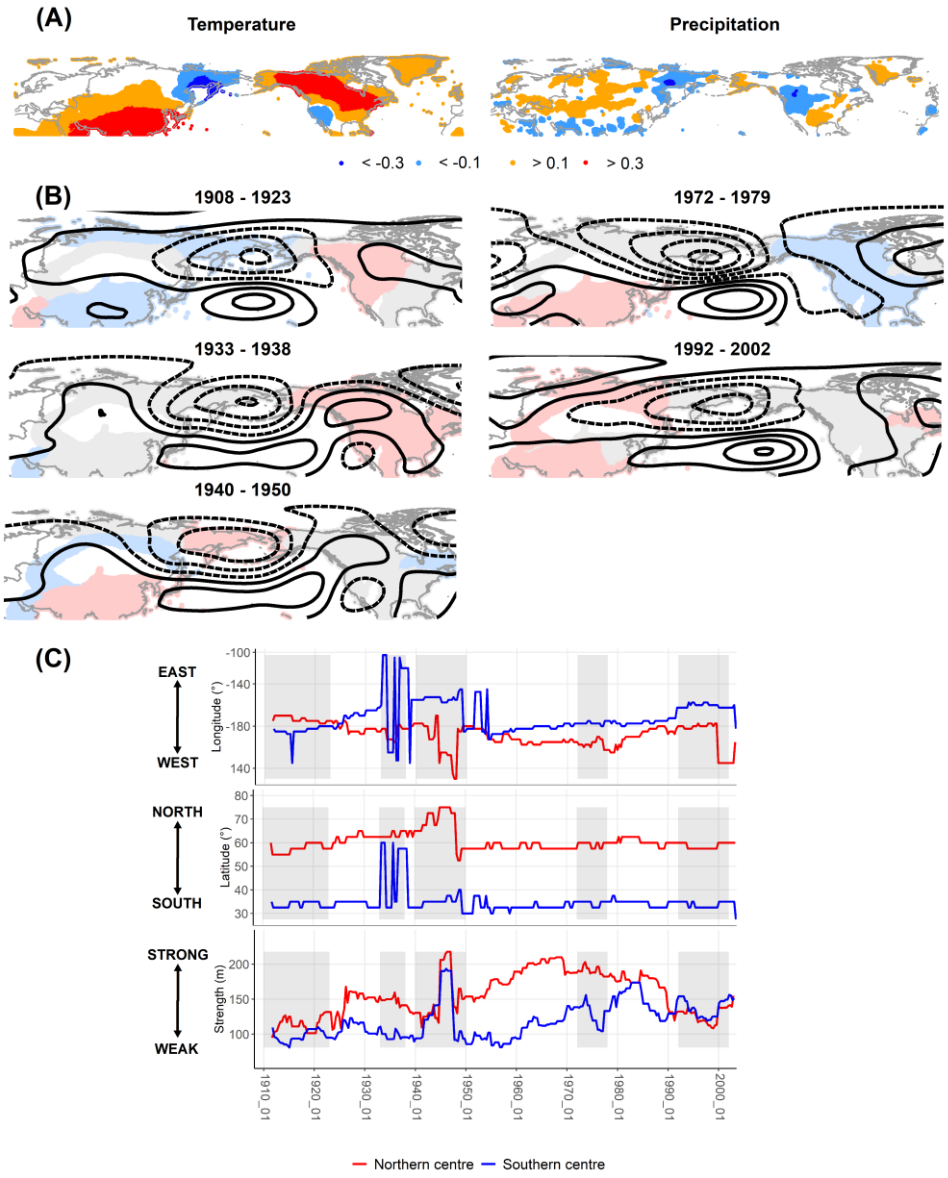

FIG. 4. WPO. (a) Long-term correlation (1901-2010, DJF) between the mode and temperature (left) and precipitation (right) anomalies. (b) Composite maps of 500 hPa geopotential heights for selected time periods. Full / dashed contours indicate positive / negative values; zero line is omitted; contour interval is 40 m. Red (blue) colours represent clusters with a strengthened (weakened) relationship with temperature in the period. Clusters in grey have normal relationship with the mode. White colour denotes clusters with missing or negligible relationship with the mode. (c) Time series of longitude, latitude (both in °), and intensity (in m) of the action centres for running periods centred on 1908 to 2003. Grey strips mark periods, for which composite differences are displayed in Fig. 4b.

The impact of WPO on North America is mostly controlled by the distance and shape of its action centres. Particularly strong correlations with temperature and precipitation in the 1930s are triggered by an extensive prolongation of the southern centre toward the continent (1933-1938; Fig. 4b,c). While this centre acquires its previous position and shape, relationships return back to normal (1940-1950). Yet, correlations with temperature substantially drop in cluster 4 afterwards due to approaching of low geopotential heights over the Labrador Sea to the cluster (1940-1950 in Fig. 4b), which intensifies advection of colder northerly air. Relationships in North America are hence modified by the intensity and shape of the additional third shallow centre over eastern Canada and the Labrador Sea (also detected in Linkin and Nigam 2008). Generally low influence of WPO on temperature in North America and precipitation in western US in the 1970s is accompanied by distant positions of both main centres (Fig. 4c) associated with an anticyclonic anomaly over eastern North America (1972-1979 in Fig. 4b).

Influence of WPO on temperature in southeastern Asia (clusters 13 and 14) is dependent on the spatial setting of the entire mode. At the beginning of the 20th century, impact of the mode is suppressed because the mode is weak (Fig. 4c), the northern centre does not considerably extend to Eurasia, and the southern centre is located solely in the Pacific while completely lacking its zonally elongated shape (1908-1923 in Fig. 4b). Conversely, when the southern centre is stronger (Fig. 4c, 1992-2002 in Fig. 4b) and/or bowed northward (1972-1979 in Fig. 4b), more pronounced advection of warmer Pacific air along its southern flank toward Asia in the positive phase of WPO accounts for the strengthened relationships. In addition, the impact of the northern centre on Asia is accentuated after the late 1970s, when the centre started to move westward toward the continent (Fig. 4c), resulting in gradually increasing influence on both temperature and precipitation in the Asian clusters, despite weakening of the centre. An even larger impact on temperature is detected after 1991, owing to the both centres stretching toward the continent (1992-2002 in Fig. 4b), although relationship with precipitation weakens due to increased anticyclonality related to southern centre (clusters 8 and 9). Large variability of the relationship between WPO and temperature in cluster 12 (the Persian Gulf) is attributed to a spatial variation of the southern belt, which modulates the inflow of air mass: strengthened relationships are associated with stronger easterly winds carrying warmer air mass (Fig. 5). Relationships near the Kamchatka peninsula (clusters 18 and 10 for

temperature and precipitation, respectively) are governed by the northern centre. Its southeasterly displacement (Fig. 4c) favours intrusion of warmer air along front side of the centre, which results in weakened correlations during the first two decades (1908-1923 in Fig 4b), whereas the northwesterly excursion and increased intensity of the centre (Fig. 4c) leads to the opposite (1940-1950 in Fig. 4b).

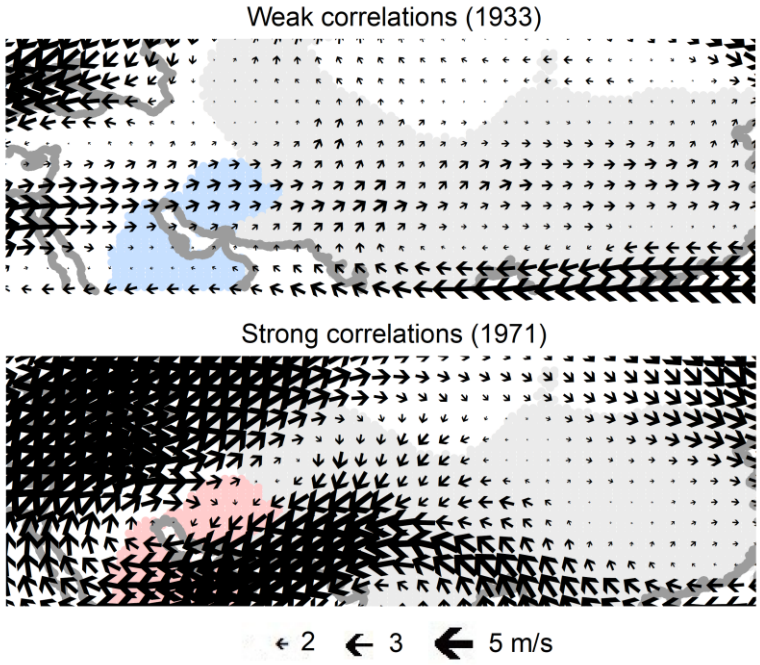

FIG. 5. Variations of wind anomalies (m/s) in 500 hPa associated with weak or strong correlations between WPO and temperature in cluster 12 (the Persian Gulf) in two selected running correlations periods. The cluster in blue (red) holds weakened (strengthened) relationship with temperature.

3.2 PNA

The PNA pattern consists of four centres: the Aleutian low in the northern Pacific and its positive counterpart located in the area of the Hawaiian high, the ridge covering northwestern parts of North America, and the trough occupying eastern US. PNA modulates the intensity of zonal flow toward North America and its positive phase is associated with more meridional circulation over the continent, while its negative phase corresponds to a zonally oriented flow (Leathers et al. 1991, Liu et al. 2015). Positive correlations with temperature over the northwestern half of North America (Fig. 6a) are result of enhanced ridging in PNA's positive

phase and consequent stronger intrusion of warmer air from the southwest, whereas intensified advection of cold air leads to a negative temperature response in southeastern USA. The positive phase of PNA tied with a southward shift of the jet stream results in a negative relationship with precipitation in central USA (Fig. 6a; Leathers et al. 1991).

Weaker relationships with temperature and precipitation over North America in the first two decades can be explained by two factors. Firstly, both the centres over North America are weaker and smaller (1912 – 1919 in Fig. 6b, Fig. 6c), which leads to reduced meridional flow and therefore close-to-zero correlations across the continent, mainly in northern and southeastern parts of North America. Secondly, the Aleutian low is shifted westwards in the beginning (Fig. 6c), which may also contribute to weakened relationships. The Aleutian Low also modulates temperature relationships over eastern Asia (Fig. 6a): its extension into the continent implies a strengthened linkage (the 1940s, the 1970s; Fig. 6b) and vice versa (1910-1930, 1912-1919 in Fig. 6b).

The specific structure of PNA during the 1940s leads to an amplified impact on temperature and precipitation. Both centres over North America are spatially extensive, the ridge shifts poleward, and the eastern American trough is particularly strong in the early 1940s (1941-1945 in Fig. 6b, Fig. 6c). Such spatial setting brings about increased meridionality and hence strengthened relationships with both climatic variables. Owing to a northwestward shift of the ridge (Fig. 6c) and its stretching in the meridional direction, lower impact on temperature and precipitation is detected between 1959 and 1964 (Fig. 6b). The subsequent episode of prevailing strengthened relationships with temperature (1969-1977 in Fig 6b) is characterized by strong centres over North America (Fig. 6c), which contribute to enhanced meridional circulation. The weakest relationships with temperature and precipitation are revealed at the end of the studied period as a result of a substantial change of PNA: the mode exhibits a more zonal appearance (1992-2002 in Fig. 6b), its action centres gradually weaken, both North American centres migrate eastward, and the Aleutian low is located more westerly (Fig. 6c), all of which indicate a reduced impact on climatic variables in North America.

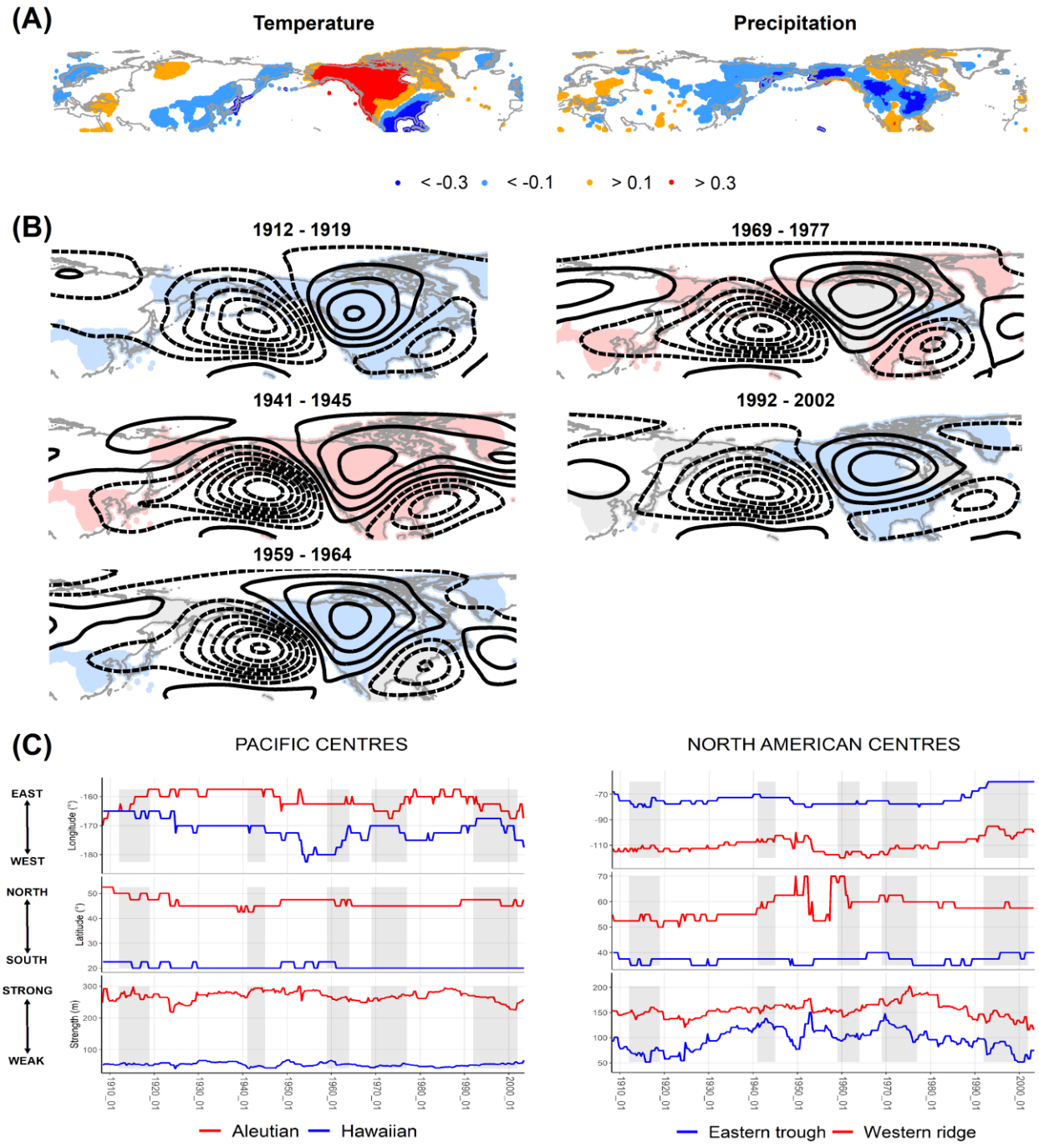

FIG. 6. As in Fig. 4, but for the PNA pattern and its four action centres.

3.3 NAO

NAO consists of two centres over the Atlantic Ocean. The northern negative (Icelandic) centre is located in the vicinity of Greenland, while the southern positive (Azores) centre extends along the 40° N parallel. NAO modifies westerlies to Eurasia, hence in its positive phase having a positive impact on temperature and precipitation over much of Eurasia, and to a lesser extent, in southern and southeastern North America (Fig. 7a). Negative correlations occur over the Mediterranean, northern Africa, northeastern North America, and Greenland (Fig. 7a; Trigo et al. 2002; Hurrell et al. 2002; Yu et al. 2019).

The impact of NAO in Eurasia is mainly dependent on the position and shape of both centres. The eastward shift of the Icelandic centre leads to increased correlations with climatic variables over much of Eurasia between 1920 and 1940, and particularly during the late 1970s and 1980s (Fig. 7b,c; Jung et al. 2003; Beranová and Huth, 2008; Luo et al. 2010). Besides, the latter period is accompanied by a fairly different spatial representation of NAO: both centres are more extensive and more zonally prolonged (1971-1993 in Fig. 7b), which results in stronger zonal circulation and hence substantially larger impact on climatic variables than in 1920-1940. Weaker correlations with temperature and precipitation around 1950 are induced by the westerly displaced Icelandic centre (Fig. 7c; Vicente-Serrano and López Moreno, 2008; Rust et al. 2021) and the split of the Azores centre into two parts, which also leads to a pronounced decrease in correlations in eastern Europe and west Asia (1947-1954 in Fig. 7b).

Temporal variations of relationships between NAO and temperature in North America are opposite to those in Eurasia and similarly relate to the shift of the centres: weaker relationships until 1935 and after 1980 (Fig. 7b) are associated with the eastward shift of both centres while relationships strengthen between 1935 and 1980 due to the centres being closer to North America (Fig. 7c).

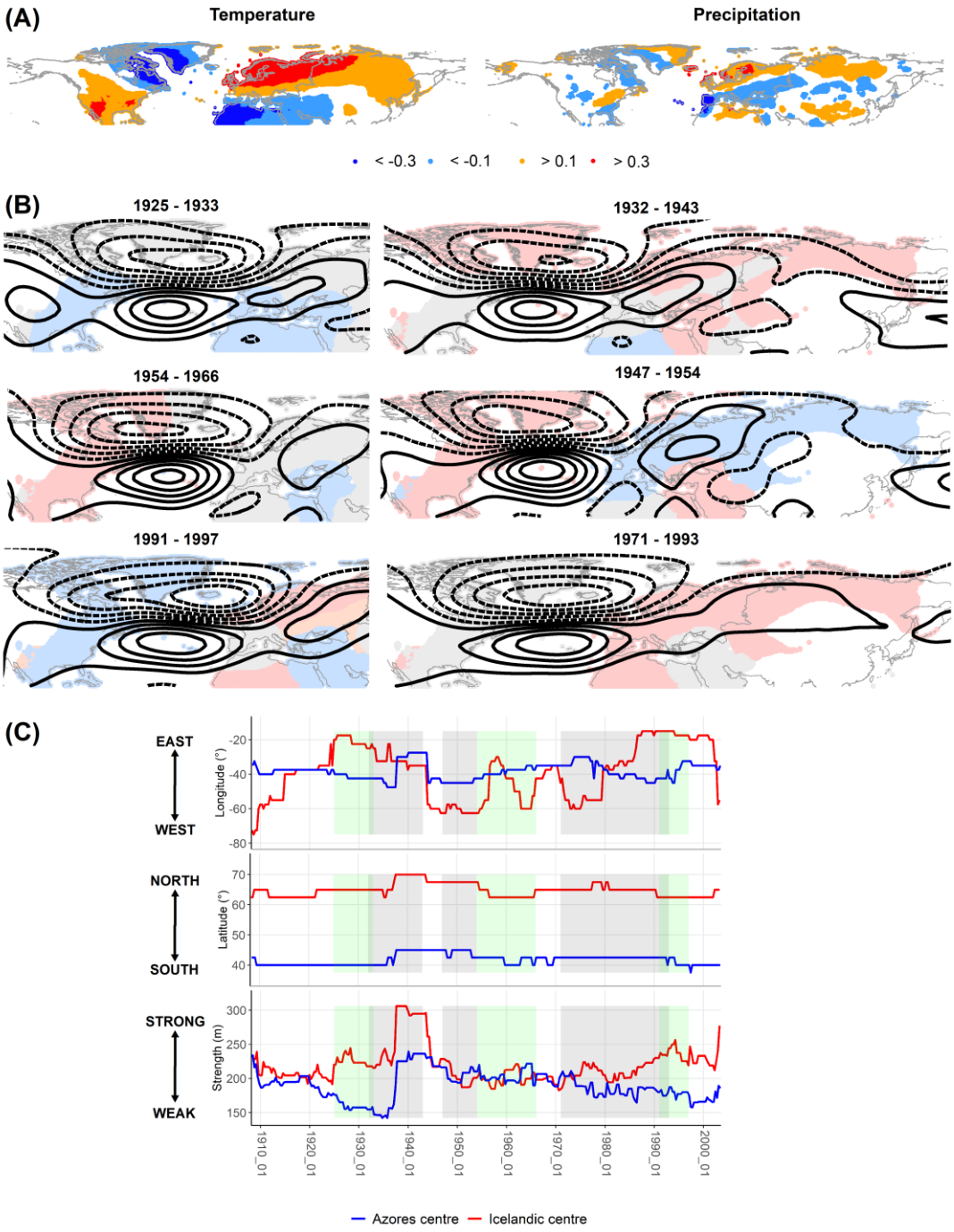

FIG. 7. As in Fig. 4, but for the NAO pattern. Green (grey) strips in Fig. 7c correspond to composite maps for North America (Fig. 7b, left) and Eurasia (Fig. 7b, right), respectively.

The Mediterranean and the Persian Gulf hold negative correlations of NAO with both temperature and precipitation (Mariotti and Dell`Aquila 2012; Donat et al. 2013; Attada et al. 2018; Seager et al. 2020). Studies generally document a rather low influence of NAO on

temperature over the Mediterranean (e.g. López-Moreno et al. 2011; Mariotti and Dell`Aquila 2012) but the intensity and spatial impact of NAO seem to be more complex and highly sensitive to locations of the NAO centres (Castro-Díez et al. 2002). Temporal variation of relationships with both temperature and precipitation in the Mediterranean is dominated by the Azores centre. Until the 1950s, it is displaced westwards, relatively far from the continent, which leads to weakened relationships. In the 1950s and 1960s, split of the Azores centre (1947-1954; 1954-1966 in Fig. 7b; Vicente-Serrano and López Moreno, 2008) may also contribute to weakened relationships with both temperature and precipitation. As the centre subsequently stretches and approaches toward Eurasia (1971-1993 in Fig. 7b, Fig. 7c), a gradually increasing impact on the Mediterranean is observed (Trigo et al. 2004; Beranová and Huth, 2008; Rust et al. 2021) due to larger anticyclonality associated with drier conditions, and intensified northeasterly advection tied with colder conditions.

3.4 Other modes

In this section, we briefly describe temporal variations of relationships with the remaining circulation modes, in the order of their explained variance.

EU2 is the fourth most prominent circulation mode in the Northern Hemisphere, explaining 7.2% of variance. Two of its main centres occupy northern Europe and central Asia, while the third weaker centre is located nearby Greenland. Weakened relationships with temperature are observed when both the centres are weaker (Fig. 8b) and the northern centre is somehow zonally oriented, which limits inflow of warmer Atlantic air far into northern Europe and Greenland and colder air into the Near East and central Asia in EU2's positive phase. Weakened relationships with temperature are detected between 1920 and 1940 and after 1985 (1920-1935 and 1990-1998 in Fig. 8a); strengthened relationships in the Asian clusters in the latter period are probably caused by the shape of the central Asian centre elongated in the northeast direction. On the contrary, strengthened relationships in northern Europe and Asia in the 1950s and 1960s are induced by both centres being stretched in the southwest to northeast direction, allowing a more pronounced temperature advection (1952-1962 in Fig. 8a). The impact of the mode is further accentuated by a higher intensity of both centres in this period (Fig. 8b). Temporal evolution of relationships with precipitation is less straightforward. Weakened relationships with majority of clusters prevail until 1940 and

strengthen afterwards. Northeastward shift of the northern centre leads to a smaller impact on precipitation between 1960 and 1980 in western and southern Europe, contrarily to larger impact on temperature in Greenland and northern Europe (1972-1980 in Fig. 8a, Fig. 8b).

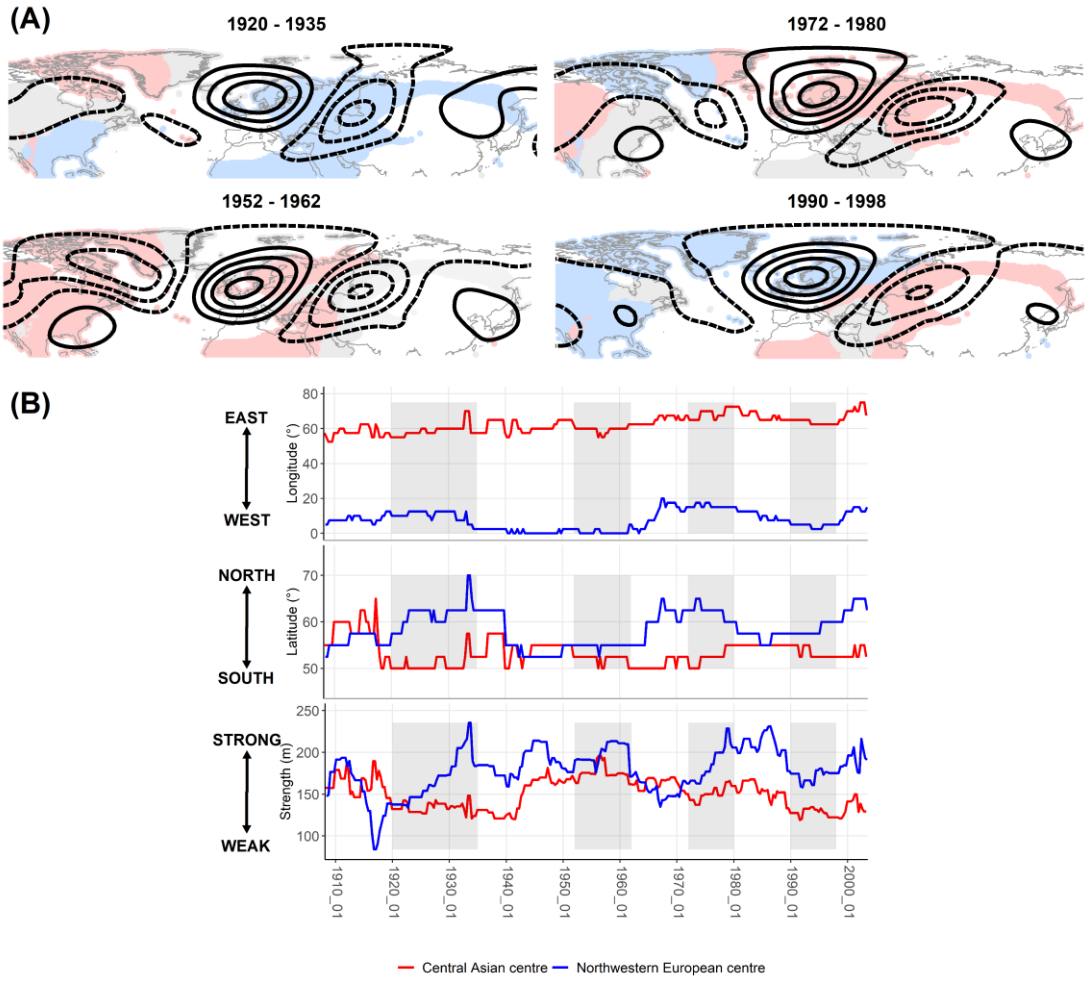

FIG. 8. As in Fig. 4, but for the EU2 pattern and without maps of correlations.

The North Asian pattern consists of three centres spread over Eurasia. Changes in the shape of the main negative centre control the intensity of advection toward the northern half of Asia: as the centre is more inclined toward west, the impact of the mode on both temperature and precipitation in the approximately central to eastern Asia is smaller until 1920 due to weakened advection (1908-1919 in Fig. 9a). Conversely, the centre extending eastward enhances the influence of the mode farther to the east; strengthened relationships with both climatic variables are consequently observed in 1960-1980 (1961-1968 in Fig 9a), and with precipitation only between 1920-1940. Relationships with temperature and precipitation in

central and southern Asia are modified by the positive centre in eastern Asia: strengthened relationships are linked with its larger intensity (1930-1950; 1936-1941 in Fig. 9a; Fig.9b), weakened relationships are associated with either a zonal shape of the centre (1961-1968 in Fig. 9a) or its weakening (1992-1996 in Fig. 9a; Fig.9b). Negative relationships with precipitation over the British Isles and the Mediterranean are modulated by spatial variations of the negative centre over western Europe: when the centre is more pronounced (1936-1941 in Fig. 9a), correlations are stronger.

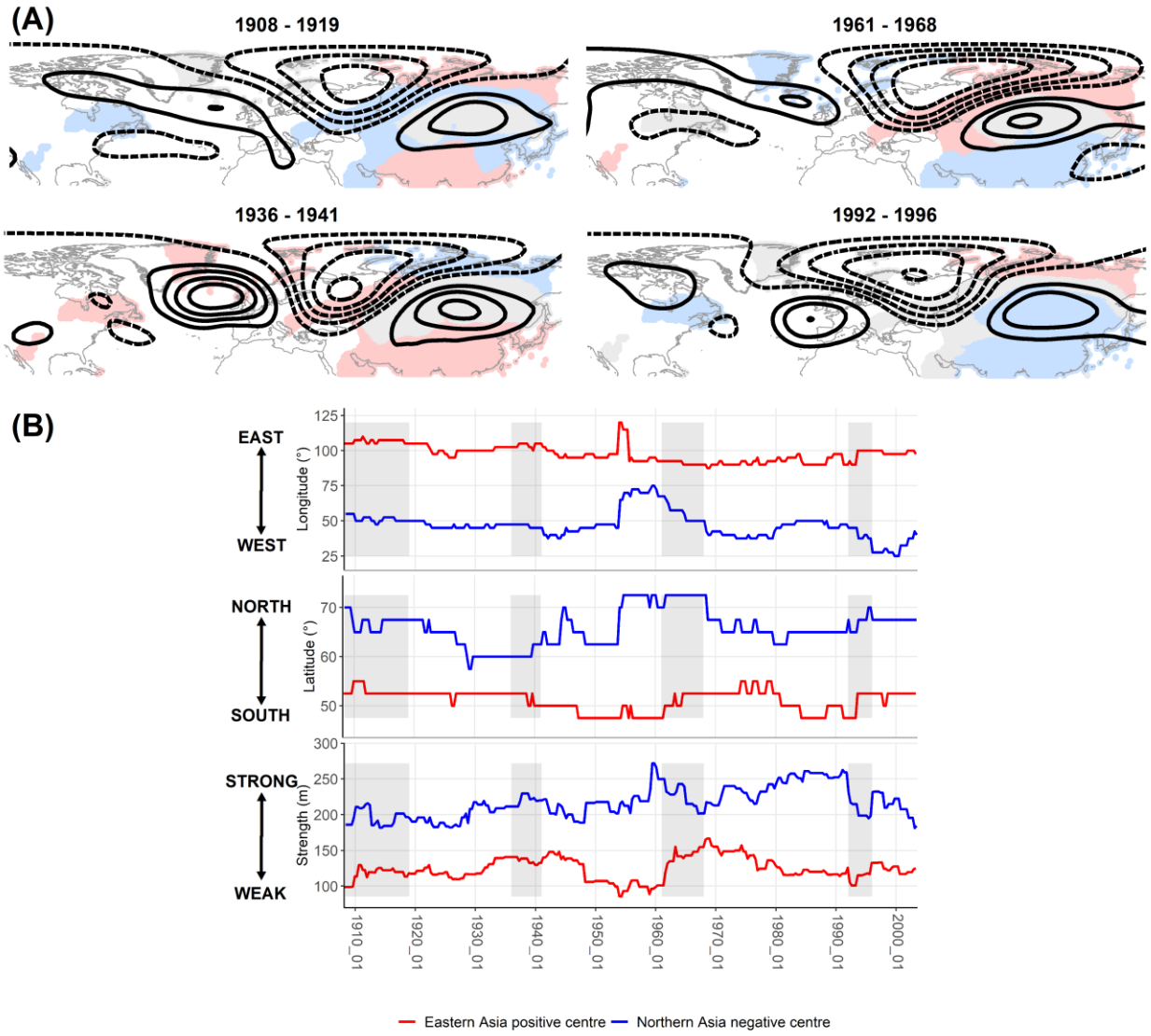

FIG. 9. As in Fig. 8, but for the NA pattern.

Relationships between EA and temperature in Eurasia are modified mainly by changes in the position and strength of the southern centre (Lionello and Galati, 2008; Gao et al. 2016). This centre stretches northeastwards and strengthens in the 1930s, 1950s and early 1960s (Fig. S5b), which, along with strengthening of the northern centre, is likely to result in a larger influence on temperature in the Mediterranean, Europe, and western Asia (1933-1940 and 1956-1968 in Fig. S5a). On the contrary, correlations drop in Europe around 1980, owing to split of the southern centre and weakening of the northern centre (1979 in Fig. S5a; Beranová and Huth 2008). Expansion of the northern centre toward the British Isles is associated with increased cyclonicity there and hence strengthened relationships between EA and precipitation (1930s, 1933-1940 in Fig. S5a), whereas shift of the centre toward Atlantic leads to weakened relationships with precipitation (1940-1970, 1956-1968 in Fig. S5a). Most striking is a decreasing impact on precipitation over the Iberian Peninsula in the last three decades, arising from the position of the southern centre close to the region, which causes larger anticyclonicity there in the positive phase of EA (Fig. S6).

The EP pattern is formed by one centre over the central Pacific and the other over the Beaufort Sea. Relationships with EP in the first two decades are weakened for both temperature and precipitation almost everywhere. This arises from a small geographical extent of both centres (1908-1921 in Fig. S7). A substantial change is detected in the 1920s: both centres strengthen and expand, the negative centre almost circumglobally, and an additional positive centre over Iceland is formed (1924-1931 in Fig. S7). Such spatial setting results in strengthened relationships around 1930 in the majority of clusters. The Iceland centre amalgamates with the northern Pacific centre in the 1940s, creating a single positive centre. As the southern negative belt shrinks in the 1940s (1938-1948 in Fig. S7), its impact on temperature in North America weakens. Spatial representation of EP is fairly stable in the second half of the 20th century; the mode modulates relationships with climatic variables mainly by minor spatial changes of its centres (Fig. S7).

Considering the TNH pattern, its negative centre over Ontario governs relationships with TNH in the majority of North America. Combination of a zonal appearance of this centre and its large intensity leads to strengthened relationships with temperature over North America during 1908-1930 and mostly from the 1960s onwards (Fig. S8a, FigS8b). Weakening of the

centre between 1930 and 1950 is analogously responsible for weakened relationships over North America (1931-1934 in Fig S8a). Variation of relationships with precipitation are not well pronounced, yet, strengthened relationships in North America in the 1960s seem to be caused by stronger negative centre favouring stronger advection (Fig. S8b).

The weak northern centre of EU3 similarly results in weakened relationships with temperature and precipitation in northern Asia (1938-1942 in Fig. S9a) and vice versa (1959-1961 and 1981-1986 in Fig. S9a). Relationships in central and southern Asia are modulated by the negative centre over eastern Asia/western Pacific: strengthened temperature response is detected when the centre is stronger and located closer to Asia (1959-1961 and 1981-1986 in Fig. S9a, Fig. S9b). Relationships with precipitation are also governed by two additional centres nearby Europe, both of which are lacking until 1940, resulting in a minimized impact on the precipitation, particularly over the Iberian Peninsula. Their formation and gradual strengthening lead to the increase of correlations, mainly after 1970 (not shown).

4. Discussion

Discussion is structured into two parts. Firstly, changes of circulation modes responsible for temporal variation with climatic variables are summarized and discussed. Then, uncertainties linked with the utilized reanalysis are described.

4.1 Mechanisms explaining time variation of relationships with climatic variables

Temporal nonstationarity between circulation modes and surface climatic variables is caused by four mechanisms related to various changes in action centres. The first one is their position: the displacement of action centres shifts the anomalous circulation, which results in a weakened or strengthened advection, depending on the position relative to the centres. For example, the shift of action centres of WPO toward North America in the 1930s leads to strengthened correlations there, whereas a retreat of the mode westward results in weaker correlations in the 1970s. Secondly, the shape and size of action centres also modify advection and the influence of a mode on climatic variables. For example, spatially extensive centres of PNA over North America in the 1940s result in a larger impact on climate there, while zonally elongated centres contribute to weakened relationships after 1990. Thirdly, the strength of action centres governs the intensity of advection: stronger centres imply stronger

advection, which in turn results in stronger effect on climatic variables. Fourthly, the formation and disappearance or split of action centres affect spatial influence of the mode: formation of a new WPO centre over the Labrador Sea changes spatial correlations in North America after 1940; split of the southern centre of NAO in the 1950s and 1960s results in a decrease in correlations mainly in the Mediterranean.

Regarding precipitation, aforementioned mechanisms may also manifest in spatial changes in cyclonicity and antiyclonicity of centres. For example, when the anticyclonic centre extends into an area of prevailing cyclonicity associated with positive correlations, relationships with precipitation consequently weaken, as detected for EA in cluster 4 (the Iberian Peninsula) from the 1980s onward. On the contrary, strengthened relationships between EA and precipitation in the British Isles are tied to increased cyclonicity related to a closer position of the negative northern centre of the mode.

Based on the review of literature, we further seek for the primary climatic patterns or factors responsible for spatial changes of the modes. Several studies attribute the interdecadal variability of the Pacific modes to changes in El Niño-Southern Oscillation (ENSO), shifts of the Pacific Decadal Oscillation (PDO), and long-term changes in sea ice extent. The PDO shift in 1924 (Mantua and Hare 2002; Newman et al. 2016) may account for substantial spatial changes of the modes, such as weakening of the Aleutian Low and the TNH, strengthening of WPO, and the formation of the new centre of EP over Iceland. The shift might also trigger migration of the southern centres of WPO and EP towards North America between 1925 and 1940, leading to strengthened relationships there. As those centres retreat back during the 1940s, relationships in turn weaken. This westward shift, also detected for other modes (PNA, the negative centre of TNH), may be associated with another PDO shift in 1946. To our knowledge, however, no study directly investigating changes of spatial appearance of the modes before 1950, particularly the excursion of southern centres of WPO and EP toward North America between 1925 and 1940, was conducted; hence, additional research clarifying this topic is needed.

The most prominent shift of PDO in 1976 (Mantua and Hare 2002; Yeh et al. 2011; Newman et al. 2016) is considered as a turning point in a non-stationary relationship between some circulation modes and ENSO (Mo and Livezey 1986; Wang et al. 2007; Mo 2010; Franzke et

al. 2011; He et al. 2013; Yuan et al. 2015; Dai et al. 2017; Schulte and Lee 2017; Dai and Tan 2019; Soulard et al. 2019). ENSO modulates Rossby waves through changes in the intensity of convection and sea surface temperatures in the Tropics, which can subsequently affect the Pacific jet stream and therefore the Pacific modes, too (Mo 1986; Hoerling et al. 1997; Jo et al. 2015; Tan et al. 2015; Soulard et al. 2019). Studies document strong (weak) linkage between ENSO and WPO (PNA) before 1976, with the inversed relationships afterwards (Wang et al. 2007; He et al. 2013; Yeh et al. 2018; Park et al. 2018; Soulard et al. 2019), although results depend on pressure levels and domain utilized for the identification of modes (Aru et al. 2021). A generally stronger impact of PNA on climatic variables is found during its weak connection with ENSO before 1976 mainly in southeastern and northeastern parts of North America (Fig. S5 in Soulard et al. 2019), which is consistent with our results. The shift of PDO in 1976 is associated with a large change of PNA and WPO: both weaken and centres over the Pacific gain more zonal shapes directing toward Asia, which lead to an increased impact on precipitation and temperature there (Wang and Chen, 2007; Marshall 2021). Lee et al. (2012) report the same behaviour of PNA after 1980 and conclude that the change in its appearance is caused by the PDO shift in 1976 and a subsequent change in the position of storm track. A more zonal appearance after 1976 is also evident for TNH, while almost no change of EP is observed. To conclude, all the Pacific modes except EP undergo weakening and gain zonal appearance after the 1976 PDO shift.

Some studies point out that the sea ice extent affects spatial representation of circulation modes. For example, eastward motion of the both WPO centres during the 1990s (also evident for the pair of the North American centres of PNA) is attributed to sea ice extent anomalies in the Barents Sea (Linkin and Nigam 2008; Yuan et al. 2015; Xu and Fan 2020). According to our results, this shift has negligible impact on climatic elements, although Xu and Fan (2020) detect increased westerlies after the shift.

Generally, there is a scarcity of studies analysing primary mechanisms responsible for changes of non-Pacific circulation modes. Possible causes responsible for an eastward migration of the NAO centres in the late 1970s refer to stronger mean westerly winds and northerly displaced jet stream core (Luo and Gong 2006, Luo et al. 2010), the dependence on the prevailing phase of NAO (Peterson et al. 2003), greenhouse gas forcing (Ulbrich and

Christoph 1999), and Atlantic Multidecadal Oscillation, the negative phase of which favours the position of NAO closer to Europe (Börgel et al. 2020). Although NAO shifts eastward also between 1908 and 1925, its climatic impact is substantially weaker because the mode is generally weaker and less extensive at that time. Considering other modes, Wang et al. (2018) linked the behaviour of EU (here named as EU3) to changes in sea surface temperatures in the North Atlantic.

4.2. Uncertainties associated with reanalyses

Although circulation modes detected in ERA-20C are in large agreement with full-input reanalyses, such as NCEP-1 and JRA-55 (Hynčica and Huth 2020a,b; Hynčica and Huth 2022), a larger uncertainty in the first decades of the 20th century is expected due to the lack of assimilated observations, mainly over less populated areas, primarily over the North Pacific. In this period, reanalyses are more dependent on the setting of the model utilized for its calculation and less constrained by observations. This is likely to result in different outputs of pressure fields between reanalyses, which obviously influence the representation of circulation modes, their intensity, and therefore spatiotemporal relationships with surface climatic variables. A larger uncertainty of surface-input reanalyses has been documented for several other circulation characteristics; see e.g. Schneider and Fogt (2018), Bloomfield et al. (2018), Chang and Yau (2016), and Slivinski et al. (2021). Hence, future research may be devoted to a comparison of temporal variation of relationships in the first half of the 20th century between different reanalyses, such as 20CRv3, ERA-20C, and CERA-20C.

5. Conclusions

The analysis of temporal variation of associations of nine circulation modes with temperature and precipitation has been conducted for winter in period 1901-2010. We utilize the ERA-20C reanalysis for detection of circulation modes and the CRU dataset as the source of the temperature and precipitation data. To evaluate long-term relationships of circulation modes with surface climatic variables, running correlations with a 45 month (i.e., 15 year) window are calculated at each gridpoint. The time series of running correlations are then subject to cluster analysis (utilizing partitioning around medoids), the result of which is 18 clusters for temperature and 11 for precipitation, within which temporal variations of relationships with

circulation modes are consistent. Several mechanisms related to circulation modes are responsible for nonstationarity of relationships with surface climatic variables:

1) Shift of action centres: a closer proximity of centres leads to a strengthened relationship with temperature and precipitation (e.g. WPO and North America in the 1930s; NAO and Eurasia between 1920 and 1940 and in the 1980s) and vice versa (e.g. WPO and North America in the 1970s, NAO and Eurasia around 1950).

2) Varying shape and extent of action centres: a larger action centre affects a larger area (e.g., more extensive centres of PNA in North America in the 1940s result in a larger impact on climate there, analogously for EU2 in Europe in the 1950s and 1960s, and EP in the 1920s), and vice versa. This mechanism also affects relationships with precipitation due to changes in cyclonicity and anticyclonicity related to action centres.

3) Changing intensity of action centres: a strengthening of action centres leads to stronger anomaly circulation, and hence a strengthened relationship with climatic variables, and vice versa. For example, a larger intensity of the main negative centre of TNH over North America contributes to strengthened relationships with temperature from the 1980s; weakening of the positive centre of NA over eastern Asia during the 1990s leads to its decreased impact on climatic variables there.

4) Formation and disappearance or split of action centres: split of the southern centre of NAO in the 1950s and 1960s leads to a smaller impact on temperature and precipitation, mainly in the Mediterranean; formation of the new EP centre over Iceland in the 1920s brings about larger correlation with temperature in the North Atlantic and Northern Europe.

Several studies point to the impact of ENSO, shifts of PDO, and sea ice extent on circulation modes residing in the Pacific (WPO, PNA, EP, and TNH), although a deeper research on the behaviour of those modes in the first half of the 20th century is needed. However, causes of spatiotemporal changes of other circulation modes still remain unclear or unknown. Nevertheless, natural variability of the climate system should be taken into account as important factor influencing circulation modes.

Acknowledgments

This research was supported by the Czech Science Foundation, project 17-07043S. Martin Hynčica was also supported by the Grant Agency of the Charles University, student project 426216. We further acknowledge ECMWF for ERA-20C and CRU for the CRU TS v 4.03.

Data Availability Statement

The ERA-20C reanalysis and the CRU dataset are publicly available.

References

Araneo, D. C., and R. H. Compagnucci, 2004: Removal of systematic biases in S-mode principal components arising from unequal grid spacing. *J. Climate*, **17**, 394-400.

Aru, H., S. Chen, and W. Chen, 2021:. Comparisons of the different definitions of the western Pacific pattern and associated winter climate anomalies in Eurasia and North America. *Int. J. Climatol.*, **41**, 2840-2859.

Attada, R., H. P. Dasari, J. S. Chowdary, R. K Yadav, O. Knio, and I. Hoteit, 2018: Surface air temperature variability over the Arabian Peninsula and its links to circulation patterns. *Int. J. Climatol.*, **39***,* 445-464.

Barnston, A. G., and R. E. Livezey, 1987: Classification, seasonality and persistence of low-frequency atmospheric circulation patterns. *Mon. Weather Rev.*, **115**, 1083-1126.

Beranová, R., and R. Huth, 2008: Time variations of the effects of circulation variability modes on European temperature and precipitation in winter. *Int. J. Climatol.*, **28**, 139-158.

Bloomfield, H. C., L. C. Shaffrey, K. I. Hodges, and P. L. Vidale, 2018: A critical assessment of the long-term changes in the wintertime surface Arctic Oscillation and Northern Hemisphere storminess in the ERA20C reanalysis. *Environ. Res. Lett*., **13**, 094004.

Börgel, F., C. Frauen, T. Neumann, and H. M. Meier, 2020: The Atlantic Multidecadal Oscillation controls the impact of the North Atlantic Oscillation on North European climate. *Environ. Res. Lett.*, **15**, 104025.

Brönnimann, S., E. Xoplaki, C. Casty, A. Pauling, and J. J. C. D. Luterbacher, 2007: ENSO influence on Europe during the last centuries. *Clim. Dyn.,* **28**, 181-197.

Castro-Díez, Y., D. Pozo-Vázquez, F. S. Rodrigo, and M. J. Esteban-Parra, 2002: NAO and winter temperature variability in southern Europe. *Geophys. Res. Lett.*, **29**, 1-1-1.4.

Chang, E. K. M., and A. M. W. Yau, 2016: Northern Hemisphere winter storm track trends since 1959 derived from multiple reanalysis datasets. *Clim. Dyn*., **47**, 1435-1454.

Compo, G. P., and Coauthors, 2011: The twentieth century reanalysis project. *Q. J. R. Meteorol. Soc*., **137**, 1-28.

Dai, Y., S. B. Feldstein, B. Tan, and S. Lee, 2017: Formation mechanisms of the Pacific–North American teleconnection with and without its canonical tropical convection pattern. *J. Climate*, **30**, 3139-3155.

Dai, Y., and B. Tan, 2019: Two types of the western Pacific pattern, their climate impacts, and the ENSO modulations. *J. Climate*, **32**, 823-841.

Donat, M. G., and Coauthors, 2013: Changes in extreme temperature and precipitation in the Arab region: long-term trends and variability related to ENSO and NAO. *Int. J. Climatol.*, **34**, 581-592.

Filippi, L., E. Palazzi, J. von Hardenberg, and A. Provenzale, 2014: Multidecadal variations in the relationship between the NAO and winter precipitation in the Hindu Kush–Karakoram. *J. Climate*, **27**, 7890-7902.

Franzke, C., S. B. Feldstein, and S. Lee, 2011: Synoptic analysis of the Pacific–North American teleconnection pattern. *Q. J. R. Meteorol. Soc*., **137**, 329-346.

Gao, T., J. Y. Yu, and H. Paek, 2016: Impacts of four northern-hemisphere teleconnection patterns on atmospheric circulations over Eurasia and the Pacific. *Theor. Appl. Climatol.,* **129**, 815-831.

Harris, I., T. J. Osborn, P. Jones, and D. Lister, 2020: Version 4 of the CRU TS monthly high-resolution gridded multivariate climate dataset. *Sci. Data*, **7**, 1-18.

He, S., H. Wang, and J. Liu, 2013. Changes in the relationship between ENSO and Asia–Pacific midlatitude winter atmospheric circulation. *J. Climate*, **26**, 3377-3393.

Hertig, E., C. Beck, H. Wanner, and J. Jacobeit, 2015: A review of non-stationarities in climate variability of the last century with focus on the North Atlantic–European sector. *Earth-Sci. Rev.*, **147**, 1-17.

Hoerling, M. P., A. Kumar, and M. Zhong, 1997: El Niño, La Niña, and the nonlinearity of their teleconnections. *J. Climate*, **10**, 1769-1786.

Hurrell, J. W., 1995: Decadal trends in the North Atlantic Oscillation: Regional temperatures and precipitation. *Science*, **269**, 676-679.

Hurrell, J. W., M. P. Hoerling, and C. K. Folland, 2002: Climatic variability over the North Atlantic. In *International Geophysics* (Vol. 83, pp. 143-151). Academic Press.

Huth, R., 2006: The effect of various methodological options on the detection of leading modes of sea level pressure variability. *Tellus A: Dynamic Meteorology and Oceanography*, **58**, 121–130.

Hynčica, M., and R. Huth, 2020a:. Modes of atmospheric circulation variability in the Northern Extratropics: A comparison of five reanalyses. *J. Climate*, **33**, 10707-10726.

Hynčica, M., and R. Huth, 2020b: Gridded versus station temperatures: time evolution of relationships with atmospheric circulation. *J. Geophys. Res. Atmos*., **125**, e2020JD033254.

Hynčica, M., and R. Huth, 2022: Temporal evolution of relationships between temperature and circulation modes in five reanalyses. *Int. J. Climatol.*, **42**, 4391-4404.

Jo, H. S., S. W. Yeh, and S. J. Lee, 2015: Changes in the relationship in the SST variability between the tropical Pacific and the North Pacific across the 1998/1999 regime shift. *Geophys. Res. Lett.*, **42**, 7171-7178.

Jung, T., M. Hilmer, E. Ruprecht, S. Kleppek, S. K. Gulev, and O. Zolina, 2003: Characteristics of the recent eastward shift of interannual NAO variability. *J. Climate*, **16**, 3371-3382.

Kaufman, L., and P. J. Rousseeuw, 1990: Partitioning around medoids (program pam). In: *Finding groups in data: an introduction to cluster analysis* (eds. L. Kaufman and P.J. Rousseeuw), 68-125.

Krichak, S. O., P. Kishcha, and P. Alpert, 2002: Decadal trends of main Eurasian oscillations and the Eastern Mediterranean precipitation. *Theor. Appl. Climatol.,* **72***,* 209-220.

Leathers, D. J., B. Yarnal, and M. A. Palecki, 1991: The Pacific/North American teleconnection pattern and United States climate. Part I: Regional temperature and precipitation associations. *J. Climate*, **4**, 517-528.

Lee, Y. Y., J. S. Kug, G. H. Lim, and M. Watanabe, 2012: Eastward shift of the Pacific/North American pattern on an interdecadal time scale and an associated synoptic eddy feedback. *Int. J. Climatol.*, **32**, 1128-1134.

Linkin, M. E., and S. Nigam, 2008: The North Pacific Oscillation–west Pacific teleconnection pattern: Mature-phase structure and winter impacts. *J. Climate*, **21**, 1979-1997.

Lionello, P., and M. B. Galati, 2008: Links of the significant wave height distribution in the Mediterranean sea with the Northern Hemisphere teleconnection patterns. *Adv. Geosci*., **17**, 13-18.

Liu, Y., L. Wang, W. Zhou, and W. Chen, 2014: Three Eurasian teleconnection patterns: Spatial structures, temporal variability, and associated winter climate anomalies. *Clim. Dyn.,* **42**, 2817-2839.

Liu, Z., Z. Jian, K. Yoshimura, N. H. Buenning, C. J. Poulsen, and G. J. Bowen, 2015: Recent contrasting winter temperature changes over North America linked to enhanced positive Pacific-North American pattern. *Geophys. Res. Lett.*, **42**, 7750-7757.

López-Moreno, J. I., S. M. Vicente-Serrano, E. Morán-Tejeda, J. Lorenzo-Lacruz, A. Kenawy, and M. Beniston, 2011: Effects of the North Atlantic Oscillation (NAO) on combined temperature and precipitation winter modes in the Mediterranean mountains: Observed relationships and projections for the 21st century. *Glob. Planet. Change*, 77, 62-76.

Luo, D., and T. Gong, 2006: A possible mechanism for the eastward shift of interannual NAO action centers in last three decades. *Geophys. Res. Lett.*, **33**.

Luo, D., Z. Zhu, R. Ren, L. Zhong, and C. Wang, 2010: Spatial pattern and zonal shift of the North Atlantic Oscillation. Part I: A dynamical interpretation. *J. Atmos. Sci.*, **67**, 2805-2826.

Mantua, N. J., and S. R. Hare, 2002: The Pacific decadal oscillation. *J. Oceanography.,* **58**, 35-44.

Mariotti, A., and A. Dell'Aquila, 2012: Decadal climate variability in the Mediterranean region: roles of large-scale forcings and regional processes. *Clim. Dyn.,* **38**, 1129-1145.

Marshall, G. J., 2021:. Decadal variability in the impact of atmospheric circulation patterns on the winter climate of northern Russia. *J. Climate*, **34**, 1005-1021.

Mo, K. C., and R. E. Livezey, 1986: Tropical-extratropical geopotential height teleconnections during the Northern Hemisphere winter. *Mon. Weather Rev.*, **114**, 2488-2515.

Mo, K. C., 2010: Interdecadal modulation of the impact of ENSO on precipitation and temperature over the United States. *J. Climate*, **23**, 3639-3656.

Newman, M., and Coauthors, 2016: The Pacific decadal oscillation, revisited. *J. Climate*, **29**, 4399-4427.

Park, Y. H., B. M. Kim, G. Pak, M. Yamamoto, F. Vivier, and I. Durand, 2018: A key process of the nonstationary relationship between ENSO and the Western Pacific teleconnection pattern. *Sci. Rep.*, **8**, 1-13.

Peterson, K. A., J. Lu, and R. J. Greatbatch, 2003: Evidence of nonlinear dynamics in the eastward shift of the NAO. *Geophys. Res. Lett.*, **30**.

Poli, P., and Coauthors, 2016: ERA-20C: An atmospheric reanalysis of the twentieth century. *J. Climate*, **29**, 4083-4097.

Pozo-Vázquez, D., S. R. Gámiz-Fortis, J. Tovar-Pescador, M. J. Esteban-Parra, and Y. Castro-Díez, 2005: El Niño–Southern Oscillation events and associated European winter precipitation anomalies. *Int. J. Climatol.*, **25**, 17-31.

Rust, W., J. P. Bloomfield, M. O. Cuthbert, R. Corstanje, and I. P. Holman, 2021: Non-stationary control of the NAO on European rainfall and its implications for water resource management. *Hydrol. Process.,* **35**.

Schneider, D. P., and R. L. Fogt, 2018: Artifacts in century-length atmospheric and coupled reanalyses over Antarctica due to historical data availability. *Geophys. Res. Lett.*, **45**, 964-973.

Schulte, J. A., and S. Lee, 2017: Strengthening North Pacific influences on United States temperature variability. *Sci. Rep.,* **7**, 1-12.

Seager, R., H. Liu, Y. Kushnir, T. J. Osborn, I. R. Simpson, C. R. Kelley, and J. Nakamura, 2020: Mechanisms of Winter Precipitation Variability in the European–Mediterranean Region Associated with the North Atlantic Oscillation. *J. Climate*, **33**, 7179-7196.

Slivinski, L. C., and Coauthors 2019: Towards a more reliable historical reanalysis: Improvements for version 3 of the Twentieth Century Reanalysis system. *Q. J. R. Meteorol. Soc*., **145**, 2876-2908.

Slivinski, L. C., and Coauthors 2021: An evaluation of the performance of the Twentieth Century Reanalysis version 3. *J. Climate*, **34**, 1417-1438.

Soulard, N., H. Lin, and B. Yu, 2019: The changing relationship between ENSO and its extratropical response patterns. *Sci. Rep.,* **9**, 1-10.

Tan, B., J. Yuan, Y. Dai, S. B. Feldstein, and S. Lee, 2015: The linkage between the eastern Pacific teleconnection pattern and convective heating over the tropical western Pacific. *J. Climate*, **28**, 5783-5794.

Trigo, R. M., T. J. Osborn, and J. M. Corte-Real, 2002: The North Atlantic Oscillation influence on Europe: climate impacts and associated physical mechanisms. *Clim. Res.,* **20**, 9-17.

Trigo, R. M., D. Pozo-Vázquez, T. J. Osborn, Y. Castro-Díez, S. Gámiz-Fortis, and M. J. Esteban-Parra, 2004: North Atlantic Oscillation influence on precipitation, river flow and water resources in the Iberian Peninsula. *Int. J. Climatol.*, **24**: 925–944.

Ulbrich, U., and M. Christoph, 1999: A shift of the NAO and increasing storm track activity over Europe due to anthropogenic greenhouse gas forcing *Clim. Dyn.,* **15**, 551-559.

Vicente-Serrano, S. M., and J. I. López-Moreno, 2008: Nonstationary influence of the North Atlantic Oscillation on European precipitation. *J. Geophys. Res. Atmos*., **113**(D20).

Wallace, J. M., and D. S. Gutzler, 1981: Teleconnections in the geopotential height field during the Northern Hemisphere winter. *Mon. Weather Rev.*, **109**, 784-812.

Wanner, H., S. Brönnimann, C. Casty, D. Gyalistras, J. Luterbacher, C. Schmutz, D. B. Stephenson, and E. Xoplaki, 2001: North Atlantic Oscillation–concepts and studies. *Surv. Geophys.*, **22**, 321-381.

Wang, L., W. Chen, and R. Huang, 2007: Changes in the variability of North Pacific Oscillation around 1975/1976 and its relationship with East Asian winter climate. *J. Geophys. Res. Atmos*., **112**.

Wang, L., Y. Liu, Y. Zhang, W. Chen, and S. Chen, 2018: Time-varying structure of the wintertime Eurasian pattern: role of the North Atlantic sea surface temperature and atmospheric mean flow. *Clim. Dyn.,* **52**, 2467-2479.

Xu, T., Z. Shi, H. Wang, and Z. An, 2016: Nonstationary impact of the winter North Atlantic Oscillation and the response of mid-latitude Eurasian climate. *Theor. Appl. Climatol.,* **124**, 1-14.

Xu, Z., and K. Fan, 2020: Prolonged Periodicity and Eastward Shift of the January North Pacific Oscillation Since the Mid-1990s and Its Linkage With Sea Ice Anomalies in the Barents Sea. *J. Geophys. Res. Atmos*., **125**, e2020JD032484.

Yadav, R. K., K. Rupa Kumar, and M. Rajeevan, 2009: Increasing influence of ENSO and decreasing influence of AO/NAO in the recent decades over northwest India winter precipitation. *J. Geophys. Res. Atmos*., **114** (D12).

Yeh, S. W., Y. J. Kang, Y. Noh, and A. J. Miller, 2011: The North Pacific climate transitions of the winters of 1976/77 and 1988/89. *J. Climate*, **24**, 1170-1183.

Yeh, S. W., D. W. Yi, M. K. Sung, and Y. H. Kim, 2018: An eastward shift of the North Pacific Oscillation after the mid-1990s and its relationship with ENSO. *Geophys. Res. Lett.*, **45**, 6654-6660.

Yu, B., H. Lin, and N. Soulard 2019: A comparison of north american surface temperature and temperature extreme anomalies in association with various atmospheric teleconnection patterns. *Atmosphere*, **10**, 172.

Yuan, J., B. Tan, S. B. Feldstein, and S. Lee, 2015: Wintertime North Pacific teleconnection patterns: Seasonal and interannual variability. *J. Climate*, **28**, 8247-8263.

Zanchettin, D., S. W. Franks, P. Traverso, and M. Tomasino, 2008: On ENSO impacts on European wintertime rainfalls and their modulation by the NAO and the Pacific multi-decadal variability described through the PDO index. *Int. J. Climatol.*, **28**, 995-1006.

Zuo, J., H. L. Ren, W. Li, and L. Wang, 2016: Interdecadal variations in the relationship between the winter North Atlantic Oscillation and temperature in south-central China. *J. Climate*, **29**, 7477-7493.

Supplementary figures for

Temporal variation of relationships between circulation modes and surface climatic variables in the 20th century in winter

Martin Hynčica [1, 2], Radan Huth [1, 3]

[1] Dept. of Physical Geography and Geoecology, Faculty of Science, Charles University, Albertov 6, 128 43, Prague, Czechia

[2] Dept. of Environment, Faculty of Environment, Jan Evangelista Purkyně University, Pasteurova 15, 400 96, Ústí nad Labem, Czechia

[3] Institute of Atmospheric Physics, Czech Academy of Sciences, Boční II 1401, 141 31, Prague, Czechia

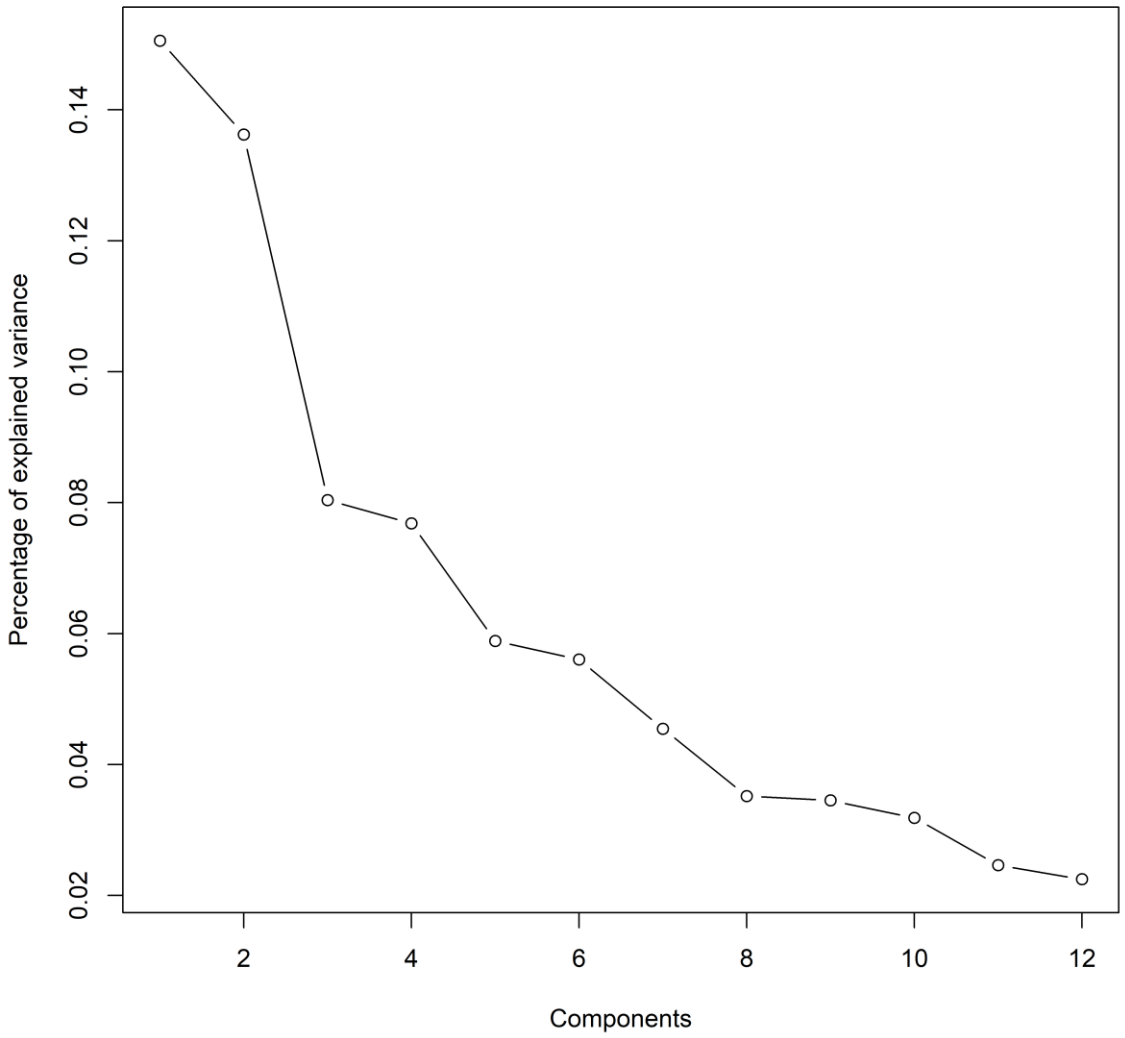

FIG. S1. Scree plot with 12 leading principal components and the percentage of their explained variance (on the y-axis) in the ERA-20C reanalysis in winter.

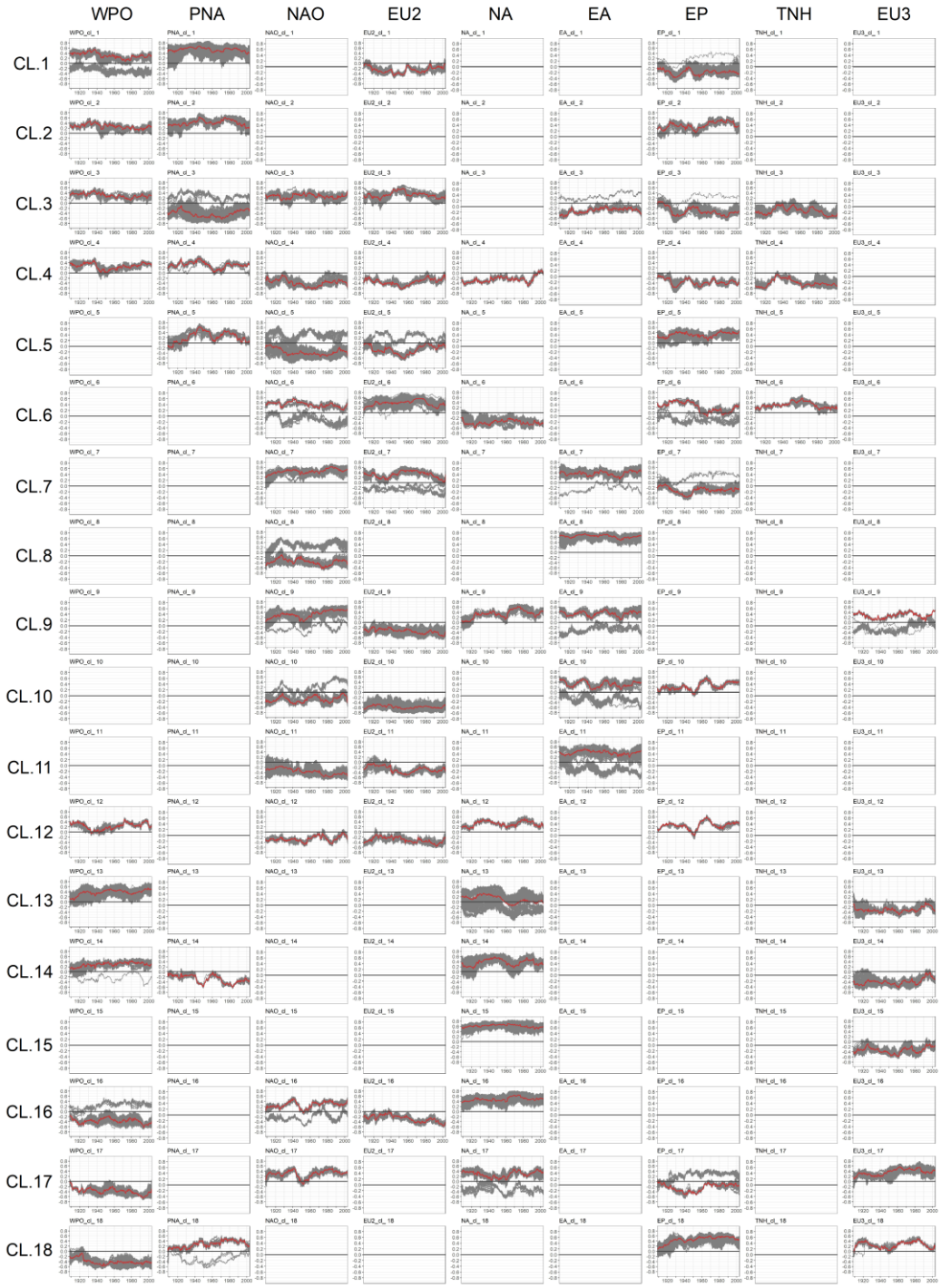

FIG. S2. Time series of running correlations between temperature anomaly and intensity of circulation modes. Clusters in rows, circulation modes in columns. Only time series satisfying conditions given in Sec. 2.3 are displayed. Red time series are the average over analysed gridpoints for each cluster and circulation mode; they correspond to the anomaly time series in Fig. 2.

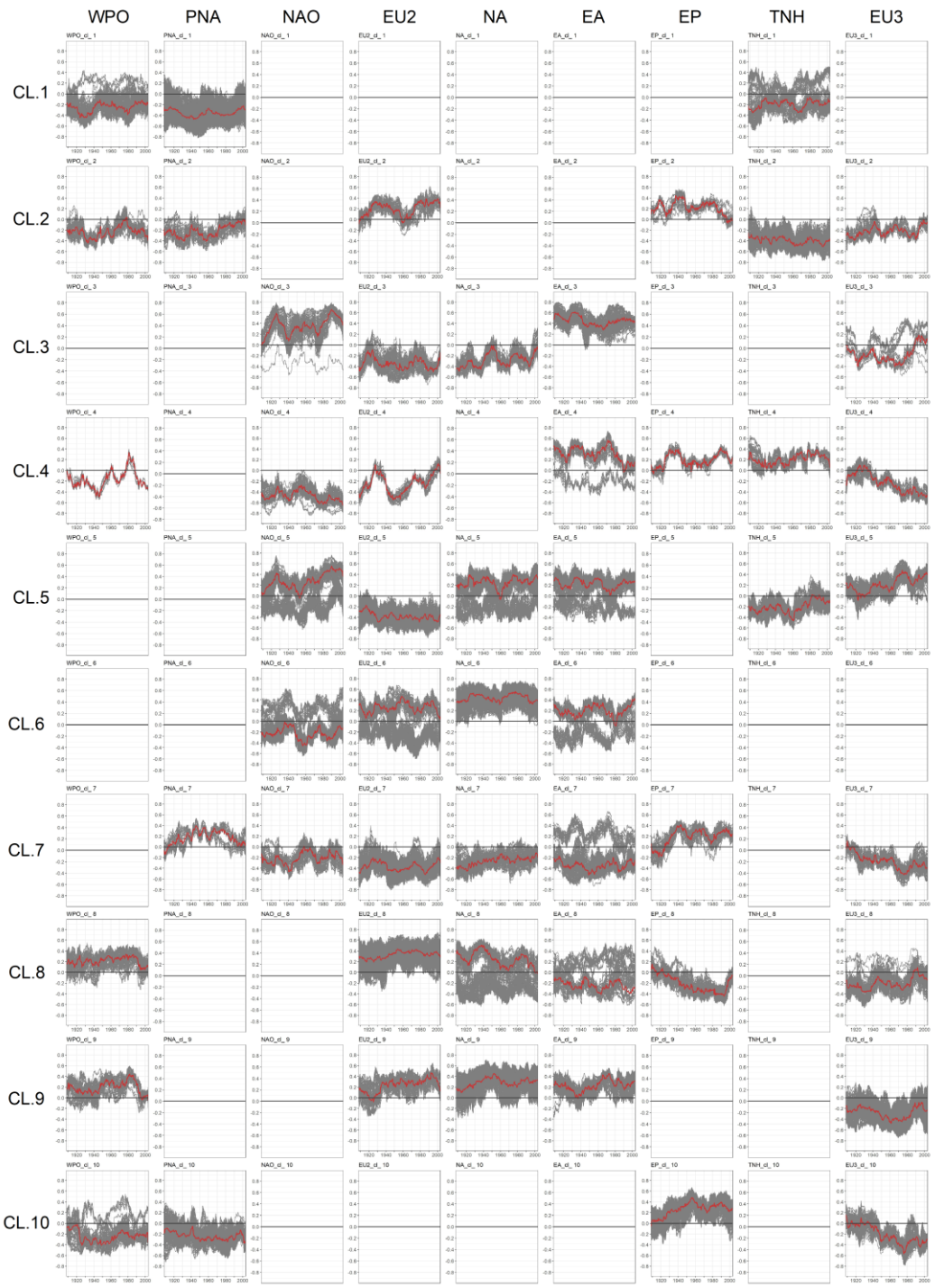

FIG. S3. As in Fig. S2 but for precipitation. Time series highlighted in red are averages over analysed gridpoints for each cluster and circulation mode; they correspond to anomaly time series in Fig. 3.

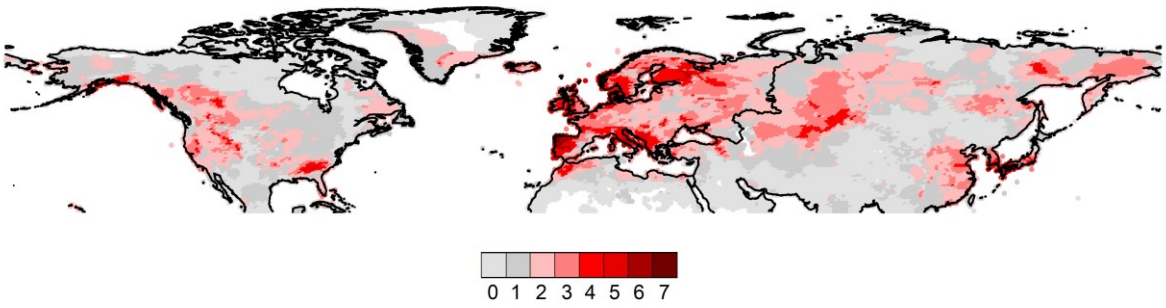

FIG. S4. Number of circulation modes meeting the criterion for a non-negligible effect on precipitation introduced in Sec. 2.3. Blank areas represent regions with no precipitation data in the CRU dataset.

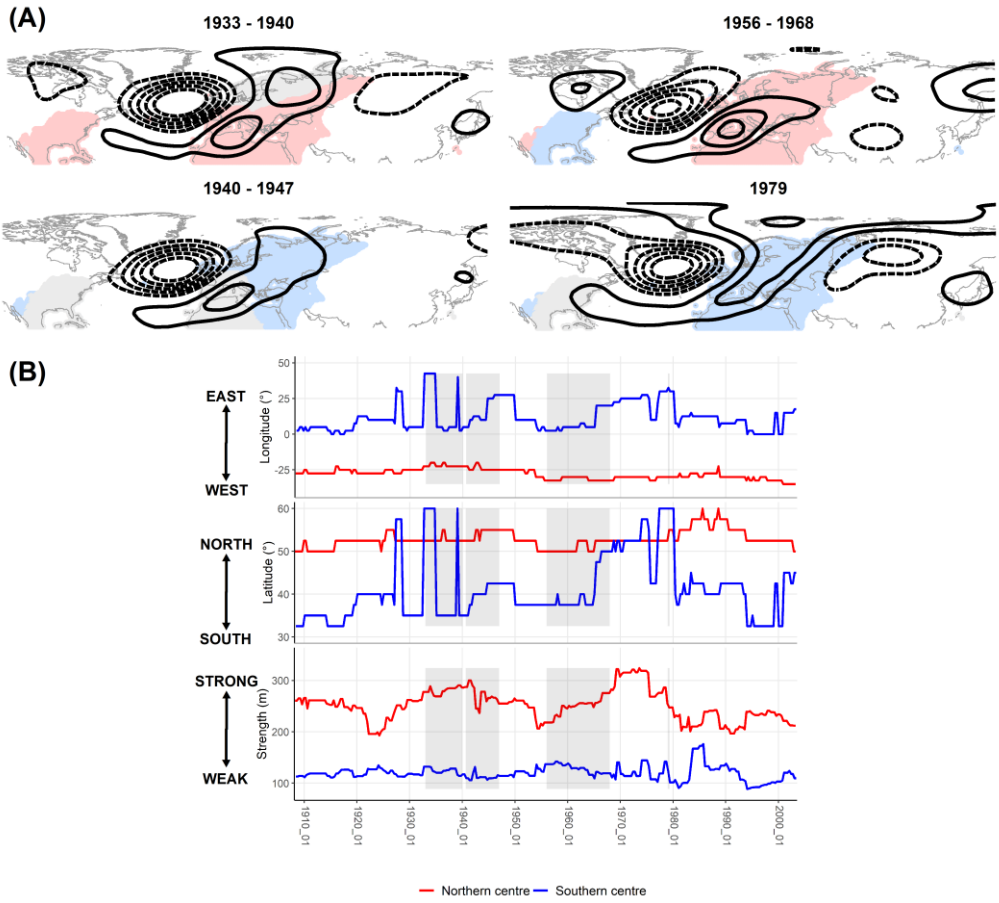

FIG. S5. As in Fig. 4, except for EA.

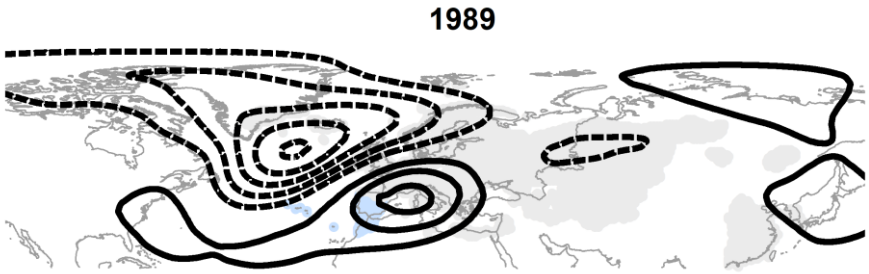

FIG. S6. As in Fig. S5a, but for correlation with precipitation in the single running period with the weakest impact of EA on precipitation in the Iberian Peninsula (cluster in blue colour).

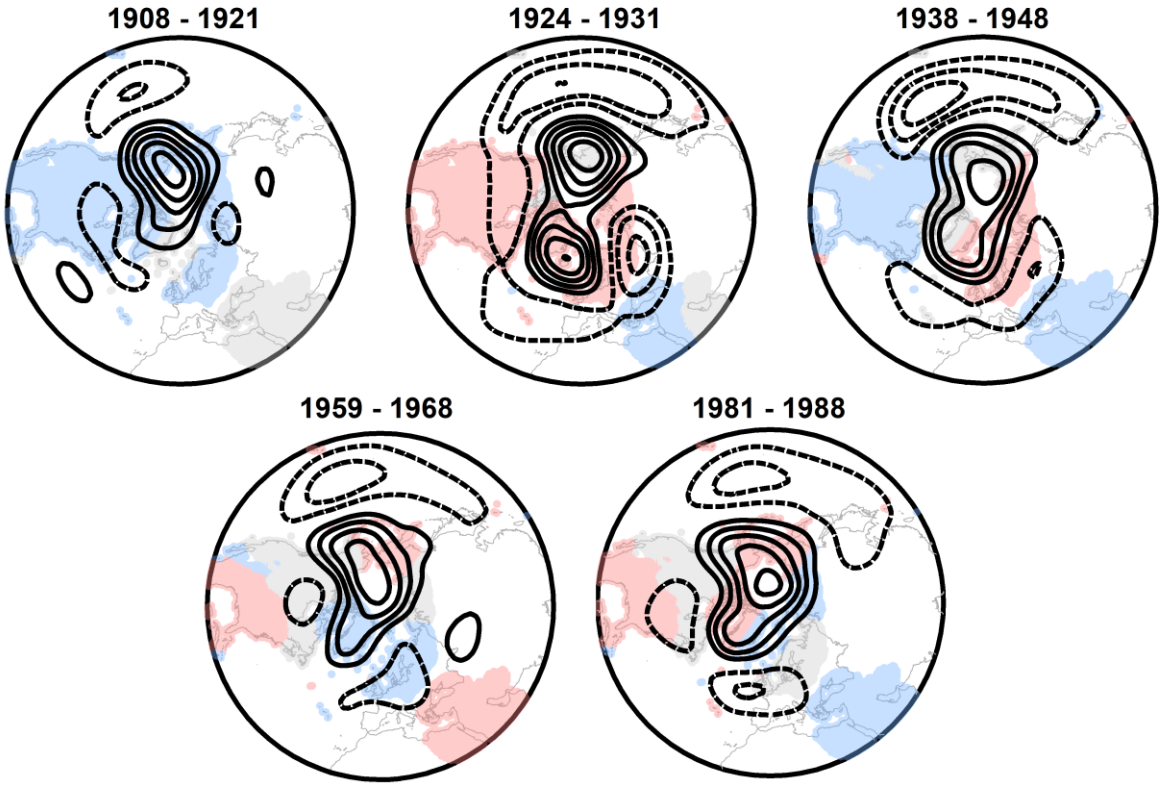

FIG. S7. As in Fig. S5, but for the EP pattern. Part B is omitted because the main positive centre often passes over the North Pole, hence causing discontinuities in the graphs.

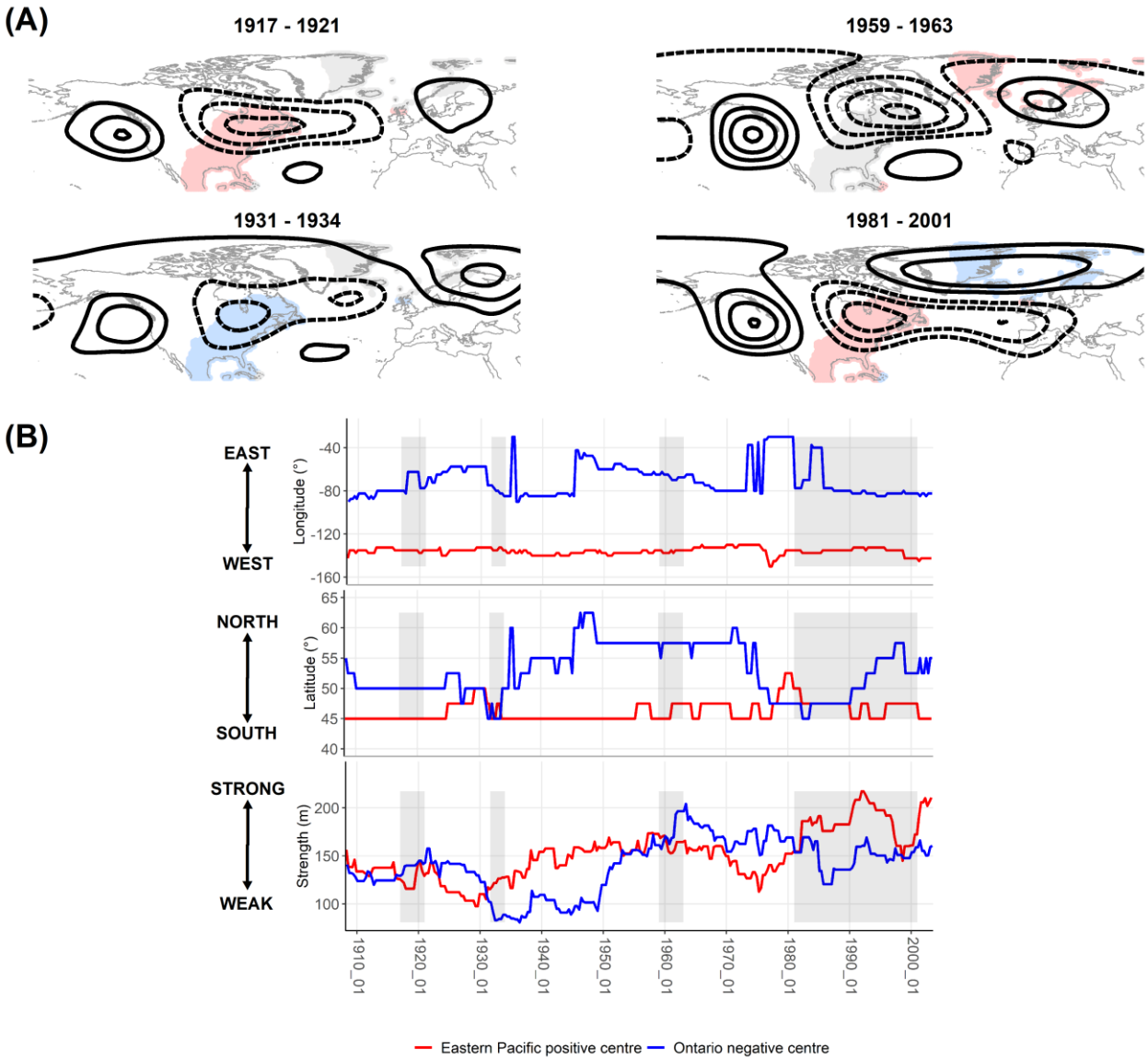

FIG. S8. As in Fig. S5, but for the TNH pattern.

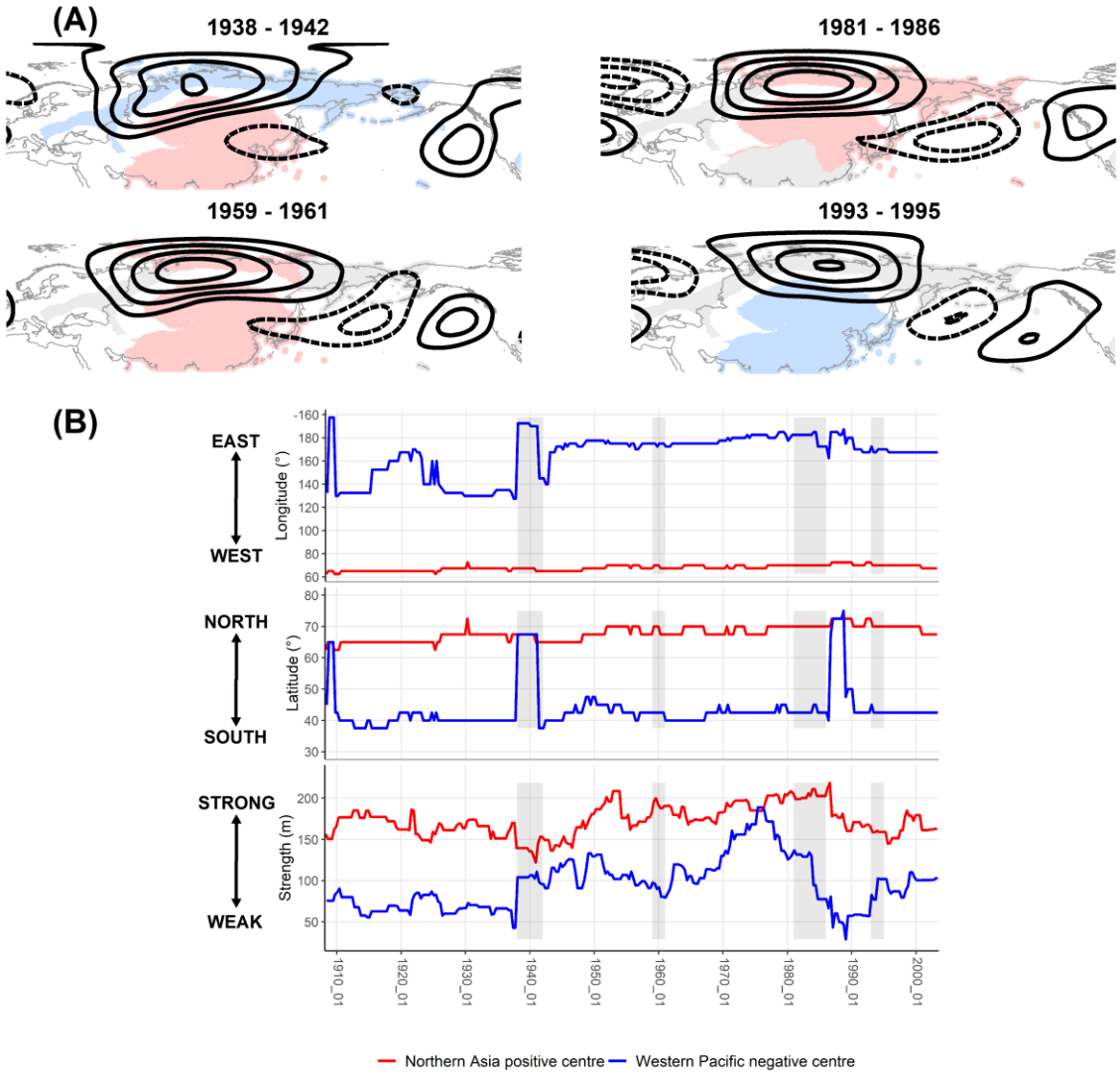

FIG. S9. As in Fig. S5, but for the EU3 pattern.

5. Conclusions and future outlook

This thesis extends research field on relationships between circulation modes and surface climatic elements. Firstly, circulation modes and their relationships with temperature are compared between reanalyses. It is demonstrated that most circulation modes are fairly similar between reanalyses in all seasons, with the largest differences detected in summer. Large congruence of datasets is clearly evident among full-input reanalyses (ERA-40, JRA-55, and NCEP-1). Contrarily to that, one of the surface-input reanalyses, 20CRv2c, suffers from errors located mainly in the southern half of Asia and subtropical eastern Pacific. Those errors manifest in different spatial representation of some circulation modes in 20CRv2c, e.g. EU1 in winter, and NAO in spring, and contribute to a different long-term evolution of relationships with surface climatic elements. For example, different spatial representation of EU1 in winter in 20CRv2c in the 1980s results in different spatial impact of the mode on temperature. Similar, albeit not so prominent issue is also related to NAO in winter. On the other hand, the recently issued version of the 20CR reanalyses family – 20CRv3 – is largely consistent with other reanalyses, suggesting that errors from the previous version have been corrected. Issues in 20CRv2c might be caused either by the model used for its creation, or the amount and quality of assimilated data; 20CRv3 utilizes updated datasets and new versions of the model. Circulation modes and relationships with temperature in the other surface-input reanalysis, ERA-20C, exhibit higher resemblance with the full input reanalyses; it suffers only from marginal issues located over the north Pacific in spring.

For the analysis of long-term temporal evolution of relationships with surface climatic elements, a reanalysis from the surface-input category should be used, because they span at least the 20th century. ERA-20C is the most suitable reanalysis because its circulation modes and relationships with temperature are similar to full-input reanalyses, which are generally considered to be more reliable due to the assimilation of upper air and satellite data.

Datasets containing surface observations are of two types: station and gridded datasets. The latter is created by interpolation of station observations into a regular grid. There is a large agreement of relationships (expressed as running correlations) between circulation modes and temperature at stations and the nearest gridpoints from the CRU dataset; differences related to island stations and higher elevated areas mainly in eastern Asia arise

from spatial distribution of station network used for the interpolation. Nonetheless, the number of locations where the temporal course of correlations between the mode and temperature at a station and at a gridpoint differ is low; the CRU dataset is shown to be reliable as the source of surface temperature and precipitation for the analysis.

Finally, the analysis of nonstationarity of effects of circulation modes on temperature and precipitation is conducted for the entire Northern Extratropics between 1901 and 2010. As noticed above, the ERA-20C reanalysis is used for the detection of circulation modes, and the CRU dataset serves as the source of surface climate data. Running correlations between the intensity of circulation modes and temperature and precipitation at gridpoints indicate temporal variations of relationships. These running correlations are consequently clustered for the sake of delimitation of clusters, that is, geographical compact regions. The temporal evolution of relationships in each cluster is then similar over all included gridpoints. Generally, the characteristics of action centres, mainly their location, strength, and shape, are proved to affect spatiotemporal impacts of circulation modes on local temperature and precipitation. For example, deepening of an action centre may lead to strengthened relationships related to stronger advection along its flanks, while an action centre shifting away results in a weaker impact on surface climatic variables. Some circulation modes vary in time considerably (e.g. WPO, PNA, NAO, and EP), whilst some are fairly stable and fluctuations of relationships with them are less recognizable (e.g. EU2, NA, and EA). Primary causes of the nonstationarity of circulation modes, such as links with the El Niño-Southern Oscillation and the Pacific Decadal Oscillation, are also discussed. Nevertheless, such analyses go beyond the scope of the thesis and, moreover, there is a lack of studies dealing with this issue, particularly before 1950 when some circulation modes, mainly WPO and PNA, underwent substantial changes in their spatial representation.

This thesis brings about new findings on circulation modes and their relationships with surface climatic variables in a somehow general sense: all circulation modes are detected simultaneously in the long time period over a large geographical area. This is, however, necessarily accompanied by a generalization of results. Future work may look at the behaviour of circulation modes in a more detailed sense, for example, focusing to a selected time period analysed in a finer temporal resolution; as noted above, the behaviour of

circulation modes before 1950 would be of a particular interest. Also, one may look at circulation modes in a specific region, but over a long time period. In either way, all such studies should contain linkage with drivers in the climate system responsible for changes in the circulation modes.

The open question remains on the long-term evolution of circulation modes in other seasons, which has been addressed rarely. The methodology used here may be applied to other seasons (spring, summer, and autumn) to detect regions with similar temporal evolution between circulation modes and surface climatic variables. Nevertheless, as also demonstrated in this thesis, circulation modes in summer are different between reanalyses, so temporal evolution of the circulation modes themselves and their relationships with surface climatic variables would be strongly dependent on the selected reanalysis. This dependence is further strengthened owing to circulation modes in summer being very regionalized. It would therefore be quite a challenge to apply the methodology in this thesis to summer; another deeper research would be needed, or different methodology may be used instead.

The research can be further extended, for example, by analysing other datasets, such as the ERA-5, MERRA, and CFSR reanalyses, all of which may be included into the comparison of reanalyses, although the majority of them do not extend before 1950, which limits they use. Even more interesting seems to be the analysis of changes of circulation modes and their associations with surface climate in historical runs in climate models, and their validation against reanalyses.

References (excluding sections 2-4)

Barnston, A. G., Livezey, R. E. (1987). Classification, seasonality and persistence of low-frequency atmospheric circulation patterns. *Mon Weather Rev*, 115, 1083-1126.

Beranová, R., Huth, R. (2008). Time variations of the effects of circulation variability modes on European temperature and precipitation in winter. *Int J Climatol*, 28, 139-158.

Börgel, F., Frauen, C., Neumann, T., Meier, H. M. (2020). The Atlantic Multidecadal Oscillation controls the impact of the North Atlantic Oscillation on North European climate. *Environ Res Lett*, 15, 104025.

Chen, D., Hellström, C. (1999). The influence of the North Atlantic Oscillation on the regional temperature variability in Sweden: spatial and temporal variations. *Tellus A*, 51, 505-516.

Compo, G. P., and Coauthors (2011). The Twentieth Century Reanalysis Project. *Q J R Metorol Soc,* 137, 1-28.

Dee, D. P., Uppala, S. (2009). Variational bias correction of satellite radiance data in the ERA-Interim reanalysis. *Q J R Metorol Soc*, 135, 1830-1841.

Dong, B., Sutton, R. T., Woollings, T. (2011). Changes of interannual NAO variability in response to greenhouse gases forcing. *Clim Dyn*, 37, 1621-1641.

Filippi, L., Palazzi, E., von Hardenberg, J., Provenzale, A. (2014). Multidecadal variations in the relationship between the NAO and winter precipitation in the Hindu Kush–Karakoram. *J Clim*, 27, 7890-7902.

Fujiwara, M., and Coauthors (2017). Introduction to the SPARC Reanalysis Intercomparison Project (S-RIP) and overview of the reanalysis systems. *Atmos Chem Phys,* 17, 1417-1452.

Gimeno, L., Ribera, P., Iglesias, R., de la Torre, L., García, R., Hernández, E. (2002). Identification of empirical relationships between indices of ENSO and NAO and agricultural yields in Spain. *Clim Res*, 21, 165-172.

Gimeno, L., De La Torre, L., Nieto, R., García, R., Hernández, E., Ribera, P. (2003). Changes in the relationship NAO–Northern hemisphere temperature due to solar activity. *Earth Planet Sci Lett*, 206, 15-20.

Gu, W., Li, C., Li, W., Zhou, W., Chan, J. C. (2009). Interdecadal unstationary relationship between NAO and east China's summer precipitation patterns. *Geophys Res Lett* ,36.

Harris, I., Osborn, T. J., Jones, P., & Lister, D. (2020). Version 4 of the CRU TS monthly high-resolution gridded multivariate climate dataset. *Sci Data*, *7*(1), 1-18.

Horel, J. D. (1981). A rotated principal component analysis of the interannual variability of the Northern Hemisphere 500mb height field. *Mon Weather Rev*, 109, 2080-2092.

Hurrell, J. W. (1995). Decadal trends in the North Atlantic Oscillation: Regional temperatures and precipitation. *Science*, 269, 676-679.

Hurrell, J. W., Kushnir, Y., Ottersen, G., Visbeck, M. (2003). An overview of the North Atlantic oscillation. *Geophysical Monograph-American Geophysical Union*, 134, 1-36.

Jung, T., Hilmer, M., Ruprecht, E., Kleppek, S., Gulev, S. K., Zolina, O. (2003). Characteristics of the recent eastward shift of interannual NAO variability. *J Climate*, 16, 3371-3382.

Kalnay, E., and Coauthors (1996). TheNCEP/NCAR40-Year ReanalysisProject. *Bull Am Meteorol Soc*, 77, 437-471.

Kobayashi, S., and Coauthors (2015). The JRA-55 reanalysis: General specifications and basic characteristics. *J Meteorol Soc Japan*, 93, 5-48.

Krichak, S. O., Kishcha, P., Alpert, P. (2002). Decadal trends of main Eurasian oscillations and the Eastern Mediterranean precipitation. *Theor Appl Climatol,* 72*,* 209-220.

Leathers, D. J., Yarnal, B., Palecki, M. A. (1991). The Pacific/North American teleconnection pattern and United States climate. Part I: Regional temperature and precipitation associations. *J Clim*, 4, 517-528.

Linkin, M. E., Nigam, S. (2008). The North Pacific Oscillation–west Pacific teleconnection pattern: Mature-phase structure and winter impacts. *J Clim* , 21, 1979-1997.

López-Moreno, J. I., Vicente-Serrano, S. M. (2008). Positive and negative phases of the wintertime North Atlantic Oscillation and drought occurrence over Europe: a multitemporal-scale approach. *J Clim*, 21, 1220-1243.

Luo, D., Gong, T. (2006). A possible mechanism for the eastward shift of interannual NAO action centers in last three decades. *Geophys Res Lett*, 33.

Marshall, G. J. (2021). Decadal variability in the impact of atmospheric circulation patterns on the winter climate of northern Russia. *J. Clim*, 34, 1005-1021.

Monahan, A. H. (2000). Nonlinear principal component analysis by neural networks: Theory and application to the Lorenz system. *J Clim*, 13, 821-835.

Opoku-Ankomah, Y., Cordery, I. (1993). Temporal variation of relations between New South Wales rainfall and the Southern Oscillation. *Int J Climatol*, 13, 51-64.

Ottersen, G., Planque, B., Belgrano, A., Post, E., Reid, P. C., Stenseth, N. C. (2001). Ecological effects of the North Atlantic oscillation. *Oecologia*, 128, 1-14.

Pokorná, L., Huth, R. (2015). Climate impacts of the NAO are sensitive to how the NAO is defined. *Theor Appl Climatol*, 119, 639-652.

Poli, P., and Coauthors (2016). ERA-20C: An atmospheric reanalysis of the twentieth century. *J Clim*, 29, 4083–4097.

Rogers, J. C. (1984). The association between the North Atlantic Oscillation and the Southern Oscillation in the northern hemisphere. *Mon Weather Rev*, 112, 1999-2015.

Rohrer, M., Brönnimann, S., Martius, O., Raible, C. C., Wild, M., Compo, G. P. (2018). Representation of extratropical cyclones, blocking anticyclones, and Alpine circulation types in multiple reanalyses and model simulations. *J Clim*, *31*, 3009-3031.

Slivinski, L. C., and Coauthors (2021). An evaluation of the performance of the twentieth century reanalysis version 3. *J Clim*, 34, 1417-1438.

Slonosky, V. C., Jones, P. D., Davies, T. D. (2001). Atmospheric circulation and surface temperature in Europe from the 18th century to 1995. *Int J Climatol,* 21, 63-75.

Soulard, N., Lin, H., Yu, B. (2019). The changing relationship between ENSO and its extratropical response patterns. *Sci. Rep.,* 9, 1-10.

Stige, L. C., Ottersen, G., Brander, K., Chan, K. S., Stenseth, N. C. (2006). Cod and climate: effect of the North Atlantic Oscillation on recruitment in the North Atlantic. *Mar Ecol Prog*, 325, 227-241.

Stryhal, J., Huth, R. (2017). Classifications of winter Euro-Atlantic circulation patterns: an intercomparison of five atmospheric reanalyses. *J Clim*, 30, 7847-7861.

Ulbrich, U., Christoph, M. (1999). A shift of the NAO and increasing storm track activity over Europe due to anthropogenic greenhouse gas forcing. *Clim Dyn*, 15, 551-559.

Uppala, S. M., and Coauthors (2005). The ERA-40 reanalysis. *Q J R Metorol Soc*, 131, 2961-3012.

Vicente-Serrano, S. M., López-Moreno, J. I. (2008). Nonstationary influence of the North Atlantic Oscillation on European precipitation. *J Geophys Res Atmos*, 113(D20).

Wallace, J. M., Gutzler, D. S. (1981). Teleconnections in the geopotential height field during the Northern Hemisphere winter. *Mon Weather Rev*, 109, 784-812.

Wang, X. L., Feng, Y., Compo, G. P., Swail, V. R., Zwiers, F. W., Allan, R. J., Sardeshmukh, P. D. (2013). Trends and low frequency variability of extra-tropical cyclone activity in the ensemble of twentieth century reanalysis. *Clim Dyn*, 40, 2775-2800.

Wang, X. L., Feng, Y., Chan, R., Isaac, V. (2016). Inter-comparison of extra-tropical cyclone activity in nine reanalysis datasets. *Atmos Res*, 181, 133-153.

Xu, T., Shi, Z., Wang, H., An, Z. (2016). Nonstationary impact of the winter North Atlantic Oscillation and the response of mid-latitude Eurasian climate. *Theor Appl Climatol*, 124, 1-14.

Zanardo, S., Nicotina, L., Hilberts, A. G., Jewson, S. P. (2019). Modulation of economic losses from European floods by the North Atlantic Oscillation. *Geophys Res Lett*, 46, 2563-2572.